Enzyme-like Catalysis

in Self-Assembled Aromatic Capsules

Qi Zhang

Die vorliegende Arbeit wurde in der Zeit von Mai 2012 bis März 2016 unter der Leitung von Jun.-Prof. Dr. Konrad Tiefenbacher an der *Juniorprofessur für Organische Chemie* der *Technische Universität München* angefertigt.

Teile dieser Arbeit wurden veröffentlicht:

Catti, L.; Zhang, Q.; Tiefenbacher, K.*, *Synthesis*, **2016**, *48*, 313.

Zhang, Q., Tiefenbacher, K.*, *Nature Chem.* **2015**, *7*, 197.

Zhang, Q., Tiefenbacher, K.*, *J. Am. Chem. Soc.* **2013**, *135*, 16213.

Acknowledgements

First of all, I would like to express my sincere gratitude to my advisor Prof. Konrad Tiefenbacher for his continuous support of my Ph.D study, for his patience and immense knowledge. Without his guidance and persistent help this dissertation would not have been possible. I still remember the time when I started as a Ph.D student and worked with him side by side in the same hood. This experience turns out to be of great benefit for me to gain practical working skills and the basic knowledge to do research work. It is a great pleasure to learn from and work with you!

I am grateful to Prof. Stefan Huber for supervising my Master's Thesis and introducing me to Prof. Konrad Tiefenbacher. I also want to thank Prof. Thorsten Bach and his group for their support. Ms. Kerstin Voigt is acknowledged for all the organizational efforts.

For proofreading I want to thank Prof. Konrad Tiefenbacher, Lorenzo Catti, Thomas Bräuer and Dr. You-Quan Zou.

I gratefully acknowledge all the members of the Tiefenbacher group for the wonderful working atmosphere. My special thanks go to Thomas Bräuer and Lorenzo Catti for providing me with help in the daily life and the fun that we had together. Johannes Richers is greatly acknowledged for the graphic design in my publications. My research students Maike Wahl, Qing-Qi Zhao and Xin-Zhe Wang are acknowledged for their contribution to this dissertation.

I also want to thank Prof. Lei Jiao, Dr. Peng Hu, Wei-Ning Zhao, Prof. Fang-Rui Zhong and Dr. You-Quan Zou for the time that we spent together. Special thanks go to Prof. Lei Jiao for the enlightening discussion and advice.

Finally, I want to thank my parents, my wife and the rest of my family for their unconditional love and support!

Deutsches Abstract

Selbstassemblierte supramolekulare Systeme haben sich als attraktive Enzymmimetika erwiesen. Die hexamere Resorcinarenkapsel **IVa** dient als ein idealer Kandidat in dieser Hinsicht: Sie ist einer der größten molekularen Kapseln, die auf Wasserstoffbrückenbindungen basieren. Des Weiteren ist sie aufgrund ihrer leichten Verfügbarkeit schon intensiv untersucht worden.

Es wurde gezeigt, dass sich Kapsel **IVa** als milde Brønsted-Säure (pK_a 5.5–6) verhält. Dieser Befund erklärt die hohe Affinität von **IVa** zur tertiären Aminen, die als protonierte Spezies eingekapselt werden und deswegen Kationen–π-Wechselwirkungen innerhalb des Hohlraumes von **IVa** eingehen können. In Anwendungen übt die Kapsel **IVa** Substratselektivität als stöchiometrischer Selektor in einer Wittig-Reaktion aus. Zusätzlich katalysiert die Kapsel **IVa** die größenselektive Hydrolysereaktion von Diethylacetalen unter milden Bedingungen.

Die Schwanz-zu-Kopf Terpenzyklisierung wird wohl als eine der komplexesten Reaktionen der Natur angesehen. Sie wurde kaum in Lösung reproduziert. Mit **IVa** als katalytischem Reaktionswirt wurde die Schwanz-zu-Kopf Terpenzyklisierung erstmals mit einem künstlichen Katalysator realisiert. Der grundlegende Operationsmodus der Cyclase wurde erfolgreich imitiert und eine Non-Stop-Zyklierung mit Geranylacetat als Substrat erzielt. Die Zyklisierung in **IVa** hat Bedeutung für den postulierten Biosynthese-Reaktionsmechanismus der Terpene. Es gibt Hinweise darauf, dass eine direkte Isomerisierung eines Geranylkations in das *cisoide* Isomer, das bisher als unwahrscheinlich angesehen wird, möglich ist.

Des weiteren wurden die Unterschiede zwischen den nahe verwandten Kapseln **IVa** und **IVc** aufgeklärt. Die gewonnenen Erkenntnisse sind von großer Bedeutung für das Verständnis der katalytische Aktivität von **IVa** und haben einen großen Einfluss auf die Gestaltung neuer katalytisch aktiver Wirtsysteme.

English Abstract

Supramolecular structures have emerged as appealing artificial catalysts in the pursuit of biomimetic catalysis. The hexameric resorcinarene capsule **IVa** serves as an ideal candidate in this regard: The hydrogen-bonded capsule **IVa** encloses a spacious cavity and intensive studies have been performed due to its ready availability.

The capsule **IVa** was found to act as a mild Brønsted acid (pK_a 5.5–6). These results accounts for the high affinity of **IVa** towards tertiary amines: The amines are encapsulated in their protonated form and stabilized by cation–π interactions within the negatively charged capsule **IVa**. We then utilized **IVa** as a stoichiometric selector to impose substrate bias in a Wittig reaction. In addition, capsule **IVa** is capable of catalyzing the diethyl acetal hydrolysis in a size-selective fashion under mild reaction conditions.

The tail-to-head terpene (THT) cyclization is arguably one of most complex reactions occurring in nature, and it has been hardly reproduced in bulk solution. With capsule **IVa** as a catalytic reaction host, the tail-to-head cyclization of monoterpenes was realized for the first time with an artificial catalyst. Capsule **IVa** successfully mimics cyclase enzymes. With geranyl acetate as the substrate, the cyclization proceeds in a highly selective and non-stop fashion. The results further indicate that the direct isomerization of a geranyl cation to the *cisoid* isomer could be relevant for the mechanism proposed for the biosynthesis of terpenes.

Moreover, the differences between the closely related capsules **IVa** and **IVc** were elucidated. The obtained results are of great significance for understanding the source of the catalytic activity of **IVa** and have a profound impact on the design of new catalytically active host systems.

Abbreviations

ATP	adenosine triphosphate
BDSB	bromodiethylsulfonium bromopetanchloroantimonate
CMP/CTP	cytidine mono/triphosphate
DABCO	1,4-diazabicyclo[2.2.2]octane
DFT	density functional theory
DMAP	4-dimethylaminopyridine
DMAPP	dimethylallyl pyrophosphate
DMSO	dimethyl sulfoxide
DOSY	diffusion-ordered spectroscopy
DOXP	1-deoxy-D-xylulose-5-phosphate
ee	enantiomeric excess
eq.	equivalent
ESP	electrostatic potential
GOAc	geranyl acetate
GOH	geraniol
GPP	geranyl pyrophosphate
HIV	human immunodeficiency virus
HSQC	heteronuclear single quantum coherence
IPP	isopentenyl pyrophosphate
LOAc	linalyl pyrophosphate
LOH	linalool
LPP	linayl pyrophosphate
MEP	methylerythritol phosphate
MVA	mevalonate
NADPH	Nicotinamide adenine dinucleotide phosphate
NBS	N-bromosuccinimide
NCS	N-chlorosuccinimide
NIS	N-iodosuccinimide
NMR	nuclear magnetic resonance
NOAc	neryl acetate
NOESY	nuclear Overhauser effect spectroscopy
NOH	nerol
SD	standard deviation
THT cyclization	tail-to-head terpene cyclization
TMS	trimethylsilyl

x

TABLE OF CONTENT

1 Introduction

1.1 Catalysis in Supramolecular Structures

1.1.1 Enzyme Catalysis

Since the discovery of enzymes as biological catalysts, studies have been performed to reveal the origin of their enormous catalytic power and delicate specificity. These questions remained puzzling until the crystallization of enzymes[1] eventually allowed their structural elucidation by X-ray crystallography.[2] Enzymes consist of linear chains of amino acids which fold into their characteristic three-dimensional structures. The resulting hydrophobic enzyme pockets select substrates of complementary size and shape from aqueous surroundings. When more than one substrate is involved, the confined space within enzymes brings reaction partners in close proximity and facilitates the intermolecular reactions by increasing local concentration. On the other hand, the formation of a compact enzyme-substrate complex efficiently shields the active sites from the bulk medium, allowing the reaction to proceed without interference.

Generally, enzymes accelerate the rate of catalyzed reactions by lowering the activation energy in three basic ways: (1) the finite confinements of enzymes exert a certain strain on bound substrates and force them to adopt reactive conformations resembling the transition state (ground-state destabilization).[3] The constraint within active sites not only assists the bound substrate in overcoming the entropic penalty of activation,[4] but also guarantees the high fidelity of steric outcomes. (2) During the binding process, the enzyme pockets act rather as flexible structures than simply rigid hosts.[5] By interacting with substrates, enzymes continuously reshape their cavity contours until the functional groups (mostly as part of hydrogen-bonding networks) residing within the pockets haven been precisely arranged[6] to complement the charge distribution of the transition state (transition state stabilization).[7] Another consequence of the precisely orientating hydrogen-bonding network is a fine-tuned

pK_a-matching[8] between substrates and protein residues, which renders substrates a higher reactivity when proton transfer is necessary for substrate activation (pK_a-shift).[9] (3) Alternatively, enzymes react expediently with substrates to form energetically more accessible covalent intermediates, which smoothly react further and collapse to desired products.[10]

1.1.2 Supramolecular Structures as Enzyme Mimetics: Structures and Properties

In parallel with the investigation of natural enzymes, attempts have been made to reproduce the hydrophobic enzyme pockets by utilizing supramolecular structures with the goal to advance the understanding of enzyme catalysis and to achieve useful catalytic applications.
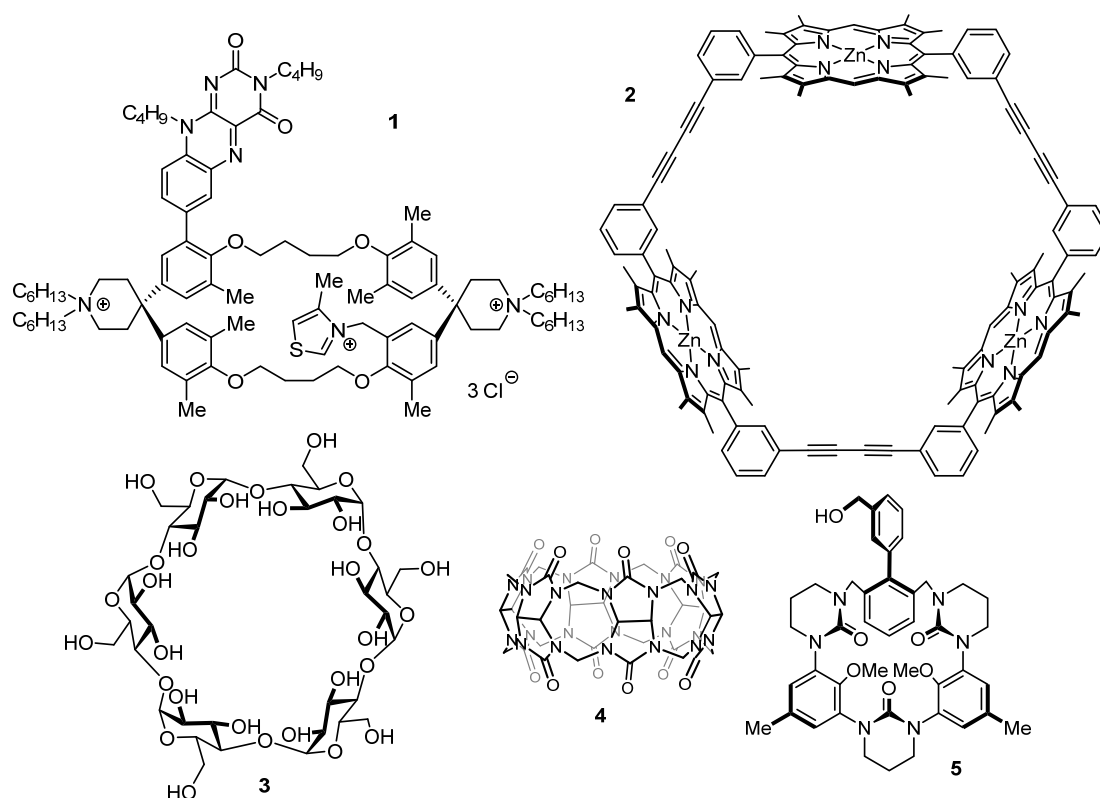

Figure 1.1: Examples of covalent supramolecular hosts employed as enzyme-mimicking catalysts: Diederich's cyclophane **1**, Sander's cyclic porphyrin trimer **2**, unfunctionalized α-cyclodextrin **3**, cucurbituril **4** and Cram's spherand **5**.

Resembling enzyme pockets, the interior of supramolecular hosts provides a specific

chemical environment different from the exterior medium. The limited space within them confers similar properties to the entrapped guest molecules as enzymatic cavities do to bound substrates: elevated effective concentration, limited freedom of motion, and restrained conformation in certain cases. Systems investigated in early times include cyclophanes,[11] cyclic porphyrin oligomers,[12] (functionalized) cyclodextrins,[13] cucurbiturils[14] and spherands[15] (Figure 1.1). After some initial success, these macrocyclic supramolecular structures, however, gradually lost their popularity due to a marked disadvantage: Their construction usually relies on connecting the sub-components *via* formation of multiple covalent bonds, which in turn results in time-consuming and step-intensive syntheses.

Instead of covalent bonds, non-covalent linkages serve as a more efficient strategy to access artificial enzyme mimics. In this approach, weak interactions, such as metal–ligand interaction,[16] hydrogen bonding[17] and hydrophobic interaction,[18] drive the spontaneous formation of assembly structures from subunits. These subunits are often equipped with carefully designed functional groups to dictate the formation of desired structures. Although based on reversible weak interactions, the accumulation of multiple interactions renders such self-assembled structures thermodynamic stability and persistency over timescale, which makes them suitable hosts for chemical reactions.

Among the supramolecular structures reported so far, based on covalent bond or non-covalent interaction, only a few of them were applied in catalysis. The major issue preventing their wider application is product inhibition.[19] This problem arises from the excessive binding of products when the reaction host fails to discriminate between products and new substrates. Strategies to circumvent this problem involve modification of substrates or *in situ* converting products to species with lower binding affinity. Discussions in this regard will be made when handling specific examples.

The most successful supramolecular assembly in the sense as enzyme-mimicking catalysts is the metal–ligand $[Ga_4L_6]^{12-}$-cluster **Ia**, developed by the Raymond research group (Figure 1.2).[20] The $[Ga_4L_6]^{12-}$-cluster **Ia** possesses a tetrahedral

symmetry with six naphthalene-based catechol ligands bridging four Gallium(III) ions that occupy the vertical of the tetrahedron. The overall negative charge (12⁻) renders the cluster good water solubility, while six ligands surround a hydrophobic cavity of approximately $450 \, \text{Å}^3$. Cluster **Ia** exhibits fruitful host-guest chemistry. It accommodates monocationic guests including tetramethylammonium salts,[21] organometallic compounds,[21-22] and reactive phosphonium species,[23] which experience cation–π interactions inside the cavity of **Ia**. Attributed to the hydrophobic effect, complexation of neutral guests by **Ia** is also observed.[24] Cluster **Ia** selectively encapsulates guests with remarkable discrimination. Exposed to a mixture of tetramethyl-, tetraethyl- and tetrapropylammonium salts, cluster **Ia** preferentially incorporates the middle-sized ammonium species.[20] The guest uptake and release occur through a nondissociative mechanism. The host deforms to create a passage along its C_3-axis, whereby the guest undergoes conformational changes to enter or depart from the host's cavity.[21] The encapsulated guests exchange with those in the bulk solution. The exchanging dynamic is influenced by the binding strength of the incorporated guest and the guests associating from the exterior.[25] Kinetic trapping is only observed for sizable guests, such as decamethylcobaltoceinium.[21]
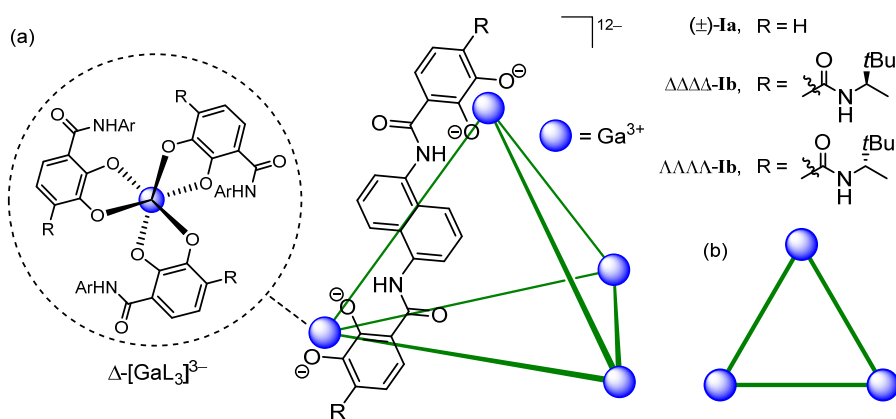
Figure 1.2: Metal–ligand $[Ga_4L_6]^{12-}$-cluster **Ia** and **Ib**: schematic structure (a) and simplified symbolic representation (b).

Upon encapsulation, the methylene groups of tetraethylammonium experience diastererotopic splitting, which provides the first indication for the chiral environment within the cluster **Ia**. The crystal structure of an iron-analogue of cluster **Ia** unambiguously reveals that the cluster is a racemic mixture of both homochiral

ΔΔΔΔ- and ΛΛΛΛ-enantiomers.[20] The chirality results from the strong mechanical coupling between each tris-bidentate Gallium(III) ion within the same cluster. The enantiomeric mixture of cluster **Ia** can be resolved with the aid of an externally associating chiral cation.[26] Sequential treatment of the resolved enantiopure **Ia** with ion-exchange chromatography allows **Ia** to be obtained as its $K_{12}[Ga_4L_6]$-salt. Nevertheless, the obtained ammonium-free cluster **Ia** requires basic reaction conditions or 1eq. NMe_4^+ as a stabilizing agent to maintain its enantiopurity and integrity. Another approach to access the ΔΔΔΔ- or ΛΛΛΛ- cluster involves the introduction of a chiral amide-auxiliary on the catechol moiety.[27] The enantiopure chiral amide functionality dictates the helical configuration of the vertical Gallium(III) ions and enables the diastereoselective formation of ΔΔΔΔ-**Ib** or ΛΛΛΛ-**Ib**. The synthesis of **Ib** necessitates no cationic species as templating agents and the resulting K_{12}**Ib**-complex shows improved stability at elevated temperatures, aerobic and low pH conditions compared to K_{12}**Ia**. In addition, **Ib** displays higher catalytic efficiency as its ammonium-free cavity is more readily available for potential substrates.

The Nitschke research group reported related metal–ligand host structures of tetrahedral symmetry[28] (Figure 1.3). Cluster **IIa** self-assembles from four iron(II) ions and six biphenyl ligands which are formed *in situ via* imine-bond formation from 4,4'-diaminobiphenyl-2,2'-disulfonic acid and 2-formylpyrindine subcomponents under basic conditions. The $[Fe_4L_6]^{4-}$-host **IIa** dissolves well in water owing to its anionic nature, whereas its biphenyl-ligands enclose a hydrophobic cavity of 141 $Å^3$. Driven by the hydrophobic effect, appropriately sized hydrocarbons are accommodated within **IIa**.[29] The incorporation of smaller guests is kinetically more favorable, as more extensive deformation of the host is needed to create the portal for sizable guests. In contrast to Raymond's $[Ga_4L_6]^{12-}$-cluster, the encapsulation of cationic guests is completely resisted by **IIa**, which is rationalized by the following two aspects: (1) a lower overall charge of **IIa** for the Coulomb interactions; (2) while the positive charges of the apical Gallium(III) ions in Raymond's systems are masked by the surrounding catecholates, the uncompensated positive charge of the iron(II)

ions in **IIa** prevents the ammonium cations from binding. Instead of encapsulation, the ammonium species rather associate with the peripheral sulfonates, as was shown with the guanidinium cation. Generally, the release of guests from **IIa** is achieved by addition of a competing guest of higher hydrophobicity, such as benzene. More tightly bound guests like cyclohexane are liberated by deconstructing the host *via* imine exchange or pH switching. It is noteworthy that the host can be regenerated by reestablishing the original pH of the aqueous solution.
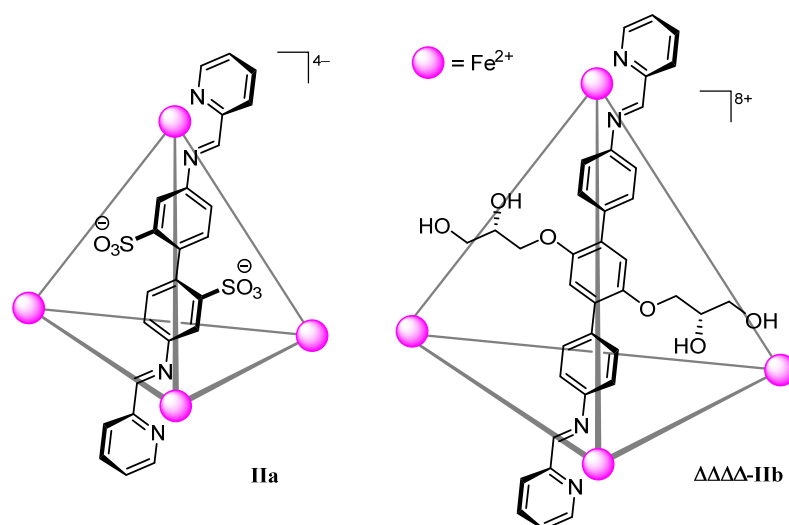

Figure 1.3: Schematic representation of metal–ligand $[Fe_4L_6]^{n\pm}$-cluster **IIa** and **IIb**.

To expand the guest scope, the Nitschke group developed a larger cluster $[Fe_4L_6]^{8+}$ (**IIb**) by employing a neutral terphenyl ligand bearing chiral glyceryl functionalities (Figure 1.3).[30] Besides imparting water solubility to **IIb**, the glyceryl groups help the host to enclose a void with a calculated volume of 418 $Å^3$. Owing to its larger cavity and higher flexibility, **IIb** manifests a wider guest spectrum: A variety of hydrophobic guests of different sizes, even those containing polar functional groups, are encapsulated. Furthermore, the chiral centers of the glyceryl groups serve as remote directing groups to dictate the helical configuration of the apical iron(II) ions, which finally determine the stereochemistry of the formed cluster. For instance, the optically pure $\Delta\Delta\Delta\Delta$-**IIb** is obtained with (*S,S*)-terphenyl ligands. *Via* proton NMR spectroscopy, enantiopure **IIb** is found able to discriminate between two enantiomers of a chiral molecule. However, the preferential binding of one enantiomer is not

observed.

In metal–ligand–based supramolecular structures, the metal-template effect serves as a crucial factor to determine the structure of the formed complexes. As hydrogen bonding lacks sufficient rigidity and directionality, the shape and geometry of hydrogen-bonded supramolecular structures often rely on their well-shaped subcomponents. The Rebek research group designed a *C*-shaped molecule **6** of self-complementing functional groups which enable hydrogen bonding.[31] In organic solvents like chloroform, benzene or *p*-xylene, molecule **6** dimerizes to build up the pseudospherical cage **III** with an internal volume between 240 and 320 Å^3 (Figure 1.4).[17a] The cage-like structure of **III** is stabilized by up to 16 intermolecular hydrogen bonds and its cavity is occupied by two solvent molecules. Cage **III** is capable of encapsulating guests of suitable size such as admantane and ferrocene, as well as their derivatives, which display slow exchanges with their free counterparts. The inclusion of guest molecules is entropically favored by releasing the solvent shells of free guests and replacing the pre-encapsulated two solvent molecules by one larger guest. From enthalpic aspects, functionalized guests capable of hydrogen-bonding to the host are more favorable due to electrostatic attraction; van der Waals interactions between the host and streamlined guests also contribute to the binding processes. Replacement of the resident guest by a better one is measured as a slow process, since a multitude of hydrogen bonds have to be ruptured until a suitable aperture for the guest substitution has been created.[32]
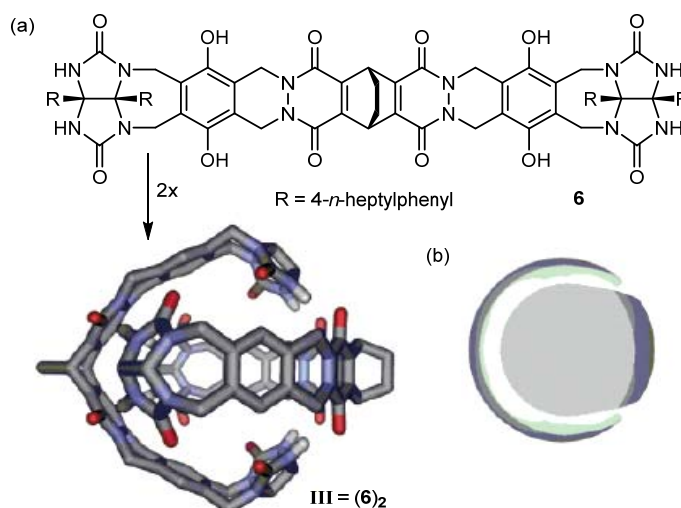
Figure 1.4: Self-assembly of cage **III** from two molecules of **6** (a) and its schematic representation (b). The figure is partly reproduced from reference[32] with the permission of Royal Society of Chemistry.

Another intensively studied system is the calixarene-based capsule **IVa** introduced by the Atwood research group.[33] In water saturated apolar organic solvents such as chloroform and benzene, capsule **IVa** self-assembles from six molecules of resorcinarene **7a** and eight water molecules to form an octahedral hydrophobic cavity enclosing an internal volume of $1375 \, \text{Å}^3$ (Figure 1.5). Capsule **IVa** owns its thermodynamic stability in both solid[33] and liquid phase[34] from sixty intra- and intermolecular hydrogen bonds. As a consequence, conditions or substances detrimental to hydrogen-bonding interactions, for instance heat, competitive solvents[35] or excess salts[36], denature the assembly of **IVa**. Exceptions are observed for alcohol species, which are demonstrated to play several roles when interacting with **IVa**.[37] Similar to other supramolecular structures, capsule **IVa** accommodates a wide range of guest molecules, including cationic species[38] (cation–π interaction) and neutral compounds of certain polarity[39] or those capable of hydrogen bonding.[32] In contrast to the metal–ligand clusters reported by Raymond and Nitschke, encapsulation occurs through a dissociative mechanism, whereby a resorcinarene unit must be completely removed by interrupting several hydrogen bonds to generate a pentameric intermediate of **7a** suitable for guest uptake.[36] Solvent molecules residing inside the cavity are replaced by the incoming guest. The encapsulation process is

therefore favored due to the entropy gain. The formed host-guest complexes are stable due to the mechanical barrier posed by the capsule's wall. Surprisingly, the stability of such complexes decreases with larger guests. The lowered stability is believed to stem from the lower entropy gain as larger guests experience more constraint inside the confinement of **IVa**.
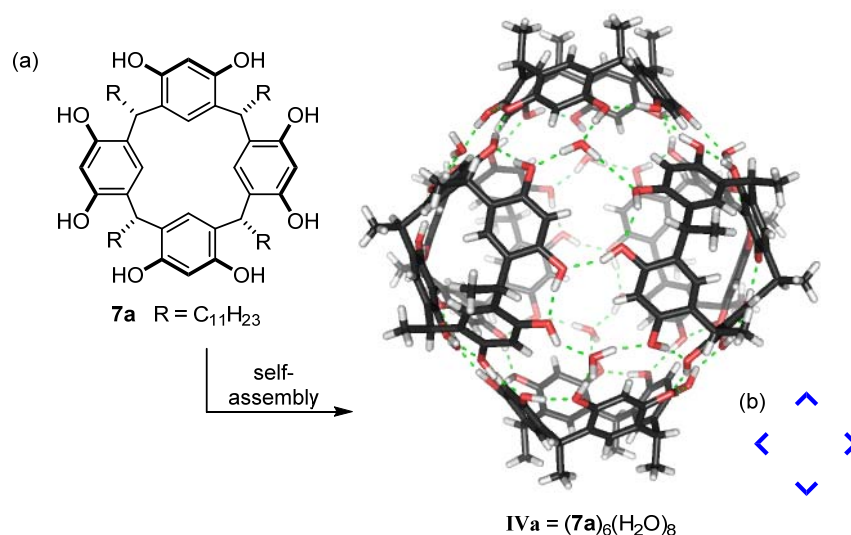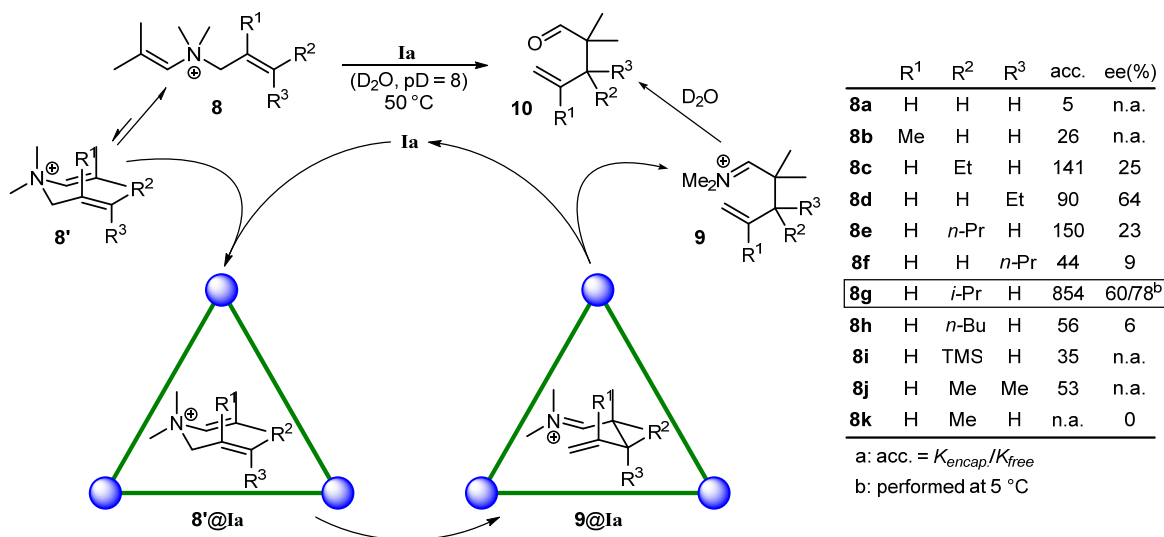

Figure 1.5: Self-assembly of cage **IVa** from six molecules of resorcinarene **7a** (a) and its schematic representation (b).

1.1.3 Catalysis in Supramolecular Capsules

Given that cluster **Ia** is prone to bind positively charged guests, the groups of Raymond and Bergman first explored the cationic aza-Cope rearrangement with **Ia** as a stoichiometric host (Scheme 1.1).[40] Allyl enammoniums **8,** readily accommodated by cluster **Ia**, undergo a [3, 3]-sigmatropic rearrangement to form iminiums **9**. Once iminiums **9** dissociate from the host **Ia**, they are hydrolyzed to γ,δ-unsaturated aldehydes **10**. The reaction was also realized with catalytic amounts of **Ia**. The source of the catalysis arises from the dominant affinity of **Ia** to charged substrates over neutral products, enabling the formation of productive complexes after each catalytic cycle. Competitive inhibition was observed with the strongly binding guest NEt_4^+. Compared to free substrates, the encapsulated enammonium cations all experience accelerated reactions. The amplification of reactivity is believed to result from some
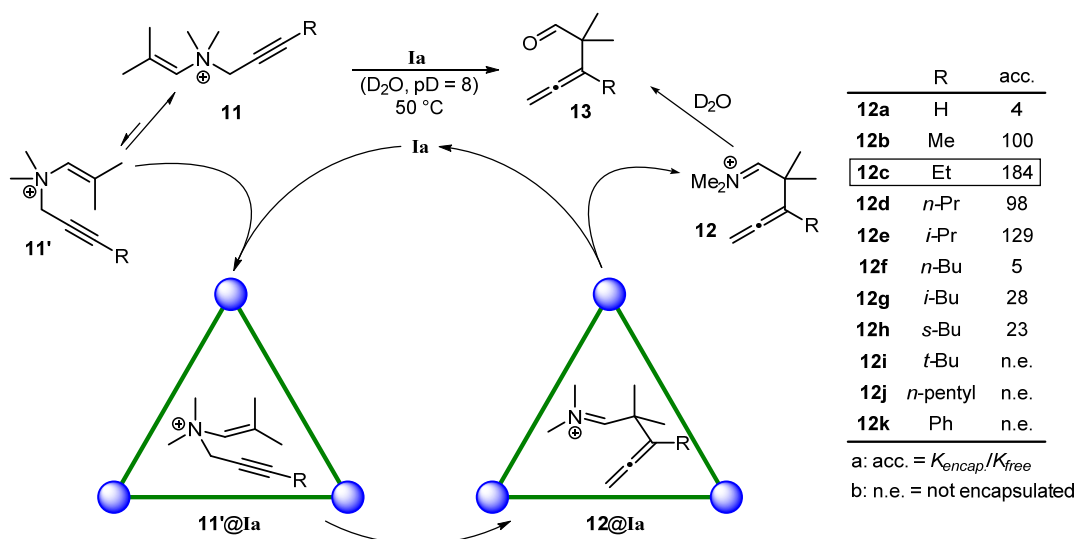
delicate interactions between the substrate and the reaction host, which is sensitive to the size, shape and substitution pattern of the substrate.[41] Substrate **8g** seems to fit the host **Ia** the best and enjoys the highest reaction acceleration inside the cavity (factor 854). Any structural modification on substrate **8g** leads to a less pronounced increase in the reaction rate. Even the *cis*- and *trans*-isomers (**8c** and **8d**, **8e** and **8f**) display totally different reactivities. It is proposed that **Ia** only incorporates the more compact chair-like conformer that resembles the transition state, as indicated by NOESY-NMR spectroscopy. The preorganization of substrates is also confirmed by the positive entropy of activation. The enthalpic barrier decreases slightly as the bound substrate is constrained inside the cavity (ground-state destabilization). The authors were also able to perform the reaction in an enantioselective fashion with the resolved ΔΔΔΔ-**Ia**.[42] Up to 64% ee was achieved, which was further improved to 78% at a lower temperature (5 °C). Computational modeling suggests that the enantioselectivity is induced by the interaction between the bound substrate and the chiral metal center of **Ia**.

	R^1	R^2	R^3	acc.	ee(%)
8a	H	H	H	5	n.a.
8b	Me	H	H	26	n.a.
8c	H	Et	H	141	25
8d	H	H	Et	90	64
8e	H	*n*-Pr	H	150	23
8f	H	H	*n*-Pr	44	9
8g	H	*i*-Pr	H	854	60/78[b]
8h	H	*n*-Bu	H	56	6
8i	H	TMS	H	35	n.a.
8j	H	Me	Me	53	n.a.
8k	H	Me	H	n.a.	0

a: acc. = K_{encap}/K_{free}
b: performed at 5 °C

Scheme 1.1: Aza-Cope rearrangement of allyl enammonium cations catalyzed by **Ia**.

Next, the Raymond and Bergman groups expanded the scope of the **Ia**-catalyzed rearrangement reaction to the less reactive propargylic substrates **12** (Scheme 1.2),[43] which normally require elevated temperatures to react. Addition of suitably sized substrates to **Ia** led to the formation of host-guest complexes and subsequent

conversion, while encapsulation of more bulky substrates was completely rejected. The reaction rates were determined for encapsulated (with stoichiometric amounts of **Ia**) and free substrates. Reactions inside **Ia** displayed generally faster conversion. The acceleration factor correlates with the size and shape of the substrate. The medium-sized substrate **12c** bearing an Et-substituent seemingly fits best the host's interior and enjoyed the highest rate increase. As for allyl enammonium substrates, the acceleration of reactions is the result of a lowered entropic barrier by means of encapsulating the preorganized substrates. Kinetic studies with substrate **12b** reveal that the reaction is 0th-order in substrate concentration under saturation conditions, which indicates that the encapsulated substrate is the resting state and the rearrangement is the rate-determining step.

	R	acc.
12a	H	4
12b	Me	100
12c	Et	184
12d	*n*-Pr	98
12e	*i*-Pr	129
12f	*n*-Bu	5
12g	*i*-Bu	28
12h	*s*-Bu	23
12i	*t*-Bu	n.e.
12j	*n*-pentyl	n.e.
12k	Ph	n.e.

a: acc. = K_{encap}/K_{free}
b: n.e. = not encapsulated

**Scheme 1.2**: Aza-Cope rearrangement of propapyl enammonium cations catalyzed by **Ia**.

Encouraged by the successful aza-Cope rearrangement reactions catalyzed by **Ia**, the groups of Raymond and Bergman sought for other reactions involving cationic transition states. In this context, they reported the **Ia**-catalyzed hydrolysis of orthoformates **14** in basic solution (Scheme 1.3).[44] Since orthoformates are exceptionally stable under neutral and basic conditions, the unprecedented reactivity probably stems from the propensity of **Ia** for positively charged species, facilitating the formation of charged intermediates **15** inside the cavity via protonation. In the following steps, the protonated substrate extrudes two equivalents of alcohol to

produce intermediate **16**, which equilibrates with the bulk solution and is hydrolyzed to formate **18** in the basic medium. Formate **18** is repelled by the electron rich aromatic host because of its anionic nature, which thereby enables the catalytic turnover. Kinetic studies[45] showed that the reaction is 1st-order in the concentration of protons and **Ia**, and 0th-order in the concentration of substrates under saturation conditions. Experiments with ^{13}C-labelled substrates indicate that the encapsulated neutral substrate is the resting state of the catalysis. Along with the negative entropy of activation and a normal solvent isotope effect of $k(H_2O)/k(D_2O) = 1.6$, the A-S$_E$2 hydrolysis mechanism is deduced for the **Ia**-mediated catalysis with the protonation of the bound substrate as the rate-limiting step. This mechanism differs from the known A-1 mechanism for orthoformate hydrolysis in bulk solution. The substrate scope clearly demonstrates size selectivity and highlights the essential role of cluster **Ia**. All substrates smaller than tri-*n*-pentyl orthoformate (**14g**) were readily hydrolyzed, while substrates, too large to fit the cavity of **Ia**, remained intact under the reaction conditions. Upon encapsulation, the reactivity of bound substrates was greatly enhanced. The tri-*n*-propyl orthoformate (**14c**) displayed one of the largest rate accelerations (factor 3900) detected in supramolecular catalysis at that time. The presented example parallels enzyme catalysis in several aspects: The hydrophobic effect drives the encapsulation of substrates, and the encapsulated substrates exist in fast equilibrium with their free counterparts in the bulk solution. The reaction was accelerated within the host and the effect vanished when the host was blocked by a strongly binding inhibitor.
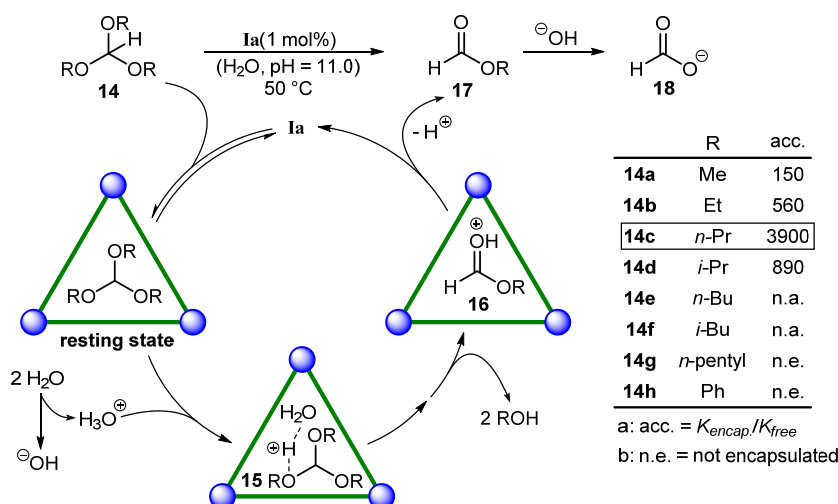
Scheme 1.3: Hydrolysis of orthoformates catalyzed by **Ia** and the proposed mechanism.

As an extension of the previous investigation, the groups of Raymond and Bergman also studied the acetal hydrolysis catalyzed by **Ia** (Scheme 1.4).[46] A wide variety of open-chained and cyclic acetals was cleaved with excellent yields under similar conditions as used in the former studies. The internal volume of **Ia** has a major influence on the substrate scope: The ones of suitable dimensions readily reacted. Acetal **19f** and **19m**, however, were not hydrolyzed though they have similar molecular weights as **19j.** The lack of reactivity is likely ascribed to their hindered accommodation by the host because of the tedious side chains.
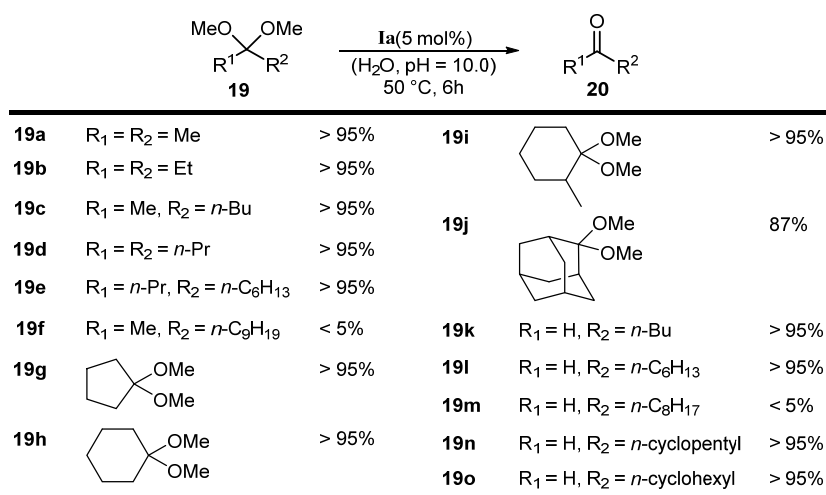

NMR-yields based on an internal standard (DMSO) are reported.

**Scheme 1.4**: Substrate scope of the hydrolysis of acetals catalyzed by cluser **Ia**.

Kinetic and mechanistic studies[47] performed with acetal **19a** illustrate some

resemblances to the hydrolysis of orthoformates. The hydrophobic effect drives the formation of the host-guest complex as the resting state of the catalysis. The encapsulation of the substrate was observed with the bulky 2,2-dimethoxyadamantane **19j**. Smaller substrates form rather kinetically unstable complexes and display fast exchange between the species inside and outside the host cavity, as reflected by the broadening of the substrates' signals in NMR spectroscopy. Under saturation conditions, the reaction rate shows 1st-order correlation with the concentration of protons and host **Ia** but independence on the substrate concentration. Reaction acceleration (factor 190 for **19a**, factor 980 for 1,1-diethoxyethane) was determined for encapsulated substrates. Contrasting to the hydrolysis of orthoformates, the inverse solvent isotope effect of $k(H_2O)/k(D_2O) = 0.62$ indicates that the A-2 mechanism is in operation with the attack of water rather than the protonation of encapsulated neutral substrates determining the overall rate of the catalysis (Scheme 1.5). The authors argued that the difference was based on the higher basicities of acetals compared to those of orthoformates. Two factors are the keys to realize the catalytic turnover. After completion of the reaction, the aldehyde products are converted to the corresponding hydrates under basic conditions, which are less favored by the hydrophobic cavity of **Ia** as compared to the less polar acetal substrates. Additionally, binding studies with **19j** and **20j** reveal that the acetal binds the host more strongly than the ketone, thus allowing the displacement of products by new substrates.
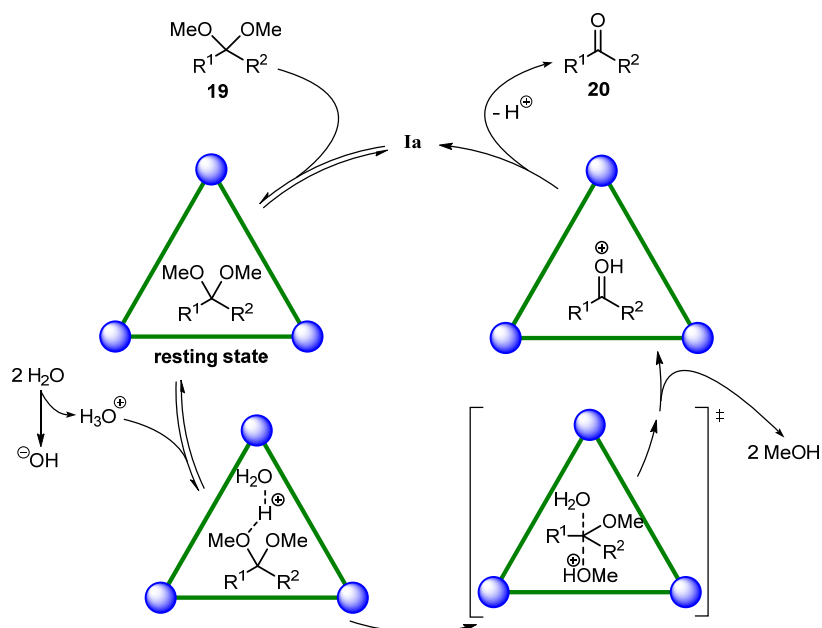
Scheme 1.5: Proposed mechanism for the hydrolysis of acetals within **Ia**.

The groups of Raymond and Bergman also explored the Nazarov cyclization catalyzed by **Ia** which involves the conrotatory electrocyclization of substrates **21** (Scheme 1.6).[48] Preliminary attempts showed complete conversion of **21** (as a mixture of three isomers) to the cyclopentadiene derivative **22** after 12 h under aqueous basic conditions, and the reaction was completely shut down when **Ia** was blocked with a strong binding inhibitor. To gain further insight into this reaction, rate studies were performed in a solvent mixture (D_2O/DMSO-d_6 = 1/1) to improve the solubility of products. Nevertheless, reaction rates decreased with progressing time, which was caused by the competitive binding of accumulated products to the reaction host. This problem was tackled by trapping the product **22** in a successive Diels–Alder reaction with maleimide **24**. The formed tricyclic product **23** binds the host only very weakly, and up to 160 turnovers were achieved with 7 mol% **Ia** as the catalyst.
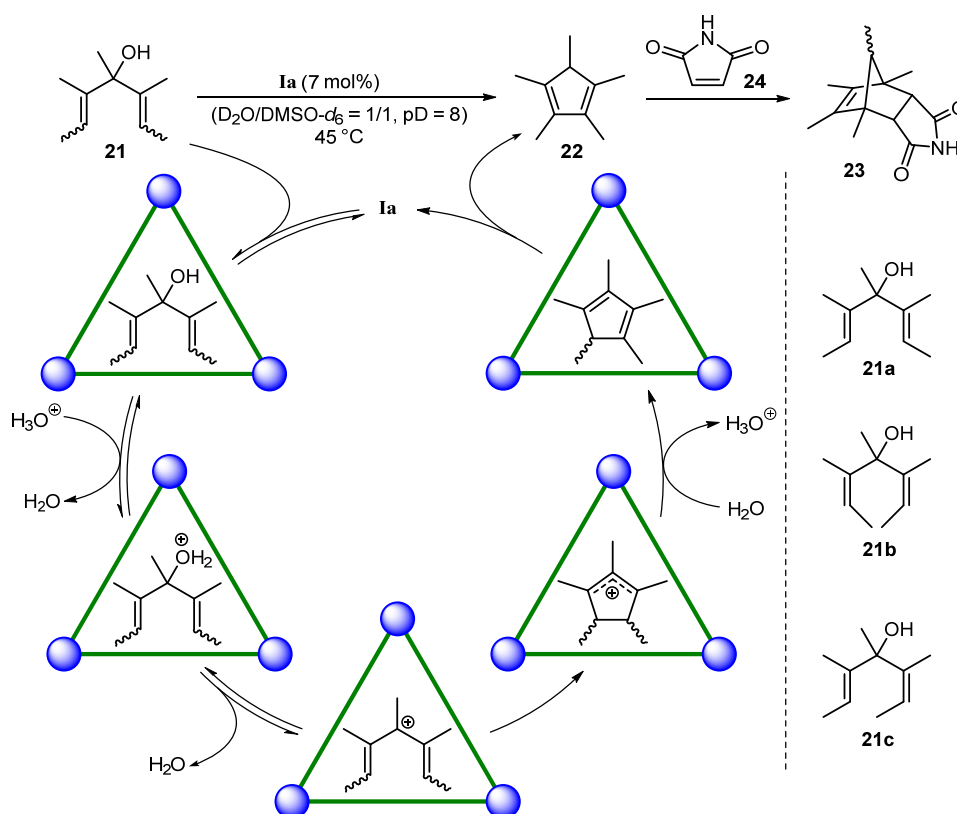
Scheme 1.6: Nazarov cyclization catalyzed by **Ia** and the proposed mechanism.

Compared to the background reactions, rate enhancements of six orders of magnitude (factor 2 100 000 for **21b**, factor 1 700 000 for **21c**) were measured for encapsulated substrates, which even rivals those achieved in enzymatic catalysis! The kinetics and mechanism were investigated in more detail to clarify the enormous acceleration effect.[49] The reaction rate was measured to be pseudo-first-order in the substrate concentration, 1st-order in the concentration of **Ia** and an apparent order of 0.5 in pD. Experiments with ^{13}C-labeled substrates imply that the encapsulated neutral substrate is the resting state of the catalysis. The negative entropy of activation is indicative of preorganization of substrates inside the cavity. In solution, the electrocyclization is considered as the rate-limiting step following the reversible protonation and water loss. On the contrary, the hydrophobic cavity poses a significant barrier for the water exchange and slows down this step. As a result, no single rate-limiting step was determined for the encapsulated Nazarov cyclization, which provided a possible explanation for the unusual 0.5th-order dependence on pD. According to DFT-calculations, the cationic intermediates are more stabilized inside the cavity than

in bulk solution. Taken together, three factors are believed to account for the unprecedented rate acceleration: (1) The preorganization of encapsulated substrates in the productive conformation lowers the entropic barrier for cyclization; (2) the preference of **Ia** for cationic species as guests facilitates the formation of charged intermediates within the cavity; (3) the formed intermediates are stabilized by **Ia** due to cation–π interactions.
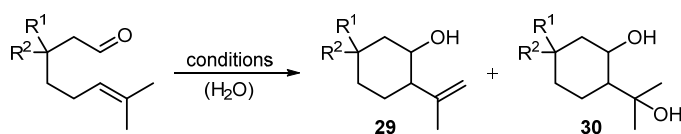
An interesting aspect of the **Ia**-catalyzed Nazarov cyclization is that dihydrofulvene **26**, isomeric to the normal product **22**, was formed in a selective fashion (**26/22** > 9/1) from the *E,E*- and *Z,Z*-isomers (**21a** and **21b**) when the reaction was performed in unbuffered D$_2$O, while the *E,Z*-isomer **21c** produces the same product **22** as under basic conditions (Scheme 1.7).[50] Why was dihydrofulvene **26** not detected before? It was confirmed in a later experiment that **26** is readily converted to the thermodynamically more stable **22** under basic conditions and trapped by maleimide **24**. The authors proposed that the selectivity was dictated by the stereochemistry of intermediate **25**, which derives from the configuration of substrate **21**. Control experiments conducted with alcohols **27** in acidic solution ruled out any intrinsic preference of carbocation **25** for the two deprotonation sites. Accordingly, cluster **Ia**, very likely, served as the biasing element. Encapsulation of the *trans*-configured **25a** somehow hinders the access to the proton, which after deprotonation leads to the cyclopentadiene product **22**. Alternatively, the more accessible terminal proton is abstracted to produce **26** as the kinetic product.
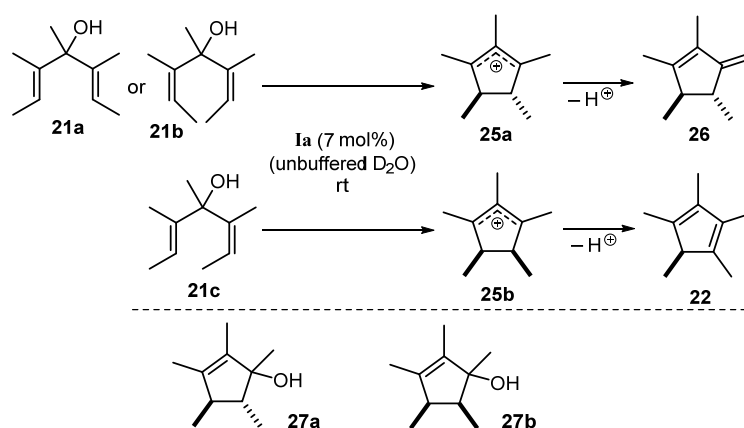
Scheme 1.7: **Ia**-mediated regioselective deprotonation of **25** in the Nazarov cyclization.

The aforementioned regioselective deprotonation mediated by **Ia** bears analogy to that observed with the geranyl cation in the biosynthesis.[51] This interesting resemblance to enzymatic systems encouraged the groups of Raymond, Bergman and Toste to investigate the **Ia**-catalyzed monoterpene-like Prins-cyclization of aldehyde **28** (Scheme 1.8).[52] The cyclization is triggered by protonation of the carbonyl functionality of substrate **28**, which is then attacked by the alkene moiety. In acidic aqueous solutions, the resulting cationic intermediate is captured by water to generate cyclic diols **30**, while the hydrophobic cavity of **Ia** prevents the entrance of water and allows the formation of alkene products **29** *via* elimination. Moreover, encapsulation thoroughly alters the steric outcome of the cyclization with the *trans*-configured alkene **29** prevailing (*trans/cis* = 65/35), which contrasts the slight preference for *cis*-products **30** in bulk solution (*trans/cis* = 40/60).

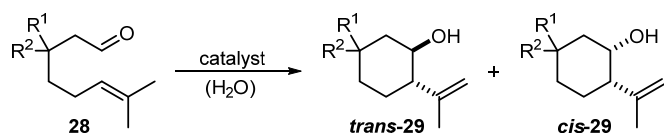**Scheme 1.8**: Chemoselectivity and stereoselectivity of the **Ia**-catalyzed Prins-cyclization of **28**.

A similar *trans*-selectivity inside cluster **Ia** was observed for derivatives **28b** and **28c**. The structural difference in the C3-position, however, led to contradicting cyclization behaviors in bulk solution: The product distribution of substrate **28b** containing *gem*-dimethyl groups was akin to that of aldehyde **28a**; the one without substituents at

C3 (**28c**) produced a promiscuous mixture. A lack of conformational control is supposedly responsible for the unselective reaction of **28c** in acidic solution. This in turn attests that cluster **Ia** constrains the encapsulated substrates and prompts them to adopt the reactive conformation for cyclization. In a follow-up study, the dependence of stereoselectivity on the host-guest interaction is probed in detail with various substrates and reaction hosts.[27, 53] The larger clusters **Ia(ext)** and **Ib(ext)** are formed with the pyrene-containing ligands **31**. The more spacious hosts demonstrate faster conversions of substrates and improved selectivity to *trans*-products. The higher catalytic efficiency could be explained by the more facile substrate uptake by the extended clusters. The higher stability of **Ib** and **Ib**(ext) under acidic conditions allows the reaction to proceed at low pD, thus facilitating the protonation of substrates. Catalytic turnover of up to 840 was achieved over two weeks with 0.045% ΔΔΔΔ-**Ib**. DFT-calculations suggest that the transition states of the *trans*-products are less destabilized in cluster **Ia**(ext) and **Ib**(ext), which is in line with the decreased steric constraint of the confined species in a larger space. On the other hand, a reasonable steric interaction between the reaction hosts and substrates seems to help the hosts to discriminate between the enantiomeric transition states. Evidence in this regard was provided by the attempt to induce enantiomeric excess with ΔΔΔΔ-**Ib** and ΔΔΔΔ-**Ib**(ext). With the achiral substrate **28c**, an enantiomeric excess of 61% was obtained within the smaller ΔΔΔΔ-**Ib**, while only 33% ee were realized with the larger ΔΔΔΔ-**Ib**(ext).

It was found that the aldehyde substrate equilibrates with its hydrate in bulk solution. And the host only binds the less polar aldehyde species due to the hydrophobic effect. Upon activation *via* protonation, cyclization occurs either stepwise (k_1, k_2) or in a concerted fashion (k_3). Finally, the product is released to close the catalytic cycle (Scheme 1.9). The displacement of products from the reaction host is facile, as the products enjoy better solvation in the aqueous bulk solution than they do in the hydrophobic cavity. Kinetic studies reveal rate accelerations of a factor of 10^4–10^5 for the host-catalyzed reactions compared to the background reactions.
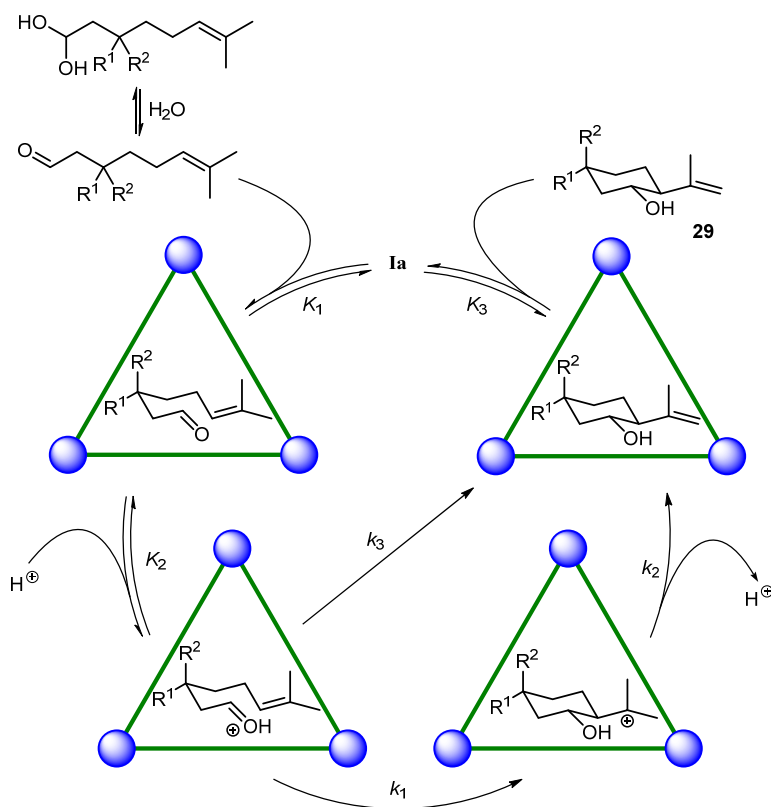
Scheme 1.9: Proposed mechanism[53] of the **Ia**-catalyzed Prins-cyclization of **28**.

Conformational control *via* encapsulation not only has an impact on the stereochemistry of a reaction but also can alter its course and outcome. The latter case is exemplified by the study on the **Ia**-catalyzed aza-Prins cyclization reported by the groups of Raymond, Bergman and Toste (Scheme 1.10).[54] The transformation features the formation of an unusual product *via* a through-space hydride-shift enabled by encapsulation. In solution, the iminium intermediate **34y**, formed *in situ* from amine **32** and formaldehyde, prefers the chair-like transition state affording the intermediate **35y** with the bulky isopropyl group placed in the equatorial position. A water molecule attacks the carbeniumion **35y** in a successive step to produce tertiary amine **36** as the product in bulk solution. However, the encapsulated iminium **34x** has to orientate the olefin moiety into the energetically less favored axial position to adapt to the restriction of **Ia**'s interior. The hydrophobic cavity prevents access of water to the carbocation formed. The close proximity of the isopropyl cation to the N-Me group paves the way for the unusual transannular 1,5-hydride transfer, which is proven by the complete deuterium incorporation using derivative **32a-*d₃***. The relative

configuration of piperidine product **33** also provides evidence for the arrangements of substituents in the transition state. Competition reactions were performed with **32a**, **32a-d_1** and **32a-d_3** to determine the kinetic isotope effect involved in the hydride-shift step. Factors of 1.1 and 2.1 were measured for the intermolecular and intramolecular kinetic isotope effect, respectively. The absence of an intermolecular isotope effect indicates that the rate determining step occurs before the 1,5-hydride transfer.

Ia-catalyzed cyclization of **32** to **33**

	R^1	R^2	conversion
32a	Me	Me	100%
32a-d_1	Me	CDH$_2$	n.d.
32a-d_3	Me	CD$_3$	n.d.
32b	H	Me	100%
32c	Me	Et	53%
32d	Me	n-Pr	43%
32e	Me	n-Bu	9%
32f	Me	i-Pr	0%^{a}
32g	H	Cy	0%^{a}
32h	Me	i-Pr	25%
32i	Me	Bn	51%^{a}
32j	Me	(MeO-substituted benzyl)	0%

a: performed at 60 °C
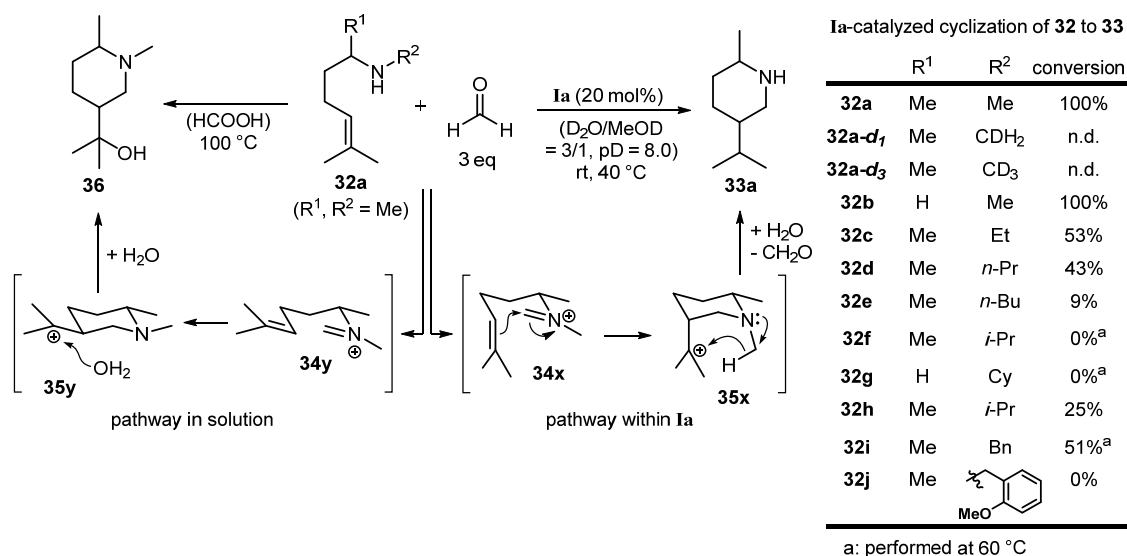
Scheme 1.10: **Ia**-catalyzed aza-Prins-cyclization of **32**.

For the **Ia**-catalyzed cyclizations, the reactivity diminished for substrates with larger groups on the nitrogen atom (Scheme 1.10). This observation is consistent with the higher energy barrier for incorporating more bulky substrates. Substrate **32f** and **32g** completely resist cyclization even at elevated temperatures, which is likely a consequence of the hindered iminium formation. Interestingly, no 1,5-hydride shift was observed for substrate **32k** (Scheme 1.11). Instead, the carbocation is quenched by proton elimination. The authors explained the different reactivity with the lowered hydricity α to the nitrogen atom due to the electron withdrawing CF$_3$-group. The derivative **32k** was employed for kinetic studies since its fluorine substituent enables the convenient quantification *via* ^{19}F-NMR. An unusual saturation behaviour was observed for the reaction host **Ia**. It is assumed that encapsulation of the iminium species determines the rate of the catalysis at low **Ia**-concentrations, whereas the rate limiting step changes to the iminium formation at higher **Ia**-concentrations. An
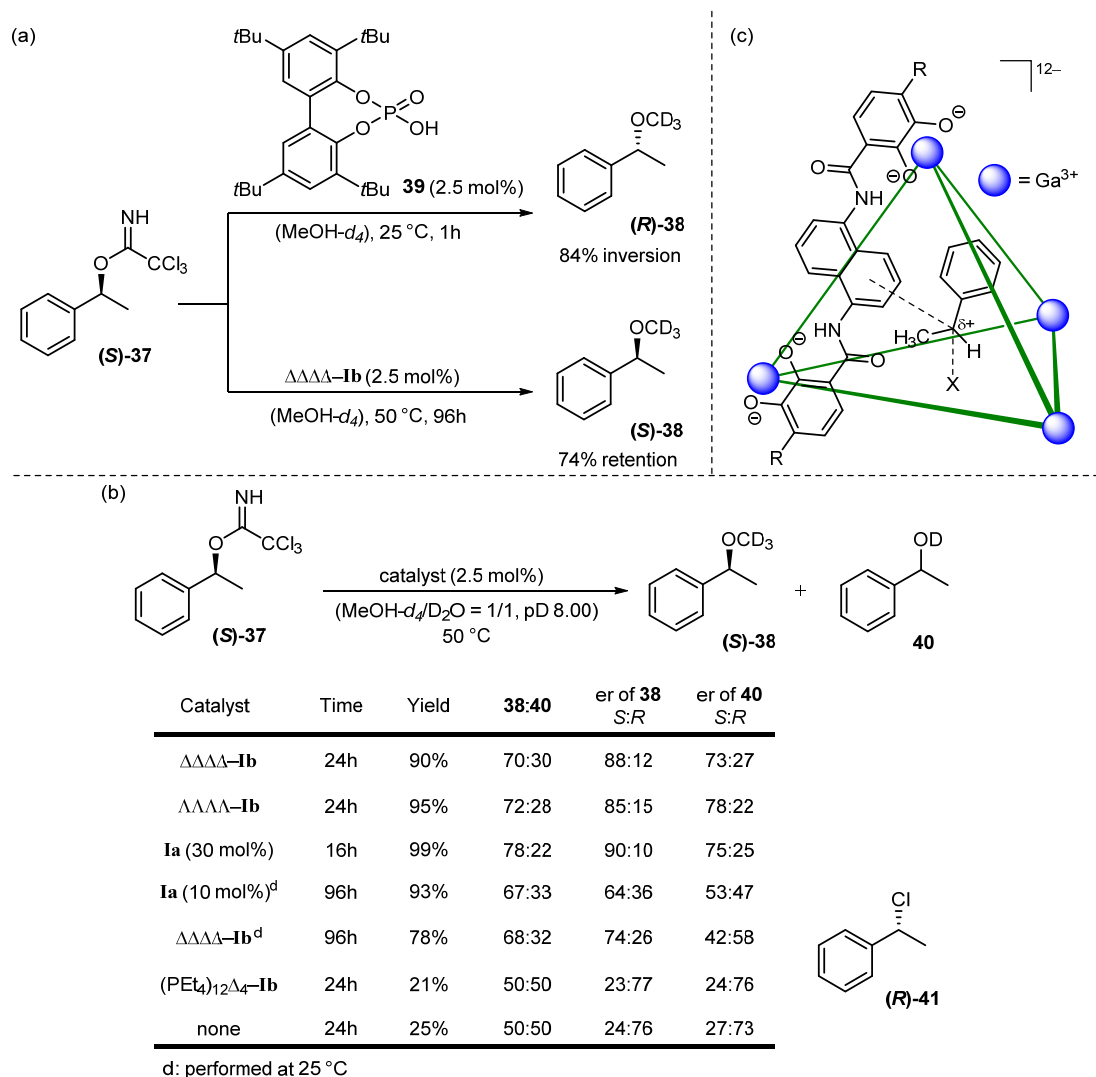
explanation for the facile catalytic turnover in this case is the preference of the reaction host for the charged iminium substrates over the neutral products.
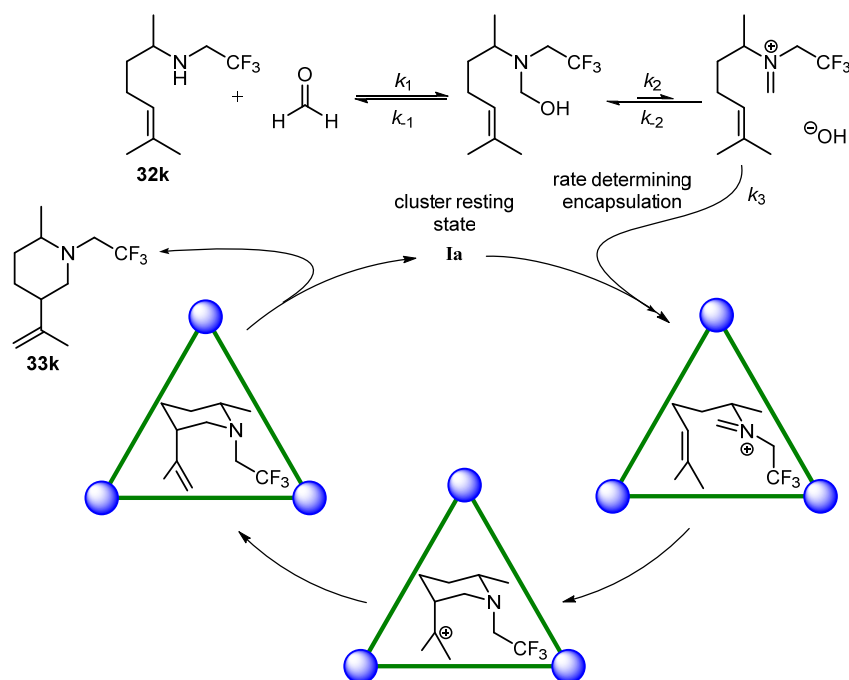
Scheme 1.11: Proposed mechanism for the **Ia**-catalyzed aza-Prins-cyclization.

The groups of Raymond, Bergman and Toste also reported the **I**-mediated nucleophilic substitution reaction with retention of stereochemistry (Scheme 1.12).[55] Under the catalytic action of ΔΔΔΔ-**Ib** (2.5 mol%), the racemic trichloroacetimidate -containing substrate **(±)-37** was readily solvolyzed by deuterated methanol to yield the ether product **38** with an enantiomeric excess of 15%. To improve the enantioselectivity, substrates and reaction hosts of different absolute configurations were probed. The enantiomeric excess of the ether product increased drastically to 74% when the reaction was conducted with the enantiopure **(S)-37**. Interestingly, the major enantiomer of the product obtained from **(S)-37** displayed the same absolute configuration as the substrate, which stood in contrast to the stereoinversion of the product formed with the achiral phosphoric acid **39** as the catalyst in solution. The stereoselectivity of the substitution reaction is maintained when switching the reaction host to the ΛΛΛΛ-enantiomer of **Ib** or racemic **Ia**. The *R*-enantiomer of **38** only became dominant when **(R)-37** was utilized as the substrate. These results

demonstrate that the determining factor of the steric outcome of this substitution reaction is rather the absolute configuration of the substrate than the chirality or enantiopurity of the reaction host. To eliminate the possibility of any acid-catalyzed background reactions , basic conditions were utilized (aqueous buffer as cosolvent). As a consequence, water serves as an alternative nucleophile and alcohol **40** was formed as a side product.


Catalyst	Time	Yield	**38:40**	er of **38** S:R	er of **40** S:R
ΔΔΔΔ–**Ib**	24h	90%	70:30	88:12	73:27
ΛΛΛΛ–**Ib**	24h	95%	72:28	85:15	78:22
Ia (30 mol%)	16h	99%	78:22	90:10	75:25
Ia (10 mol%)[d]	96h	93%	67:33	64:36	53:47
ΔΔΔΔ–**Ib**[d]	96h	78%	68:32	74:26	42:58
(PEt$_4$)$_{12}$Δ$_4$–**Ib**	24h	21%	50:50	23:77	24:76
none	24h	25%	50:50	24:76	27:73

d: performed at 25 °C

Scheme 1.12: **Ia**-catalyzed stereoretentive nucleophilic substitution (a and b) and proposed intermediate (c).

Control experiments performed with blocked host or in the absence of the reaction host yielded products with reversed stereogenic centers, confirming that the stereoretentive substitution reaction indeed proceeds inside the cavity of **I**. Furthermore, the inactivity of benzylic trichloroacetamide under reaction conditions

excludes the possibility of a doubled inversion via a preliminary 1,3-rearrangement. Intriguingly, the chloro-analogues (±)-41 and (R)-41 exhibited comparable reactivity and stereoselectivity as 37, which indicated that a common intermediate is involved in these reactions. Based on these observations, the authors proposed the following explanation for the stereoselectivity: Protonation and cleavage of the trichloroacetimidate functional group is promoted *via* encapsulation. The resulting carbocation enjoys cation–π stabilization by staying in close contact with the naphthalene walls of cluster **I**, leaving only one face of the cationic intermediate available for the nucleophilic capture. The restrictions of the interior of **I** likely retard the planarization of the carbocation and dictate the attack of the nucleophile from the same side as the leaving group departs, which results in the overall retention of the absolute configuration.

Being aware of the cationic nature of gold(I)-complexes, the groups of Raymond, Bergman and Toste investigated the encapsulation behaviour of gold (I)–phosphine complexes in cluster **Ia** (Scheme 1.13).[56] Formation of host-guest complexes was demonstrated with a series of R_3PAuX complexes **42**. It was found that the gold(I) complexes bound inside the host **Ia** in their dissociated forms, since the same encapsulated species were observed in ^{1}H-NMR regardless of the type of counter ions. R_3PAuX complexes **42** are known to catalyze the hydroalkoxylation reaction of allene compounds **43**. The complex Me_3PAuBr (**42b**), displaying the lowest catalytic efficiency in bulk solution, was investigated in combination with cluster **Ia** to test if encapsulation could enhance its reactivity. Indeed, the yield of substrate **43** was greatly improved (from 11% to 48% after 18 h) with encapsulated **42b.** The isomerized diene **45** was formed as a side product. Control experiments performed with blocked **Ia** and in the absence of **42b** confirmed that the accelerated reaction was indeed attributed to the encapsulated gold catalyst. By comparing the initial rate of the encapsulated and free reaction, 8-fold acceleration was determined for the reaction inside **Ia**. Three factors are responsible for the observed rate enhancement: (1) Ionization of gold(I) complexes facilitated by encapsulation increases the
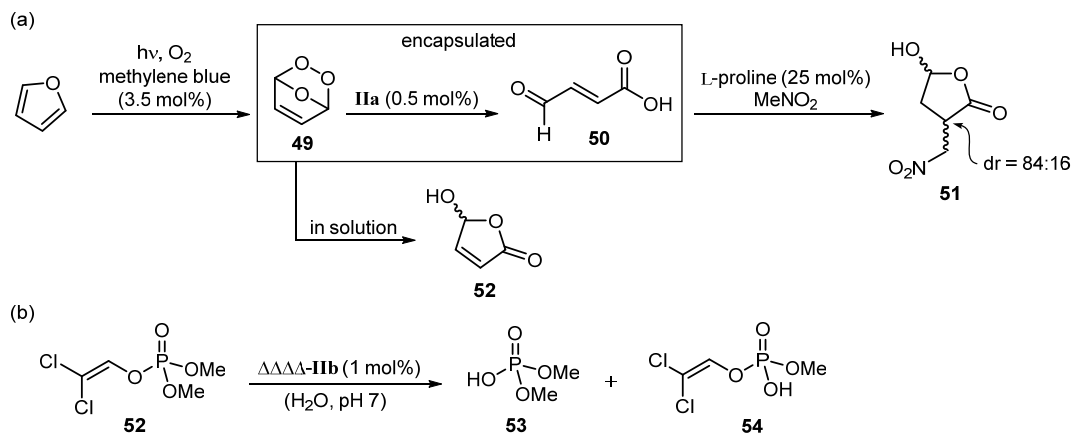
electrophilicity and the reactivity of the gold catalyst; (2) encapsulation improves the stability of gold (I) species in aqueous solutions; (3) the confinement of **Ia** promotes the formation of the reactive intermediate due to the enormously enlarged effective molarity. An interesting aspect is that product inhibition could have prevented the catalytic turnover since the less polar ether products **44** could compete with allene alcohol substrates **43** for the hydrophobic cavity of **Ia**. It is reasonable to infer that the reactivity of **43** towards gold catalysts **42** serves as an additional driving force for the displacement of products by new substrates.
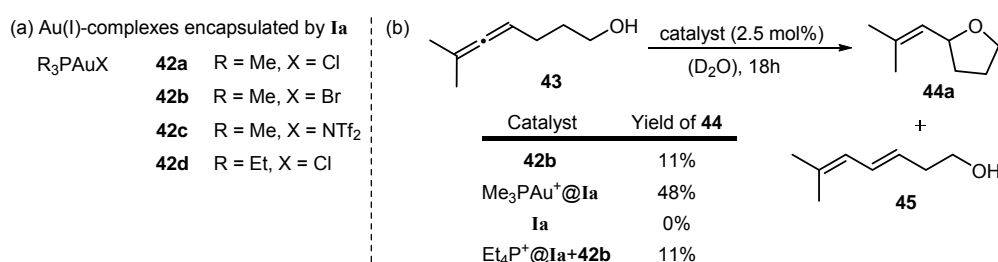
Scheme 1.13: Binding studies of gold complexes with **Ia** (a) and hydroalkoxylation reaction of **43** to cyclic ether **44** catalyzed by encapsulated gold catalyst **42b** (b).

Based on the previous studies, the groups of Raymond, Bergman and Toste reported a tandem reaction sequence combining enzymatic and supramolecular catalysis.[57] Exposure of allenic acetate **46a** to a buffered aqueous solution (pH 8) of rabbit liver esterease (25 units) and encapsulated gold catalyst (Me$_3$PAu$^+$@**Ia**, 10 mol%) at room temperature resulted in 88% conversion to tetrahydrofuran derivative **44** via enzyme-mediated acetate hydrolysis followed by gold-catalyzed cyclization. Full conversion was reached by operating at 37 °C with only 5 units enzyme. Similar results were obtained for substrate **46b** and amide substrate **47** with a variety of estereases or lipases and encapsulated gold catalyst. The reactivity of the combined system dropped dramatically in the absence of cluster **Ia**. It was proposed that the free gold catalyst bound to the amino acid residues of the enzyme and retarded the hydrolysis step. The rate study of fluoro derivative **46c**, whose hydrolysis kinetic could be followed by ^{19}F-NMR, confirmed this hypothesis. Similarly, the kinetic resolution of racemic substrates **46d** and **46e** proceeded in a more enantioselective fashion when the gold catalyst was restricted within **Ia**.

46a (R^1 = H, R^2 = Me)   **46b** (R^1 = H, R^2 = n-C$_7$H$_{15}$)

46c (R^1 = H, R^2 = CH$_2$CF$_3$)

46d (R^1 = Me, R^2 = Me)   **46e** (R^1 = Et, R^2 = Me)

Scheme 1.14: Tandem enzyme-mediated hydrolysis and Me$_3$PAu$^+$@**Ia**-catalyzed cyclization.

Another one-pot synthesis involving supramolecular catalysis was reported by the Nitschke group. The reaction sequence couples a Diels–Alder cycloaddition, a rearrangement reaction mediated by the [Fe$_4$L$_6$]$^{4-}$-cluster **IIa** and an organocatalysis (Scheme 1.15a).[58] In the acidic aqueous solution containing all the components required for the overall transformation, methylene blue catalyzes the hetero-Diels–Alder cycloaddition of furan with singlet oxygen (^{1}O$_2$) generated by irradiation. The formed unstable endoperoxide **49** decomposes to hydroxylbutenolide **52** (35%) accompanied by several side products in bulk solution, while cluster **IIa**, formed *in situ* under reaction conditions, stabilizes the high-energy intermediate *via* encapsulation and catalyzes its selective conversion to fumaraldehydic acid **50**. Upon liberation, **50** is converted in the third catalytic cycle *via* iminium formation with L-proline. Nitromethane is added to the iminium species in a 1,4-addition reaction to afford **51** as the final product in 30% overall yield. Unexpectedly, the one-pot synthesis displayed an improved stereoselectivity (dr = 84:16) for the incorporation of nitromethane over the separately performed 1,4-addition reaction (dr = 70:30). The authors explained this effect with the low steady-concentration of **50** in the relay transformation. Besides, the presence of cluster **IIa** was demonstrated to be essential for the multi-catalytic system. No trace of **51** was detected when any subcomponent necessary for the assembly of **IIa** was omitted. The compatibility within the presented system is quite remarkable, since the reactivities of the different catalytic cycles are not completely orthogonal. For instance, L-proline can compete with 2-formylpyridine for iminium formation (Figure 1.3). The formation of the bidentate ligand capable of

chelating the Fe(II) ion seemingly functions as the impetus to override the interference. In turn, the metal–ligand interaction stabilizes the Fe(II) ions and prevents their oxidization to Fe(III) species under aerobic conditions.


Scheme 1.15: Catalytic application of Nitschke's metal–ligand self-assembled cluster. (a) tandem multicatalytic system involving cluster **IIa** (b) ΔΔΔΔ-**IIb**-catalyzed hydrolysis of **52**.

The group of Nitschke also reported the hydrolysis of the pesticide dichlorovos (**52**) promoted by the larger $[Fe_4L_6]^{8+}$-cluster ΔΔΔΔ-**IIb** under neutral conditions (Scheme 1.15b).[30] In the presence of 1 mol% ΔΔΔΔ-**IIb**, the hydrolysis of **52** to the less toxic dimethyl phosphoric acid (**53**) along with dichlorovinylmethyl phosphoric acid (**54**) as a minor product is efficiently accelerated as compared to background reactions. No rate enhancement was observed with incomplete ingredients of ΔΔΔΔ-**IIb** or with blocked ΔΔΔΔ-**IIb**. A possible explanation for the acceleration effect involves the polarization of encapsulated **52** by the positively charged reaction host.

The Rebek group demonstrated that the dimeric cage **III** was prone to include two guest molecules of appropriate sizes, which raised the possibility to perform bimolecular reactions inside **III**. Early attempts involved the Diels–Alder reaction between *p*-benzoquinone (**55**) and cyclohexadiene (**56**) which was efficiently accelerated inside **III**.[59] But the reaction had to be operated with stoichiometric amounts of reaction host **III** as strong binding of the product **57** impeded the catalytic turnover. Product inhibition was eventually circumvented by identifying a Diels–Alder system, where the accommodation of substrates is more preferred by **III** than the product (Scheme 1.16).[60] Under reaction conditions, the cavity of **III** is

predominantly occupied by two copies of *p*-benzoquinone (**55**), which forms the resting state of the system. Due to the dynamic property of the host-guest complex, one **55** is occasionally replaced by thiophenedioxide (**58**). The resulting reactive complex smoothly undergoes cycloaddition to afford product **59**. Although the displacement of **59** by two **55** is entropically disfavored, the turnover is forced by the much higher affinity of **55** towards **III** (1.9×10^5 M^{-1} for two molecules of **55** and 155 M^{-1} for **59**). The rate study reveals pseudo-first-order kinetics in product formation which is in accord with the absence of product inhibition. The catalyzed reaction is accelerated 7-fold over the background reaction due to the increased effective concentration in the cavity of **III**.
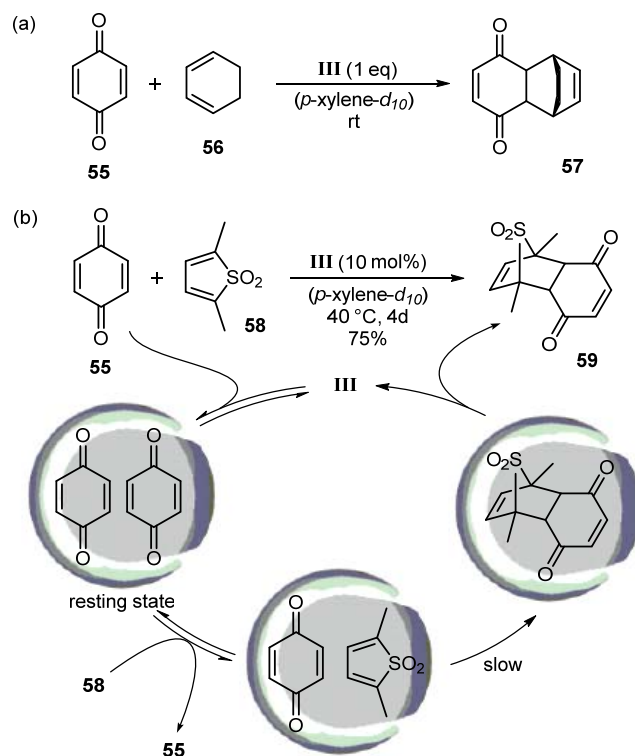
Scheme 1.16: Diels–Alder reactions mediated by Rebek's dimeric cage **III**.

The groups of Scarso and Reek reported the encapsulation of gold catalyst **61**-OTf in the hexameric resorcinarene capsule **IVa** in benzene or chloroform saturated with water.[61] Formation of a 1:1 host-guest complex was demonstrated by ^{1}H-NMR, DOSY and NOESY spectroscopy. ^{19}F-NMR indicated that the triflate counter ion was not incorporated in the capsule, and the gold catalyst is encapsulated as a cationic

species. The hydration reaction of terminal alkynes was chosen to examine the reactivity of the encapsulated **61**. In solution, **61**-OTf catalyzed the clean conversion of terminal alkynes **60** to methyl ketones **64** within 30 min. However, a mixture including methyl ketone **64** (12%), terminal aldehyde **65** (4%) and 1,2-dihydronaphthalene (**66**, 12%) was produced with the encapsulated **61** after 400 min (Scheme 1.17). The reactivity in solution was restored when the encapsulated gold catalyst was displaced by the strongly binding guest $Et_4N^+BF_4^-$. Formation of **64** and **65** likey stems from the branched intermediate **63**, which mirrors the steric requirement of the interior of **IVa**, as the more compact **63** is probably better accommodated by **IVa** than its linear counterpart **62**. As proposed by the Rebek group, removal of one resorcinarene unit is required for the binding of substrates and release of products, which provides a possible explanation for the slower reaction inside **IVa**. Considering that the reactions were conducted in benzene saturated with water, the formation of **66**, which normally necessitates anhydrous condition, evidences that water is excluded from the hydrophobic cavity of **IVa**. In a follow-up study, competitive reactions demonstrated that the reactivity with encapsulated catalyst was mainly determined by the size and shape of substrates.[62] The smaller substrates and those of a more compact shape were preferentially converted due to their facilitated encapsulation.

catalyst	time	conversion	**64:65:66**
61-OTf	30 min	100%	100:0:0
61@**IVa**	400 min	28%	43:14:43

condition: C_6D_6 (saturated with H_2O), 70 °C
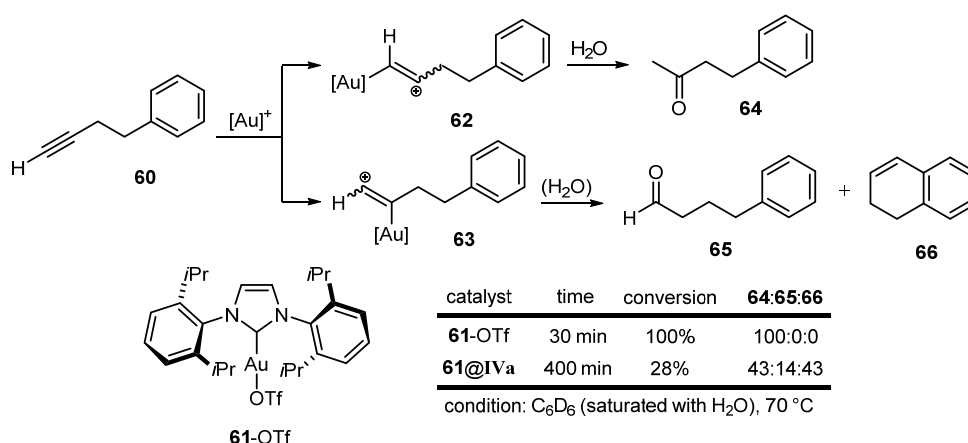
Scheme 1.17: Control over chemo- and regioselectivity *via* encapsulation of **61** within **IVa**.

In a collaboration between the Scarso and Strukul groups, **IVa**-catalyzed hydration

reactions of isonitriles were explored (Scheme 1.18).[63] Under reaction condition, kinetically stable host-guest complexes were detected by ^{1}H-NMR spectroscopy. The encapsulation of neutral isonitriles **67** is attributable to their capability to form intermolecular hydrogen bonds with **IVa**. Substrates bearing isopropyl (**67a**), benzyl (**67c**) and cyclohexyl (**67e**) substituent were quantitatively hydrolyzed within 18 h with 10 mol% **IVa** as the catalyst. Lower conversions were observed for the *tert*-butyl (**67b**) and aromatic (**67d**) isonitriles. The catalytic activity was completely suppressed when the reaction host was blocked by a competitive guest (Et$_4$N$^+$OTf$^-$).
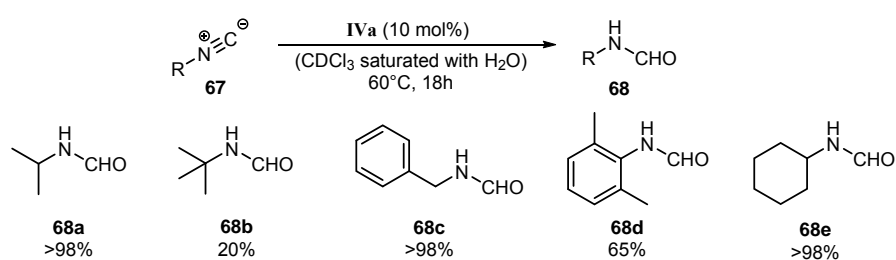
Scheme 1.18: **IVa**-catalyzed hydration reactions of isonitriles **67**.

Taking advantage of the isonitriles' affinity towards **IVa**, the Scarso group described the intermolecular [2+3] cycloaddition between isonitrile **67** and trimethylsilyl azide (TMSN$_3$, **69**) with **IVa** as the catalytic reaction host (Scheme 1.19).[64] 1H-tetrazoles were formed from aliphatic and aromatic isonitriles with moderate to excellent yields. However, no clear trend could be deduced for the reactivity of different substrates. The cycloaddition reaction did not occur without **IVa** under otherwise identical conditions. Control experiments performed with acetic acid and resorcinol ruled out acid catalysis and activation of substrates *via* hydrogen bonding. Interestingly, blocking the reaction host with a competitive inhibitor (Et$_4$N$^+$BF$_4^-$) did not completely shut down the reaction, indicating that the residual space inside **IVa** was still sufficient to catalyze the reaction but with lowered efficiency. Notably, the reaction conditions for 1H-tetrazole formation are closely related to those reported for hydration reactions, but no amide species was produced during the course of the cycloaddition reaction. Subjecting formamides to TMSN$_3$ resulted in no formation of the cyclic product. Therefore, the possibility that the amide was transiently formed as

an intermediate during the cycloaddition reaction could be eliminated. Previously described syntheses of 1*H*-tetrazoles substituted at position 1 usually involve toxic reagents[65] or harsh condition,[66] while this work provides an environment-friendly alternative to access this class of compounds.
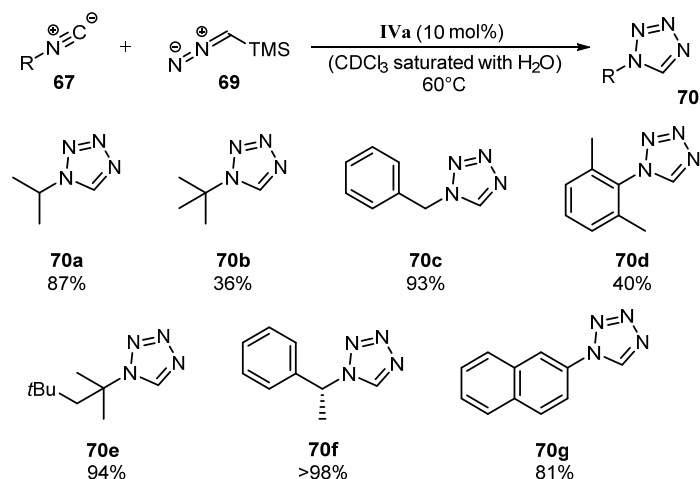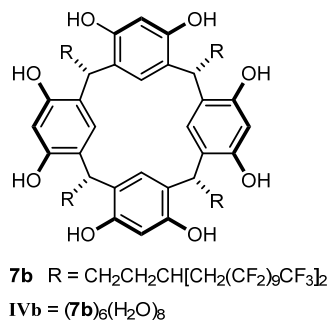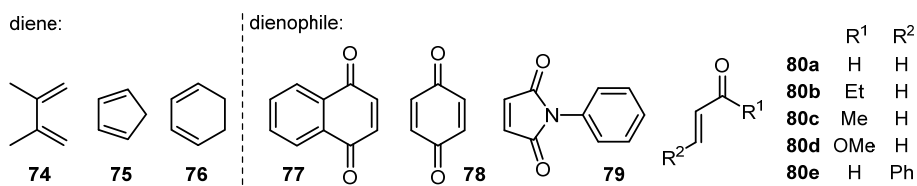

Scheme 1.19: **IVa**-catalyzed [2+3] cycloaddition between isonitrile **67** and TMS-azide **69**.

The Scarso group also reported another catalytic [2+3] cycloaddition reaction inside **IVa** involving diazoacetate **71** and electron-deficient alkene **72** (Scheme 1.20).[67] The reaction is facilitated by the high affinity of diazoacetate **71** towards the capsule **IVa**. Quantitative formation of the host-guest adduct with **71** was evidenced by ^{1}H-NMR spectroscopy under reaction conditions. Compared to background reactions, the cycloaddition reactions were accelerated or enabled in the presence of 10 mol% **IVa** for a wide range of substrate combinations. 4,5-Dihydro-1*H*-pyrozole derivatives **73** were formed as products with varying yields. The authors attributed the rate enhancement of the encapsulated reactions to the combination of stabilization of substrates by **IVa** and the dramatic increase of effective concentrations inside the reaction host. No reaction acceleration was observed when the host was blocked with competitive ammonium guests or replacing **IVa** with a Brønsted acid (resorcinol). The capsule also displayed a gentle substrate selectivity favoring the reaction of smaller alkenes with a given diazoacetate. This effect could be explained by the more efficient accommodation of smaller substrates by the reaction host.
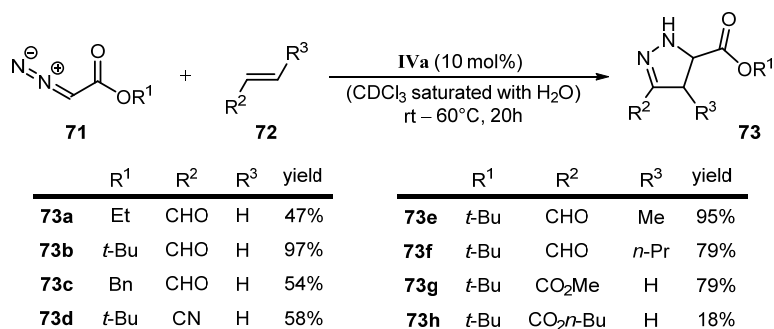
Scheme 1.20: **IVa**-catalyzed [2+3] cycloaddition between diazoacetate **71** and alkene **72**.

Resorcinarenes bearing fluorous feet **7b**, reported by the Shimizu group, form the hexameric assembly **IVb** in wet fluorous solvent such as perfluorohexane or methoxyperfluorobutane.[68] Under these conditions, it displays a much higher binding affinity towards organic compounds relative to its non-fluorinated counterpart **IVa** due to the fluorophobic effect. This property was utilized to promote intermolecular Diels–Alder reactions (Scheme 1.21).[69] As the organic diene and dienophile were readily encapsulated by **IVb** in perfluorohexane, the effective molarity of the intermolecular reaction was significantly increased in the confined space within the capsule **IVb**, reflected by the moderate rate acceleration (2.3- to 21-fold increase in yield) of these reactions. The effect of binding affinity on rate enhancement was probed by varying the fluorous content of solvent mixtures containing perfluorohexane (C_6F_{14}) and hexafluorobenzene (C_6F_6). The acceleration effect declined when the fluorous content decreased (i.e. the ratio of hexafluorobenzene increased). This observation is consistent with a lower binding affinity of substrates towards the reaction cavity with less pronounced fluorophobic effect. The capsule also showed a moderate bias regarding *endo/exo*-selectivity with the more compact *endo* product being formed preferentially. Due to the high solubility of capsule **IVb** in fluorous solvents, the catalyst can be easily recovered by decanting of the fluorous phase. The catalytic activity did not drop even after five catalytic runs.

diene:

dienophile:

	R^1	R^2
80a	H	H
80b	Et	H
80c	Me	H
80d	OMe	H
80e	H	Ph

74 **75** **76** **77** **78** **79**

7b R = CH$_2$CH$_2$CH[CH$_2$(CF$_2$)$_9$CF$_3$]$_2$

IVb = (**7b**)$_6$(H$_2$O)$_8$

diene	dienophile	yield [%]	*endo/exo*
74	**80a**	63(3)	n.a
74	**80b**	61(<19)	n.a
74	**77**	93(6)	n.a
74	**79**	64(5)	n.a
75	**80c**	67(29)	7.7:1(5.6:1)
75	**80d**	55(23)	5.5:1(2.9:1)
75	**80e**	28(10)	1.2:1(0.85:1)
76	**78**	78(15)	*endo*(*endo*)
76	**77**	35(7)	*endo*(*endo*)

a: conditions: diene (10 eq), dienophile (1 eq), **IVb**
   (1.67 mol%), hexafluorohexane/H$_2$O, 50 °C, 6h
b: values in parenthesis: without **IVb**

Scheme 1.21: Diels–Alder reactions catalyzed by capsule **IVb** bearing fluorous feet.

1.2 Terpene Cyclization

1.2.1 Biosynthesis of Terpenes

Terpenes constitute one of the largest classes of natural products. Thus far, more than 30000 terpenes[70] have been identified and display an enormous diversity in structure, stereochemistry and biological function. Intriguingly, all terpene natural products are generated by enzymes, termed terpene synthases, just from a handful of linear precursors which themselves are derived from only two isomeric five-carbon building blocks: isopentenyl pyrophosphate (IPP, **87**) and dimethylallyl pyrophosphate (DMAPP, **88**).

Two metabolic pathways are known to produce IPP and DMAPP: mevalonate (MVA) pathway and deoxyxylulose phosphate (DOX) pathway (Scheme 2.1). The mevalonate pathway[71] is operative in eukaryotes, archaea, and some bacteria and it is initiated by the biological Claisen condensation of two molecules of acetyl-coenzyme A (**81**) to form acetoacetyl-CoA (**82**), which then undergoes an aldol reaction with another copy of **81** to generate 3-hydroxy-3-methylglutary-CoA (HMG-CoA, **83**). Reduction of **83** is realized with two equivalents of NADPH (Nicotinamide adenine dinucleotide phosphate) to afford mevalonic acid (**84**). **84** is then converted to its diphosphate counterpart **86** in two successive phosphorylation reactions. Subsequent decarboxylation and dehydration sequence of the resulting diphosphomevalonate **86**, mediated by ATP (Adenosine triphosphate), provide isopentenyl pyrophosphate (IPP). Under the action of an isomerase, IPP isomerizes to dimethylallyl pyrophosphate (DMAPP).

The alternative deoxyxylulose phosphate (DOX) pathway,[70, 72] also known as non-mevalonate pathway or methylerythritol phosphate (MEP) pathway, is substantially presented in bacteria and in chloroplasts of green algae and higher plants. The reaction pathway starts from the condensation between pyruvic acid (**89**) and glyceraldehyde-3-phophate (**90**) accompanied by the loss of CO_2. The formed 1-deoxy-D-xylulose-5-phosphate (DOXP, **91**) undergoes rearrangement and

subsequent reduction to give 2-*C*-methyl-D-erythritol-4-phosphate (**93**). Compound **95** is furnished by a sequence of cytidinylation and phosphorylation of **93**. By the catalytic action of IspF protein, **95** is transformed to the cyclic phosphate **96** via the release of CMP (cytidine monophosphate). The following steps involve the ring opening reaction of **96** and the enzymatic conversion of **97** to IPP and DMAPP.
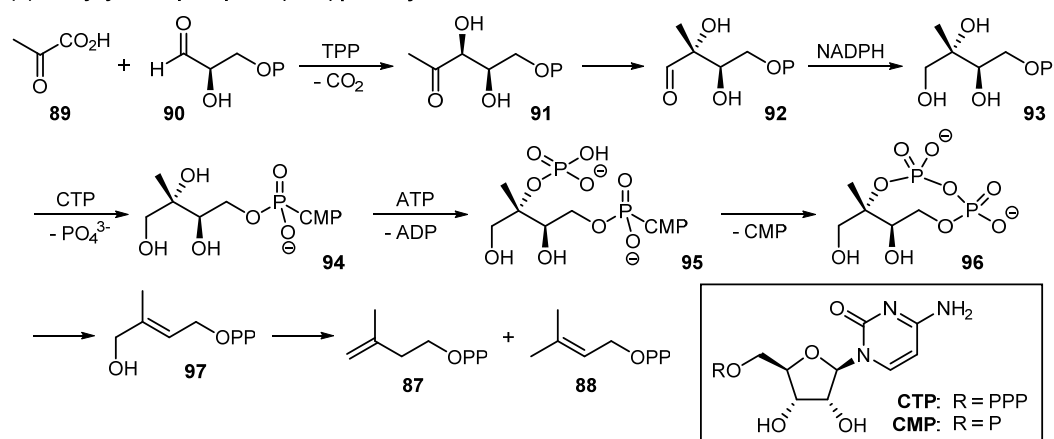
Scheme 2.1: Biosynthesis of IPP and DMAPP via the mevalonate (a) and deoxyxyluose phosphate (b) pathway.

The syntheses of the linear cyclization precursors are catalyzed by the so-called prenyltransferase which mediates the extension of DMAPP by the IPP elongation unit.[73] Mechanistically, the metal-triggered departure of the diphosphate group generates the cationic allylic intermediate, which is entrapped by the electron-rich double bond of IPP. The resulting carbocation (not shown) undergoes elimination of a proton to afford geranyl (*E*, **99**) or neryl (*Z*) pyrophosphate depending on the operational enzyme. Further elongation steps allow the access to farnesyl pyrophosphate (C_{15}) and geranylgeranyl pyrophosphate (C_{20}).

Terpene cyclization is categorized into two classes which differ in the mechanism of

substrate activation and the direction of charge propagation (Scheme 2.2).[70, 74] In the tail-to-head pathway, cyclization is initiated by activating the allylic pyrophosphate group by the trinuclear metal cluster that is coordinated by the conserved amino acid residues in the enzyme's active site. In contrast, the cationic intermediate of the head-to-tail pathway is generated by activating the distal double bond (head) with a proton or a halonium ion. During the cyclization process, the cyclizing enzyme, termed as terpene cyclase, serves as a template to dictate the reactive conformation of the flexible linear substrate and cationic intermediate. The type of terpene cyclases determines the regiochemistry and/or the steric outcome of the cyclization, and the highly variable cyclization patterns explain the enormous structural diversity of terpene natural products.
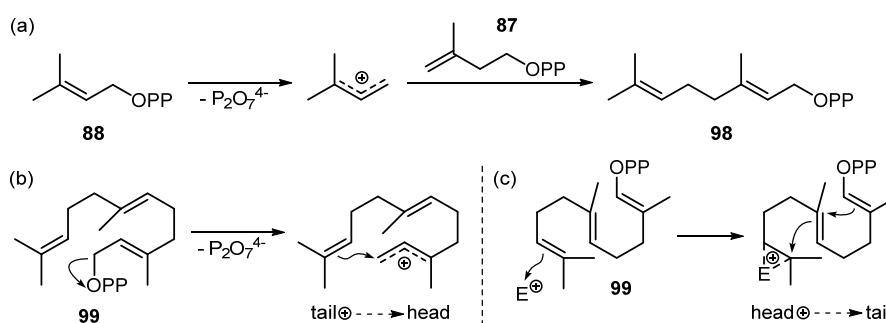
Scheme 2.2: Biosynthesis of geranyl pyrophosphate (a) and cyclization of farnesyl pyrophosphate *via* the tail-to-head (b) and head-to-tail (c) pathway.

1.2.2 Biomimetic Terpene Cyclization

Fascinated by nature's ability to access complex terpene natural products with high efficiency and fidelity, synthetic chemists have endeavored to reproduce terpene cyclization with man-made catalysts. In this context, numerous novel Brønsted and Lewis acids have been developed to trigger the cyclization reactions.

Although the acid-catalyzed terpene cyclizations have been intensively studied,[75] it is until late 1990s when the group of Yamamoto described the first enantioselective polyene cyclization mediated by the combination of a Lewis acid and a chiral Brønsted acid (LBA, Scheme 2.3).[76] The coordination of the Lewis acid (SnCl$_4$) to the (*R*)-BINOL-derivative **100** is believed to increase the acidity of the Brønsted acid

and to restrict the direction of the acidic proton which is responsible for the enantiomeric induction. The cyclization of homofarnesol **101** promoted by excessive LBA **100a** (2 eq.) proceeded with a moderate optical yield (42% ee). The cyclization product **102** is the most important commercial substitute for ambergris, due to its unique olfactive and fixative properties. The attempt to use catalytic amounts of **100a** failed since the hydroxyl group of the substrate competitively coordinates to the Lewis acid and therefore reduces the reactivity of the LBA. To solve this problem, geranyl phenyl ether **103** was used as the cyclization precursor, where the phenol ring serves as the internal nucleophilic terminator. The substrate **103** cyclized smoothly via an abnormal 1,3-rearrangement in the presence of 20 mol% LBA with greatly improved yields and enantioselectivity.
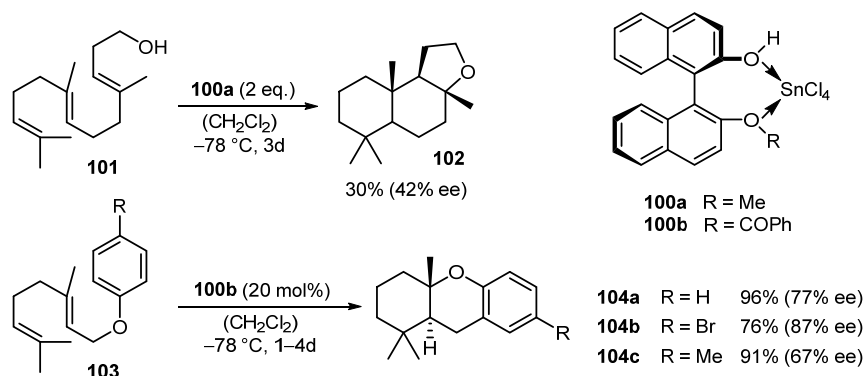
Scheme 2.3: Yamamoto's enantioselective polyene cyclization mediated by chiral LBA.

The group of Ishihara reported another highly enantioselective (up to 99% ee) polyene cyclization, which features the *in situ* formation of the electrophilic activator **106** from *N*-iodosuccinimide (NIS) and the chiral phosphoramidite **105** under controlled cryogenic conditions (Scheme 2.4).[77] The use of toluene as solvent allows **106** to exist as tight ion-pair and the double bond character of the P-N bond, which was proven crucial for the enantioselectivity. Compound **108** was formed as a minor product (**109/108** = 7/3) due to the premature quenching of the carbocation intermediate, and it can be transformed to the tricyclic product **109** with ClSO₃H in a diastereoselective fashion. As brominated and chlorinated natural products greatly outnumber the iodinated ones, the authors also tried to extend the protocol to the enantioselective bromo- and chlorocyclization. However, the enantiomeric excess

decreased dramatically to 36% with *N*-bromosuccinimide (NBS) as bromine source and no chlorinate product was formed with *N*-chlorosuccinimide (NCS).
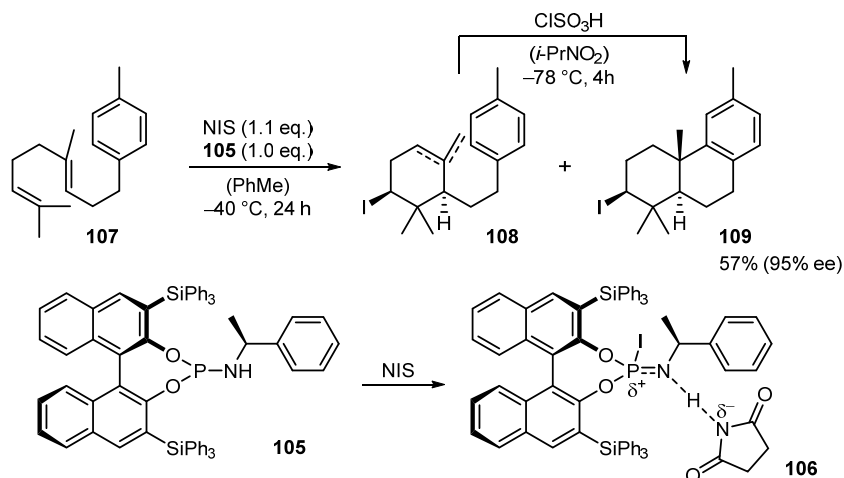
Scheme 2.4: Enantioselective iodocyclization using NIS and the chiral phosphoramidite **105**.

The Snyder group provided a solution for a highly efficient bromonium-induced polyene cyclization (Scheme 2.5) with the simple, bench-stable reagent bromodiethylsulfonium bromopentachloroantimonate (BDSB, **110**).[78] BDSB effects the fast cyclizations of a wide range of electron-rich and -deficient substrates under mild reaction conditions, affording mono- to tetracyclic products in moderate to excellent yields. The power of BDSB relies on its exceptionally short bromine-sulfur contact and the effective sequestration of the antimonate counterion, as indicated by the X-ray crystal structure. The structurally related CDSB and IDSB also demonstrate similar reactivities as BDSB. Serval racemic natural products, including the anti-HIV peyssonol A **115**, were synthesized by using the established protocol as the key steps.
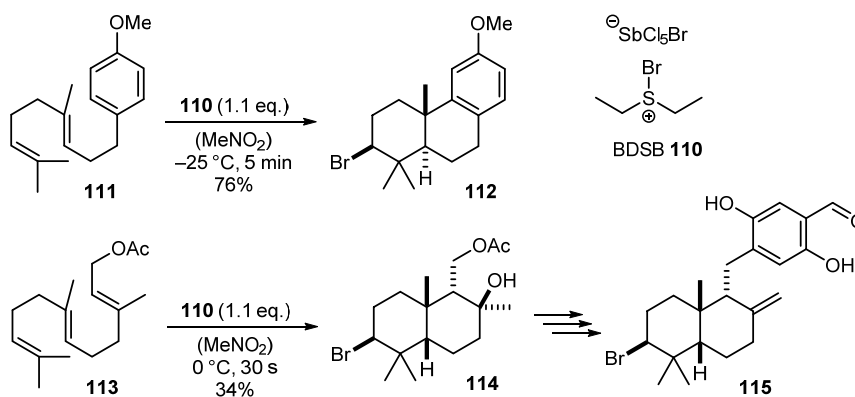
Scheme 2.5: Bromonium ion-induced polyene cyclization using BDSB.

Although the exploration of the biomimetic head-to-tail terpene cyclization has resulted in fruitful achievements, only one example of the tail-to-head pathway was recently reported by the Shenvi group using stoichiometric Lewis acid.[79] While the concertedness of the overall ring-forming process is postulated for the former cyclization branch,[80] the tail-to-head cyclization pathway proceeds in a stepwise fashion which poses the major challenge. Due to the Coulombic attraction, the reactive carbocation is kept in a close distance to the counteranion that can function as a nucleophile or a general base to prematurely intercept the cyclization cascade. Cyclase enzymes solve this problem by immobilizing the cleaved pyrophosphate group by the trinuclear metal cluster. Accordingly, the Shenvi group developed a biomimetic anion sequestration strategy by using a Lewis acid with non-dissociating ligands. After the vinyl epoxide substrate **116** is activated by a mixture of alkyl aluminium chlorides, the resulting alcoholate remains attached to the aluminium species (Scheme 2.6). The enforced charge separation facilitates the uninterrupted propagation of the cationic intermediate and allows access to the natural products β-cedrene **123** and β-funebrene **124**.
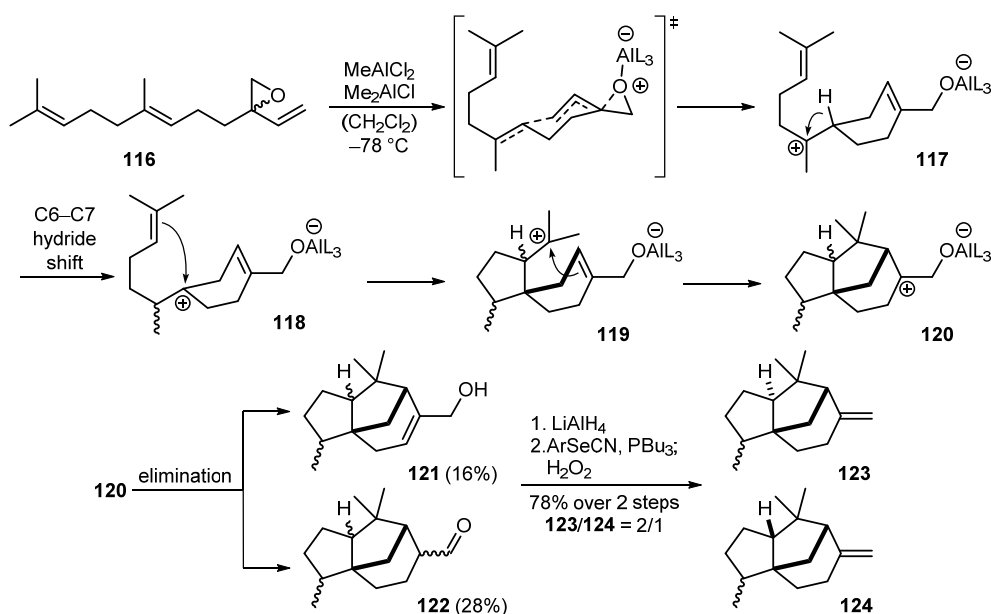
Scheme 2.6: Biomimetic tail-to-head terpene cyclization using a nondissociating Lewis acid.

2 Objective of the Thesis

In the past years, the efforts to achieve biomimetic terpene cyclizations have centered on the development of potent reagents as stoichiometric activators or catalysts. To avoid side reactions of the reactive cationic intermediates, cyclizations using such reagents need to be performed under cryogenic and/or high dilution conditions. On the contrary, cyclase enzymes effect cyclizations under mild conditions (physiologic pH and ambient temperatures), largely due to two factors: The cyclase selects the substrate from the bulk solvent and prevents side reactions with nucleophiles or bases; the aromatic residues in the active site are believed to stabilize the intermediate *via* cation–π interactions.[81]

Given these facts, we envision that aromatic supramolecular structures would make suitable surrogates for natural cyclases and provide a truly biomimetic approach for the fascinating catalytic terpene cyclization. As numerous literature precedence has demonstrated, substrate uptake should be favored for entropic reasons. And the cationic intermediate is expected to be stabilized by interacting with the aromatic walls of the reaction host. Preliminary investigations will be conducted with linear monoterpenes, such as geraniol, nerol and linalool. Although their cyclization behavior has been intensively studied with natural enzymes, the use of cell-free systems would open the possibility to gain new insights into such classical reactions. And the comparison with biological systems would, in turn, provide us with valuable guidelines for the design of more efficient enzyme-mimicking catalysts.

3 Results and Discussion

3.1 Publication Summaries

This chapter shortly summarizes the crucial aspects of the publications prepared during the course of this dissertation.

3.1.1 Hexameric Resorcinarene Capsule is a Brønsted Acid: Investigation and Application to Synthesis and Catalysis[82]

Supramolecular structures have been identified as appealing mimics for the biological catalysts. While the water-soluble metal−ligand systems have yielded fruitful catalytic transformations, applications of molecular capsules based on hydrogen bonding are still rare. Such systems have attracted our interest since they can be employed in organic solvents and are compatible with water-sensitive reagents.

We identified the hexameric resorcinarene capsule **IVa** (Figure 1.5) as an ideal candidate. Besides the ease of preparation, its spacious cavity (1375 Å^3) can accommodate guests of variable sizes and prevents the strong binding of products that impedes catalytic turnover. In pursuit of elucidating the puzzlingly high affinity of tertiary amines towards **IVa**, the surprisingly high acidity (pK_a approximately 5.5−6) of **IVa** was uncovered. The evidence collected indicated that tertiary amines were encapsulated as protonated species inside the negatively charged capsule.

These findings were then applied to synthesis. A size selective Wittig reaction was achieved with capsule **IVa** as the selector (Scheme 3.1). Analogously to tertiary amines, the smaller stabilized Wittig ylide **125** was completely protonated and encapsulated by **IVa**, while the Wittig ylide **126**, too bulky to fit the cavity of **IVa**, experienced only reversible protonation and therefore, maintained its reactivity. Treatment of this mixture with propanal led to a highly selective conversion of the bulky Wittig ylid **126**.
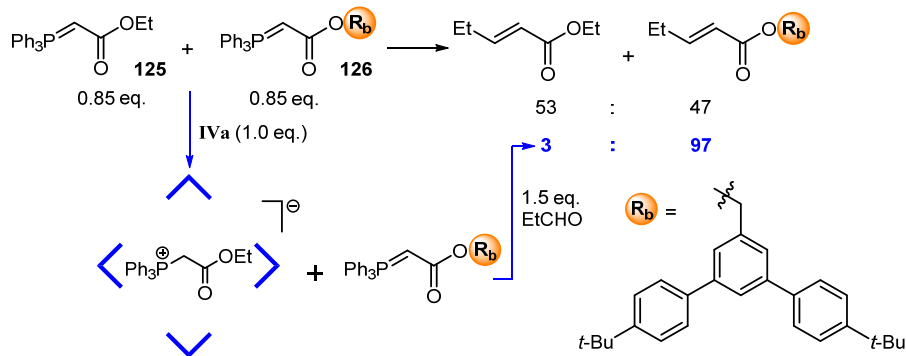
Scheme 3.1: Size-selective Wittig reaction in the presence of **IVa**.

Encouraged by the successful substrate-selective Wittig reaction mediated by capsule **IVa**, we decided to probe the viability of using **IVa** as an enzyme-like catalyst (Scheme 3.2). In a model reaction, 1,1-diethoxyethane (**127**) was smoothly hydrolyzed within 60 min at ambient temperature with catalytic amounts of **IVa**. The reaction rate dropped significantly with more bulky substrates. Blocking **IVa** with a strongly binding guest (Bu$_4$NBr) gave only a weak background reaction, indicating that the cavity of **IVa** is the source of the rate acceleration. In a competition experiment with **127** and its longer analog **128**, the hydrolysis reaction proceeded in a highly size-selective fashion favoring the cleavage of **127**. In a solution control experiment, a large excess of the much stronger trifluoroacetic acid had to be used to achieve comparable rates of conversion. Not surprisingly, a product mixture was formed.

catalyst	conv.	**129 : 130**
400 mol% TFA	33%	37 : 63
10 mol% **IVa**	85%	98 : 2
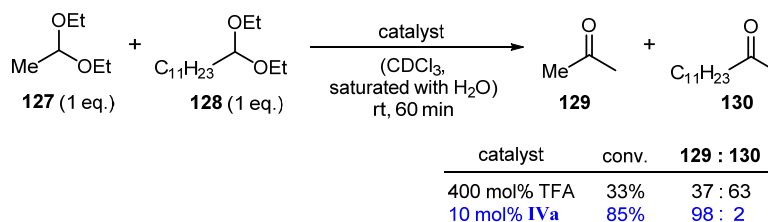
Scheme 3.2: Selective hydrolysis of acetal **127** in the presence of **128** within catalyst **IVa**.

3.1.2 Terpene Cyclization Catalyzed inside a Self-assembled Cavity[83]

In last decades, numerous catalysts or stoichiometric mediators have been developed and successfully applied to synthesis of terpene natural products by the head-to-tail (HT) approach. This is not the case for the tail-to-head (TH) terpene cyclization. Due to the lack of stabilization of the cationic intermediates, the THT cyclization has hardly been reproduced with man-made catalysts.

Based on our findings that the resorcinarene capsule **IVa** acts as a mild Brønstend acid and it functions as a catalyst for simple acetal hydrolysis reactions by stabilizing cationic transition states, we envisaged that a THT cyclization could be triggered by activating a suitable leaving group of an acyclic terpene *via* protonation. Indeed, geraniol (GOH) was converted to α-terpinene (**134**) and eucalyptol (**132**) in the presence of 10 mol% **IVa** with linalool (LOH) and α-terpineol as intermediates. Under similar conditions, nerol (NOH, **131**) was converted much faster, and eucalyptol (**132**) was formed as the dominant product. Linalool displayed a cyclization behavior which could be interpreted as a combination of those of GOH and NOH, both regarding the reaction rate and the product profile.
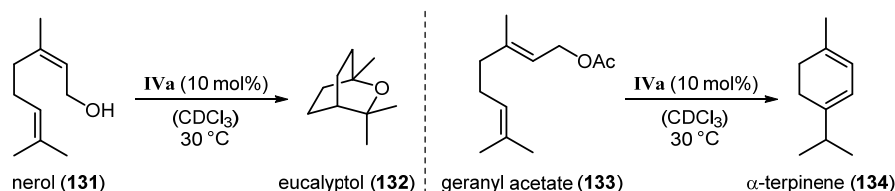
Scheme 3.3: **IVa**-catalyzed THT cyclization of nerol (**131**) and geranyl acetate (**133**).

In all cases, α-terpineol was detected as an intermediate, which resulted from the nucleophilic quenching of the transient carbocation by the cleaved water molecule. We found that the interception of cation intermediates could be efficiently suppressed when replacing the alcohol functionality with a less nucleophilic acetate leaving group. Most importantly, geranyl acetate (GOAc, **133**) was selectively transformed into α-terpinene (**134**) without the formation of any intermediates, indicating a true non-stop cyclization. With the aid of fluoro derivatives **137** and **138**, we were able to attribute the distinct cyclization behaviors of GOAc and neryl aceate (NOAc) to the

different double bond geometry of the allylic moiety. The *cis*-configuration of NOAc enables a direct cyclization in a S_N2-fashion, whereas the GOAc has to undergo an ionization step (S_N1) to form the reactive *cisoid* cationic intermediate **140** prior to cyclization.

The different reactivity displayed by linalyl acetate (LOAc, **135**) compared to GOAc is of interest . In the proposed biosynthesis, the linalyl intermediate (LPP) is suggested as intermediate for the cyclization of geranyl pyrophosphate (GPP) as the isomerization of the *transoid* **139** to the *cisoid* cation **140** is considered unlikely due to the postulated high-energy barrier. If this hypothesis applies for the system presented, such a difference between GOAc and LOAc would not be expected. This observation, in addition to the absence of any intermediates, indicates that a direct isomerization of the *transoid* cation **139** to the *cisoid* cation **140** is occurring in the **IVa**-catalyzed cyclization. Consequently, a direct isomerization between **139** and **140** could be relevant for the mechanism proposed for the biosynthesis of terpenes.
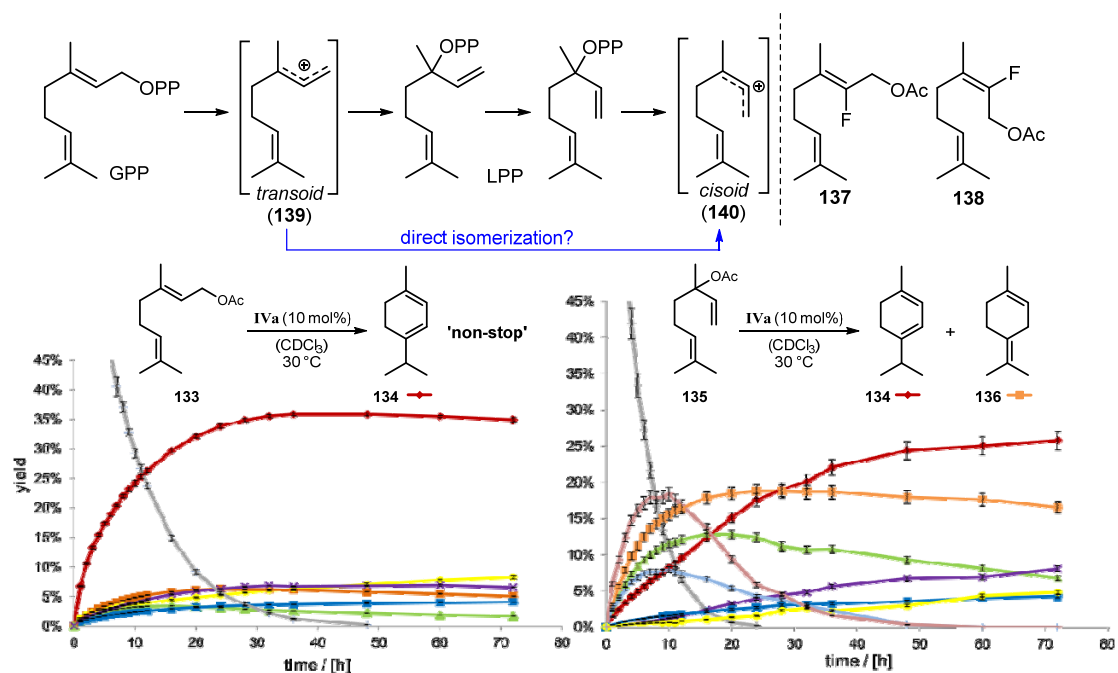
Scheme 3.4: Proposed mechanism for the biosynthesis based on the indication from the THT cyclization catalyzed by **IVa**.

3.2 To Catalyze or not to Catalyze: Elucidation of the Subtle Differences between the Hexameric Capsules of Pyrogallolarene and Resorcinarene

3.2.1 Results and Discussion

The functional mimicking of natural enzymes has been a very fascinating but also challenging research topic for decades. Several supramolecular structures have been identified that are able to catalyze reactions inside artificial enzyme-like pockets.[19, 84] Nevertheless, neither the catalytic efficiency nor the selectivity of such systems can usually compete with natural enzymes. Therefore, the refinement of known systems, as well as the development of new systems, is necessary. For the design of new artificial enzyme-like catalysts, it is of fundamental importance to understand the prerequisites for catalytic activity. We[82-83, 85] and others[63] have shown that the hexameric resorcinarene capsule **IVa**,[33-34, 38a, 39, 64, 67, 86] which self-assembles from six units of resorcinarene **IVa** and eight water molecules (Figure 3.1), is an efficient catalyst for a variety of cationic reactions. Nevertheless, the reasons for the high catalytic efficiency remained unclear. To learn more about the pivotal requirements for the catalytic activity of hexamer **IVa**, we became interested in the structurally closely related pyrogallolarene hexamer **IVc**.[35, 87] Capsule **IVc** self-assembles from six units of pyrogallolarene **7c**. Surprisingly, hexamer **IVc** displays a different encapsulation behavior than **IVa**. It was reported that hexamer **IVa** encapsulates both tertiary amines as well as alkylammonium species,[34, 36, 38a, 88] while **IVc** only binds tertiary amines.[87d, 87f] Very recently, the Cohen group disclosed that binding of ammonium salts in **II** can be observed to some extent in benzene solution.[89] The high affinity of ammonium salts for **IVa** can be explained by strong cation–π interactions. However, the surprising exclusion of alkylammonium species from **IVc** remained puzzling,[86c] especially since encapsulated tertiary amines were completely expelled after protonation by the addition of acid.[87d, 87f] This seemingly contradictory encapsulation behavior of **IVc** has remained a mystery for the last decade. We herein

elucidate the reasons for these differences. More importantly, we report herein that capsule **IVc** is catalytically completely incompetent in cationic reactions which are efficiently accelerated inside **IVa** and probe the molecular mechanisms responsible for these surprising observations.
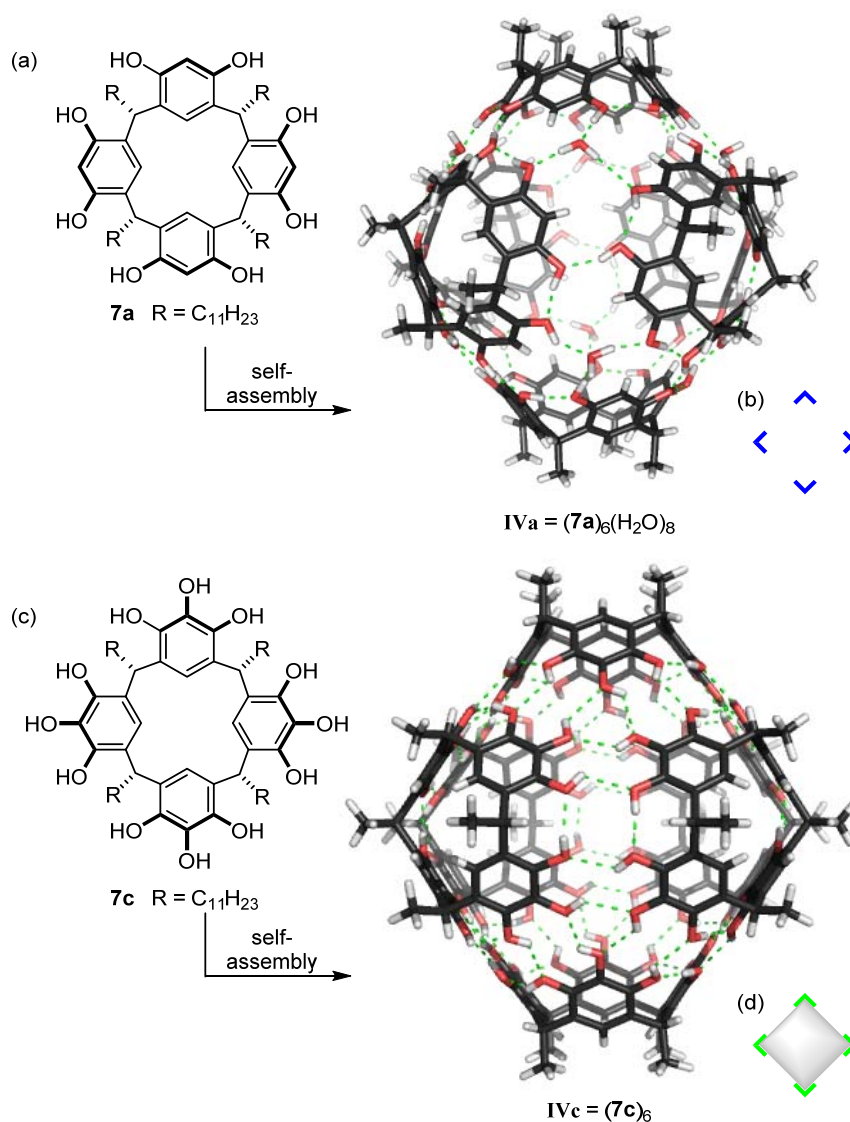

Figure 3.1: Structures of hexameric resorcinarene **IVa** (a) and pyrogallolarene **IVc** (c) capsules, and their symbolic representations (b) and (d).

Our interest in capsule **IVc** started with the observation that, while **IVa** is an efficient catalyst for cationic reactions,[63, 82-83, 85] hexamer **IVc** is catalytically incompetent in all these reactions. The tail-to-head terpene cyclization of nerol (**131**) [83] (Figure 3.2) was investigated more closely with **IVc**. ^{1}H-NMR analysis confirmed the formation of the host-guest complex **131@ IVc** (Figure 3.19). Therefore, the guest uptake cannot

explain its catalytic inertness.
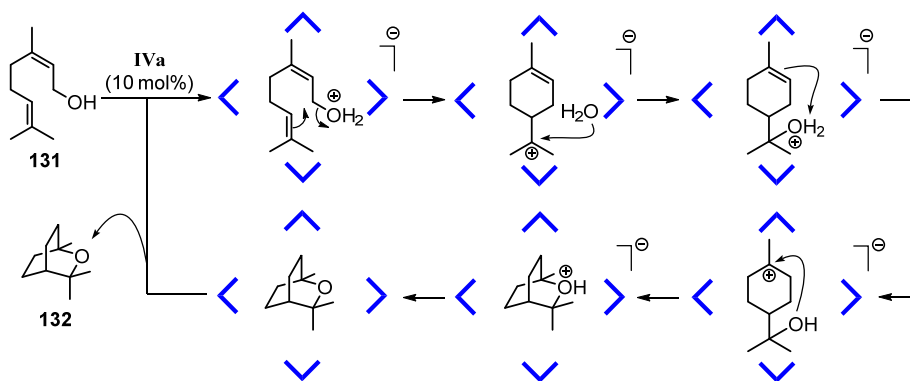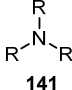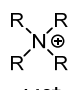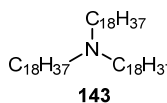
Figure **3.2**: Schematic overview of the nerol (**131**) cyclization to eucalyptol (**132**), catalyzed inside capsule **IVa** (CDCl₃, 30 °C).[83]

We first probed whether the absence of catalytic activity of **IVc** could arise from the reported resistance to bind alkyl ammonium salts,[87d] which may indicate a lack of cation–π stabilization inside the cavity. A cation–π stabilization of cationic transition states has been proposed as a possible reason for rate acceleration inside **IVa**,[83] and may thus be a potential explanation for the observed catalytic differences. Interestingly, however, it was reported that tertiary amines bind well inside **IVc**.[87d, 87f] Recently, we demonstrated that a proton transfer from capsule **IVa** to the tertiary amines is responsible for their high affinity for **IVa**.[82] This raised the question of whether the same is true inside **IVc**. Therefore, we investigated the encapsulation of differently sized tertiary amines inside **IVc**. The encapsulation of triethylamine (**141a**) in **IVc** is clearly evident in the ¹H-NMR spectrum (Figure 3.6). The integral of the phenolic groups of **IVc** diminishes upon treatment with **141a**, while a new broad peak emerges between 3 and 7 ppm. Careful integration (Scheme 3.5 and 3.6, Table 3.3), reveals that it accounts for the diminished phenolic protons, as well as for the water signal, which no longer is visible as a separate peak. These observations are consistent with our previous findings for capsule **IVa**, and thus indicate the concomitant protonation of tertiary amines upon encapsulation in **IVc**.[82] The integrity of the hexameric encapsulation complex was confirmed by DOSY spectroscopy (Figure 3.7). Therefore, the formation of smaller (dimeric, or monomeric) pyrogallolarene-cation complexes observed in methanol solution[87c] and in the solid state[87e, 90] can be

excluded.

The size of the tertiary amine has a pronounced effect on protonation and encapsulation, as shown in Table 3.1a. The degree of protonation and encapsulation drops with the increasing size of the alkyl groups, a behavior that is consistent with a decreased cation–π interaction due to steric shielding. In the case of triethylamine (**141a**), the deprotonation degree of **IVc** is considerably lower than the encapsulation degree. Therefore, a [**141**H**141**]$^+$@**IVc**$^-$-complex, also observed in capsule **IVa**,[82] is likely formed.

a)

	R	depronation degree of IVc	encapsulation degree of 141
141a	C_2H_5	29±2%	44±2%
141b	C_3H_7	19±1%	22±1%
141c	C_4H_9	12±1%	15±1%
141d	C_6H_{13}	10±1%	7±1%

b)

	R	encapsulation degree of 142$^+$	after addition of 143
142a$^+$Br$^-$	C_2H_5	nd*	nd*
142b$^+$Br$^-$	C_3H_7	4±0.3%	46±2%
142c$^+$Br$^-$	C_4H_9	0%	30±1%
142d$^+$Br$^-$	C_6H_{13}	0%	10±1%

*precipitation occured (2:1 complex, SI-Table 3)

Table 3.1: Encapsulation studies of capsule **IVc** with 1 eq. of (a) amine **141** or (b) ammonium **142** compounds. The encapsulation ratio of the ammonium guest was increased by the addition of the large amine base **143**.

These results indicate that capsule **IVc** encapsulates amines in their protonated form and therefore is able to stabilize cations inside its cavity. Indeed, our quantum chemical density functional theory (DFT: PBE–D3/def2–SVP) calculations also indicate that capsule **IVc** stabilizes cations approximately as well as capsule **IVa** (within ca. 4-12 kcal/mol; see Figure 3.5). This seems to contradict the previous observation that the ammonium salt Hex$_4$NBr (**142d$^+$Br$^-$**) was rejected by capsule **IVc**.[87d] We therefore repeated the encapsulation studies not only with **142d$^+$Br$^-$** but with differently sized ammonium salts (Table 3.1b). The small ammonium salt Et$_4$NBr (**142a$^+$Br$^-$**) is indeed encapsulated to a considerable extent (28%, Figure 3.10). With the increasing size of the alkyl residues, encapsulation drops dramatically: only 5% encapsulation is observed in the case of Pr$_4$NBr (**142b$^+$Br$^-$**), while the longer ammonium salts Bu$_4$NBr (**142c$^+$Br$^-$**) and Hex$_4$NBr (**142d$^+$Br$^-$**) do not show any degree of uptake inside **IVc**. This confirms the earlier observation that larger

ammonium salts are rejected by **IVc**, but also demonstrated that the uptake of the smaller salts is possible. Nevertheless, there is a striking difference between the capsules, as **IVa** encapsulates salts (**142a–142c$^+$Br$^-$**) quantitatively and **142d$^+$Br$^-$** to a large extent (Figure 3.9). This discrepancy is even more surprising considering that our DFT calculations suggest a comparable stabilization of cations inside **IVa** and **IVc**. To elucidate the different behavior of **IVa** and **IVc**, we calculated the electrostatic potential (ESP) map of the capsules' inner surfaces. As shown in Figure 3.3, the main difference between the two systems are high potential areas on the inner surface of **IVa**, which represent positively charged hydrogen atoms of the bound water molecules. These could potentially stabilize the anions of encapsulated ammonium salts *via* hydrogen bonds. Such a stabilization of anions inside **IVc** is lacking, and could therefore explain the dramatically weaker binding of ammonium salts. Our DFT optimizations of the capsules in presence of the ammonium salt **142a$^+$Br$^-$** confirms this hypothesis: although capsule **IVc** stabilizes cations better than capsule **IVa**, capsule **IVc** binds the ammonium salt weaker (*ca.* 3-9 kcal mol^{-1}) than **IVa**.
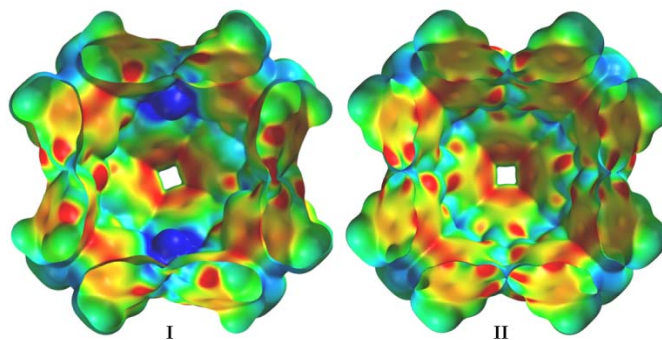
Figure. 3.3 Comparison of the electrostatic potential (ESP) surfaces of capsules **IVa** and **IVc**.

The energetically unfavorable encapsulation of anions inside **IVc** raises the question of whether the anion is encapsulated at all. Its presence would weaken the cation–π interactions, as has been shown in cyclophane hosts in organic solvents of low dielectric constants.[91] Therefore the ammonium salt EtPr$_3$N$^+$MeSO$_3^-$ (**142e$^+$MeSO$_3^-$**) containing an organic anion, detectable by ^{1}H- and ^{13}C-NMR spectroscopy, was investigated. ^{1}H- and ^{13}C-NMR (Figure 3.13, 3.14, and 3.15) unequivocally confirms that the counterion is located outside of **IVc** (Figure 3.4a). In capsule **IVa**, however,

the ion pair is encapsulated. The minute uptake of **142**[+] by neutral **IVc** is likely achieved by an energetically unfavorable charge separation in CDCl₃. This could explain the low encapsulation ratio of **142**[+] by **IVc**. If so, the addition of the large base **143**, which cannot be encapsulated due to its size, should increase the uptake of ammonium species: it would deprotonate the capsule and form an ion pair with the bromide *outside* the capsule, as depicted in Figure 3.4b. Indeed, upon the addition of **143**, the encapsulation of ammonium species increases as anticipated (Table 3.1b). These findings solve the puzzling encapsulation behavior of capsule **IVc** and also explain the expulsion of encapsulated trihexylamine (**141d**) after HCl-addition[87f] (Figure 3.4c). After the addition of HCl, the ion pair **141d**H^{+}Cl^{−} is formed, which is rejected by capsule **IVc**.
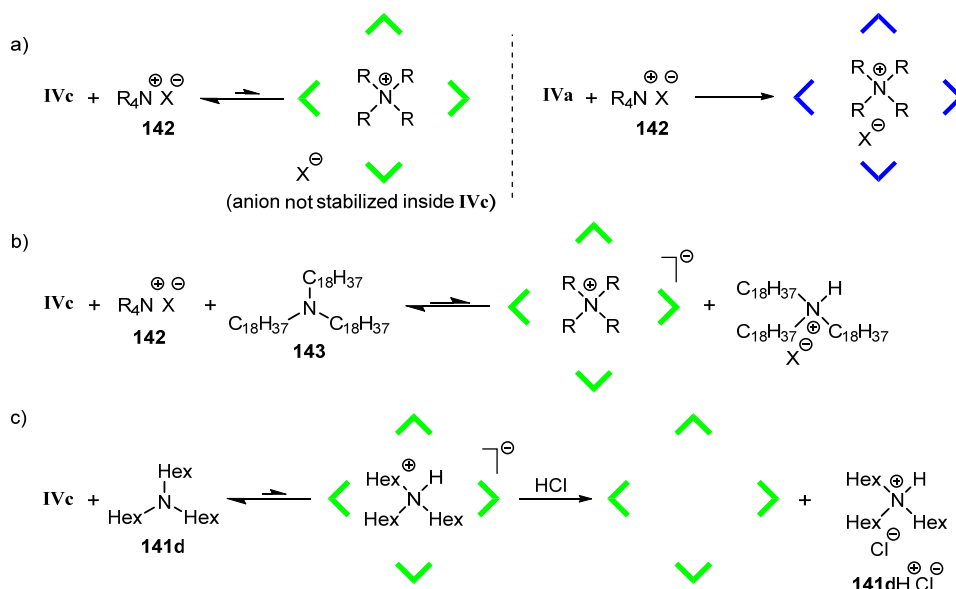
Figure 3.4: Schematic representation of encapsulation experiments of alkyl ammonium salts and amines in capsule **IVa** and **IVc**.

The evidence presented clearly indicates that capsule **IVc** is able to stabilize cations inside its cavity due to cation–π interactions. Therefore, its catalytic incompetence originates from a different source. After successful substrate uptake, protonation is required for substrate activation. Although **IVc** encapsulates protonated amines (Table 3.1a) the acidity of the system may be too low for activation of the alcohol substrate. Therefore, the acidity of hexamer **IVc** was determined analogously to **IVa** [82] by a series of protonation experiments with amines of varying basicity. The pK_a-value of

capsule **IVc** is approx. 9.5 − 10 (Figure 3.20 and 3.21; ca. four pK_a units higher than resorcinarene capsule **IVa**). These results are in excellent agreement with our DFT calculations at the PBE/def2–SVP/ε=4.81 level of theory, suggesting that the proton affinity of **IVa** is *ca*. 5 kcal mol^{-1} lower than that of **IVc** (Figure 3.23). The surprisingly low acidity of **IVc** may be a result of mesomeric destabilization of the phenolate (Figure 3.22). Our DFT calculations further suggest that the anionic defect can delocalize across several hydrogen bonds in **IVa**, while we observe a more localized defect in **IVc**, leading to a lower relative pK_a in capsule **IVa** (Figure 3.24).

Therefore, the low acidity of **IVc** is the likely cause of its catalytic incompetence (Figure 3.5a). We tried to overcome this limitation by the addition of stronger external acids, but still could not observe any reaction progress. This result, however, is not too surprising, since an external acid would form ion pair **144** with the substrate, which would impede encapsulation (Figure 3.5b).
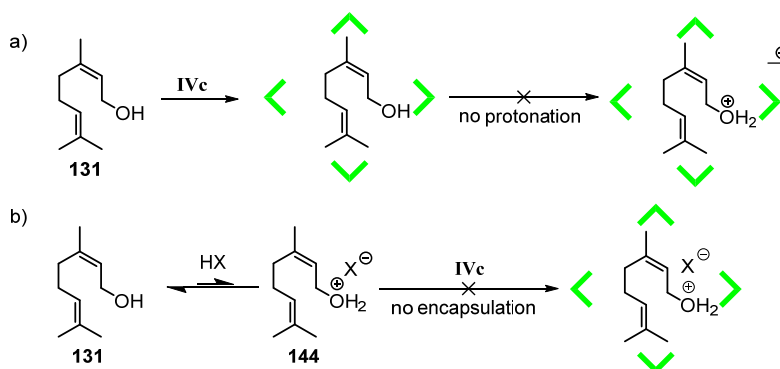
Figure 3.5: Schematic overview of nerol cyclization attempts with **IVc**.

In conclusion, the differences between the closely related hexameric capsules **IVa** and **IVc** were elucidated. Evidence was presented showing that capsule **IVc** does not stabilize anions inside its cavity, as opposed to **IVa**. Therefore, alkyl ammonium salts are encapsulated only to a small extent with concomitant charge separation. Cations, nevertheless, are stabilized inside **IVc** approximately as well as inside **IVa** *via* cation–π interactions. The much lower acidity of capsule **IVc** was determined to be the likely cause of the catalytic incompetence of capsule **IVc**. These findings are of great significance for the further development of enzyme-like catalysts and have a profound impact on the design of new catalytically active host systems.

3.2.2 Experimental Details

3.2.2.1 General information

Reactions were carried out under an atmosphere of argon, unless otherwise indicated. ^{1}H-NMR and ^{13}C-NMR spectra were recorded at 500 MHz and 126 MHz respectively, using a Bruker AV 500 spectrometer. ^{1}H-NMR and ^{13}C-NMR chemical shifts (measured at 298 K, unless otherwise stated) are given in ppm by using CHCl$_3$ and CDCl$_3$ as references (7.26 ppm and 77.16 ppm, respectively). Coupling constants (J) are reported in Hertz (Hz). Standard abbreviations indicating multiplicity were used as following: s (singlet), t (triplet), q (quartet) and m (multiplet). 2D-DOSY spectra were recorded with a Bruker AV 500 spectrometer using the Bruker standard DOSY routine. GC-analysis was performed with an Agilent GC6890 instrument equipped with a FID detector and a HP–5 capillary column (length = 29.5 m). Hydrogen was used as the carrier gas and the constant-flow mode (flow rate = 1.8 mL/min) with a split ratio of 1:20 was used.

Tetrabutylammonium bromide and tetrapropylammonium bromide were purchased from Acros Organics. CDCl$_3$ was purchased from Deutero GmbH. Dodecanal, trihexylamine and resorcinol were purchased from Alfa Aesar. Triethylamine and pyrogallol were purchased from Merck KGaA. Tetraethylammonium bromide, Tetrahexylammonium bromide, tributylamine and tripropylamine were purchased from Sigma–Aldrich. Ethanol (99.9%) was purchased from VWR. All chemicals were used as received, unless otherwise stated. Methanol and diethyl ether were purchased from Brenntag and distilled prior to use. Sonication was performed in a VWR Ultrasonic Cleaner USC–300TH. Transfer of liquids with a volume ranging from 1 to 10 µL or from 10 to 100 µL was performed with a microman M1 pipette (Gilson) equipped with 10 µL or 100 µL pipette tips, respectively.

Resorcinarene **7a**[83] and trioctadecylamine **143**[82] were synthesized according to literature procedures. Pyrogallolarene **7c** was synthesized according to a literature procedure[92]: To a stirring solution of 99.9% ethanol (60 mL) and 37% aqueous HCl

(14 mL), pyrogallol (11.4 g, 90 mmol, 1.0 eq.) was added. After the solution was cooled to 0 °C, a solution of dodecanal (20.0 mL, 90 mmol, 1.0 eq.) in 99.9% ethanol (10 mL) was added slowly into the reaction mixture over 15 min. The resulting solution was allowed to warm to 25 °C slowly and was then refluxed at 100 °C for 24 h. Afterwards, the reaction mixture was cooled to room temperature, filtered and washed with ethanol (120 mL). Air was drawn through the precipitate for 20 min (aspirator). The solid was recrystallized from ethanol (50 mL) and air was drawn through the precipitate for 20 min (aspirator). The obtained crystalline material was then dried utilizing a rotary evaporator (50 °C and 4 mbar), until the residual ethanol was removed completely. Compound **7c** (18.3 g, 70%) was obtained as an off–white crystalline solid.

Preparation of host stock solution: $CDCl_3$ (ca. 80% of the volume of volumetric flask) was added to **7a** or **7c** in a volumetric flask and the sample was homogenized by sonification, gentle heating with a heat gun and agitation to give a clear solution. The volumetric flask was filled up to the calibration mark with $CDCl_3$ and again homogenized by agitation to give a solution with a concentration as given in Table 3.2.

Table 3.2: Preparation of host stock solution.

	molecular weight (g/mol)	mass (mg)	volumetric flask (mL)	concentration (mmol/L)
resorcinarene **7a**	1106	140	2.00	63.3
pyrogallolarene **7c**	1170	295	5.00	50.4

Preparation of guest stock solution: Stock solutions of guests were prepared with a concentration of 83.3 mmol/L in $CDCl_3$.

Sample preparation: To the host solution (159 μL for **7a** and 198 μL for **7c**, 10.0 μmol, 6 eq.) in a NMR-tube was added $CDCl_3$ (320 μL for **7a**, 280 μL for **7c**) and guest stock solution (20 μL, 1.667 μmol, 1.0 eq.). The sample was homogenized by agitation. All experiments were conducted in triplicate and the average values

including standard deviation are reported. NMR spectra were recorded at least 3h after sample preparation to make sure protonation and/or encapsulation equilibria were reached.

Determination of the encapsulation ratio: In case of binding studies, the integral of the methine group (4.29 ppm for **7a** and 4.37 ppm for **7c**, t, J = 7.7 Hz, 24H) of capsule **IVa** or **IVc** were used as reference. In case of experiments with NEt$_3$ (**141a**) and Et$_4$N$^+$Br$^-$ (**142a$^+$Br$^-$**), the terminal methyl groups appearing between 0 and −1 ppm after encapsulation were utilized for calculating the encapsulation ratio. For more bulky guests, it's elusive how many of the respective alkyl groups are shifted into the negative ppm-range due to the anisotropic effect of capsule's walls. Therefore, the encapsulation degree of such guests was determined by comparing the integral of the remaining methylene groups adjacent to nitrogen atoms in tertiary amines **141** or tetraalkylammonium bromides **142$^+$Br$^-$** to their original values (6H for **141** or 8H for **142$^+$Br$^-$**, highlighted as asterisk * in the corresponding spectra). It is noteworthy that both methods yielded comparable values of encapsulation ratio for **141a** (44±2% determined by the terminal methyl groups between 0 and −1 ppm, 47±1% determined by the remaining methylene groups).

Determination of the deprotonation ratio: Depending on the deprotonation degree of the pyrogallolarene capsule **IVc**, the calculation of the deprotonation ratio was divided into three cases:

a) Little deprotonation: the broad peak of the phenol signals of **IVc$^-$** and water remained in the high-field range. The low field phenol peak of **IVc** (9.40–8.40 ppm, m, 24H, 'reference peak') was used for determining the amount of deprotonation, since it does not overlap with other signals. The ratio of deprotonation was directly determined by comparing the integral of the remaining phenolic protons to its original value (24H). This method is applicable for the experiment with imidazol (1 eq., Figure 3.21)

b) As more deprotonation occurs, the broad peak (phenol signals of **IVc$^-$** and water)

experienced some down-field shift but still remained < 4 ppm. All phenolic peaks became broad. The right halve of the 'reference peak' overlaps with the neighboring phenol signal. The deprotonation degree was determined by comparing the integral of the left halve of the reference peak (OH_A or $OH_{A'}$) to its original value (12H) as shown in Scheme 3.5. This method is applicable for the experiments with NEt_3 (0.5 – 0.7 eq.), DABCO (1 eq.) and morpholine (1 eq.).
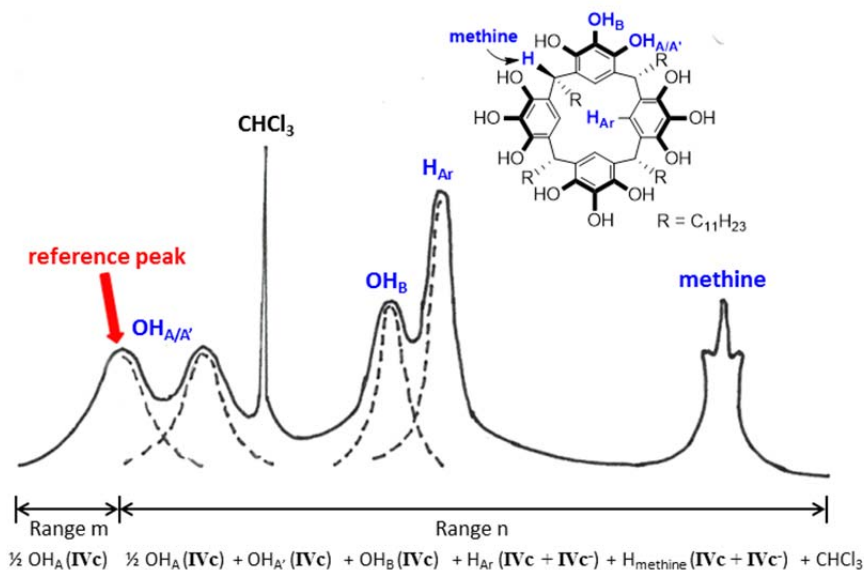
Scheme 3.5: Determination of deprotonation ratio according to method **b**.

c) At high deprotonation ratios (ca. ≥ 25%), the 'reference peak' and the neighboring phenolic group merge into a single broad peak. The broad peak corresponding to phenol signals of **IVc⁻** and water signals, shifts into the down-field region and overlaps with signals of **IVc**. The deprotonation degree is determined by comparing the integral of the left halve of the reference peak (OH_A and $OH_{A'}$) to its original value (24H) as described in Scheme 3.6. This method is applicable for the experiment with NEt_3 (0.8–1.0 eq.) and DMAP (1 eq.).
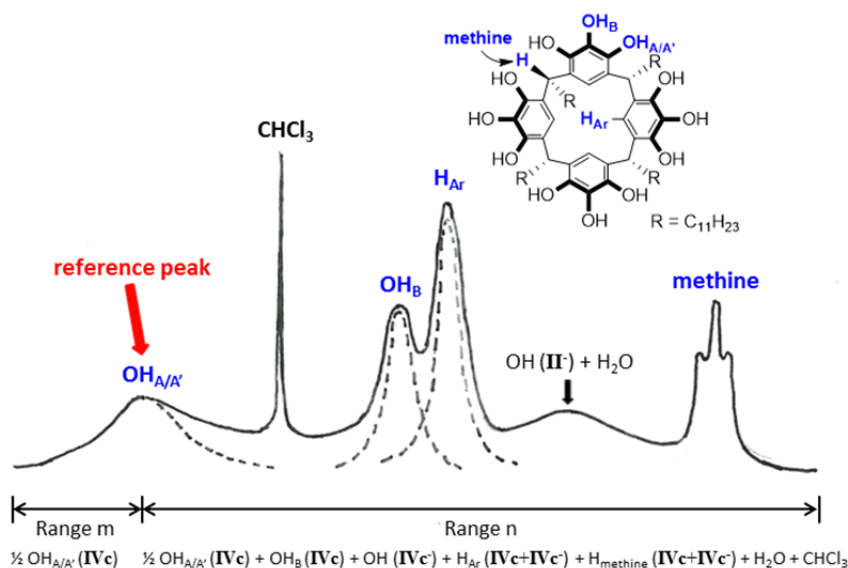
Scheme 3.6: Determination of deprotonation ratio according to method **c**.

The validity of methods **b** and **c** was verified in the titration experiment of pyrogallolarene capsule **IVc** with NEt$_3$ (Table 3.3) by comparing the calculated integrals in range **n** with the determined ones.

3.2.2.2 Binding studies with tertiary amines

^{1}H-NMR titration with triethylamine (141a)

To the stock solution of pyrogallolarene **7c** (198 μL, 11.7 mg, 10.0 μmol, 6.0 eq.) in a NMR-tube was added NEt$_3$-stock solution with a concentration of 8.4 mmol/L (a multiple of 20 μL, 0.167 μmol, 0.1 eq.). Then the sample was diluted with CDCl$_3$ to a volume of 0.50 mL, to obtain a sample of the desired **IVc**/NEt$_3$-ratio. After agitation the sample was allowed to equilibrate for $\geq$ 3 h and then subjected to NMR-spectroscopy.
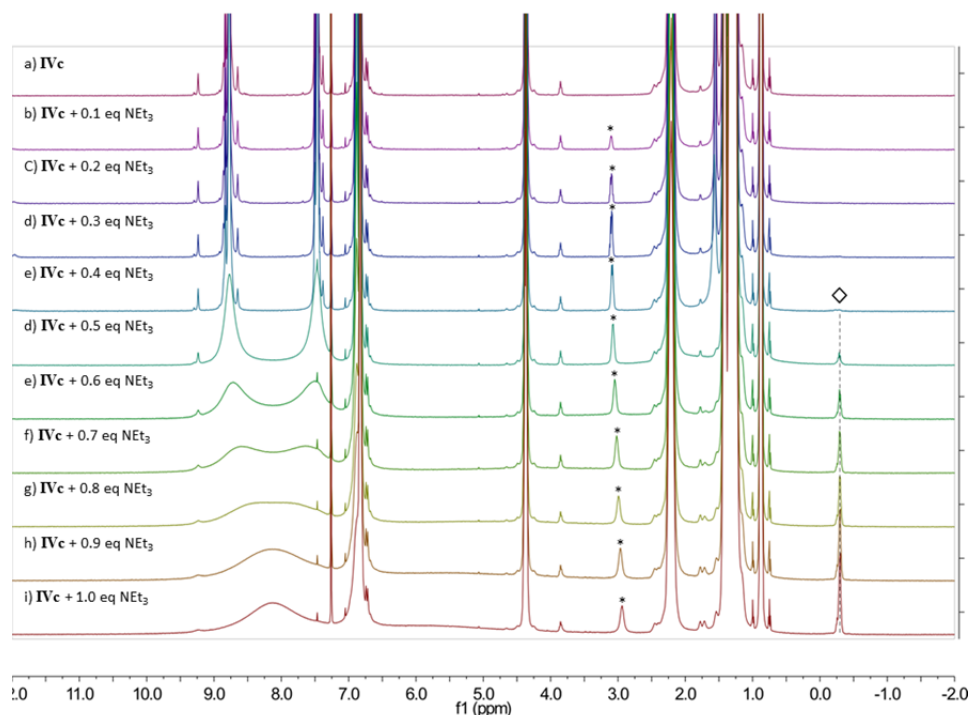
Figure 3.6: ^{1}H-NMR titration of capsule **IVc** (a) in CDCl$_3$ (3.3 mM) with various amounts of NEt$_3$ (b–i). Signals corresponding to free and encapsulated guest are highlighted by an asterisk and a square, respectively.

Table 3.3: Titration experiment of **IVc** with NEt$_3$. The methine peak (24H) was utilized as reference for integration. Integrals of H$_2$O (12.7H) and CHCl$_3$ (6.0H) were determined in a blank sample (entry 0). nd = not detectable.

entry	II/NEt$_3$	encapsulation ratio	Range n calc.	Range n determined	deprotonation method	deprotonation ratio
0	1:0		--			
1	1:0.1	0%				
2	1:0.2	2%				
3	1:0.3	4%	nd		nd	nd
4	1:0.4	6%				
5	1:0.5	10%	110.8	111.6	b	5%
6	1:0.6	22%	109.0	110.9	b	8%
7	1:0.7	28%	106.8	105.0	b	12%
8	1:0.8	37%	118.5	118.9	c	16%
9	1:0.9	40%	120.0	119.0	c	22%
10	1:1.0	45%	121.5	121.3	c	29%

Deprotonation ratios of **IVc** were determined by method **b** or **c** described in Scheme 3.5 or 3.6, respectively. The determined integrals in range n have a good correlation with the calculated values (Table 3.3).

DOSY-experiments of pyrogallolarene capsule IVc
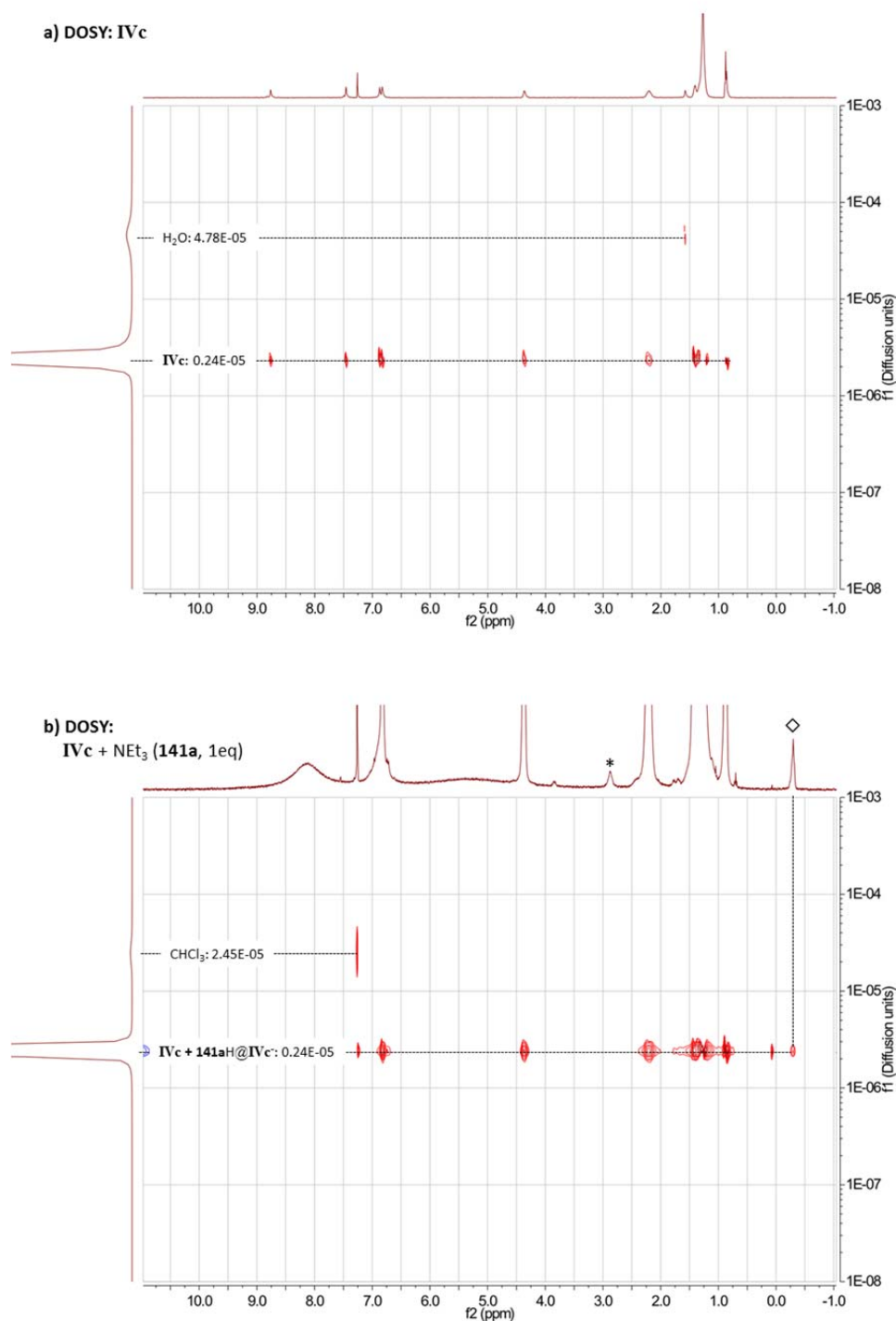
Figure 3.7: DOSY spectra of pyrogallolarene capsule **IVc**. The diffusion coefficients are given in cm^2/s. a) **IVc** (3.3 mM); b) **IVc** /NEt$_3$ = 1/1, **IVc** (3.3 mM), NEt$_3$ (3.3 mM). Signals corresponding to free and encapsulated guest are highlighted by an asterisk and a square, respectively.

Comparison of trialkylamines (141a–d)
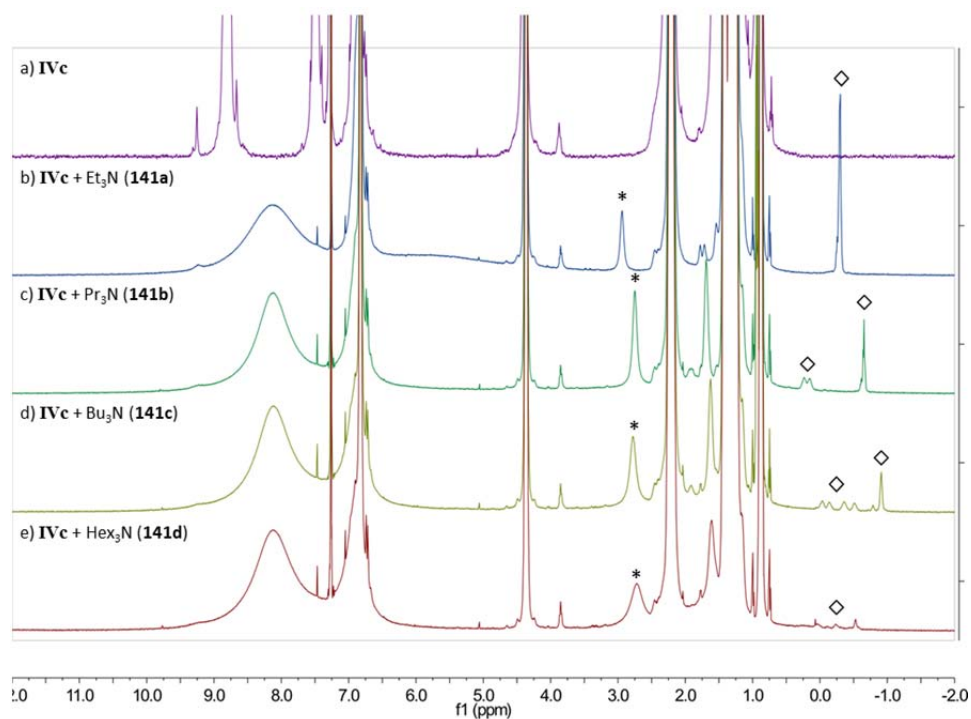
Figure 3.8: Binding and deprotonation studies of pyrogallolarene capsule **IVc**. a) **IVc** (3.3 mM), with b) Et₃N (**141a**) (3.3 mM); c) Pr₃N (**141b**) (3.3 mM); d) Bu₃N (**141c**) (3.3 mM); e) Hex₃N (**141d**) (3.3 mM). Signals corresponding to free and encapsulated guest are highlighted with an asterisk and a square, respectively.

3.2.2.3 Binding studies with tetraalkylammonium salts

Comparison of tetraalkylammonium bromides (6a–d⁺Br⁻)
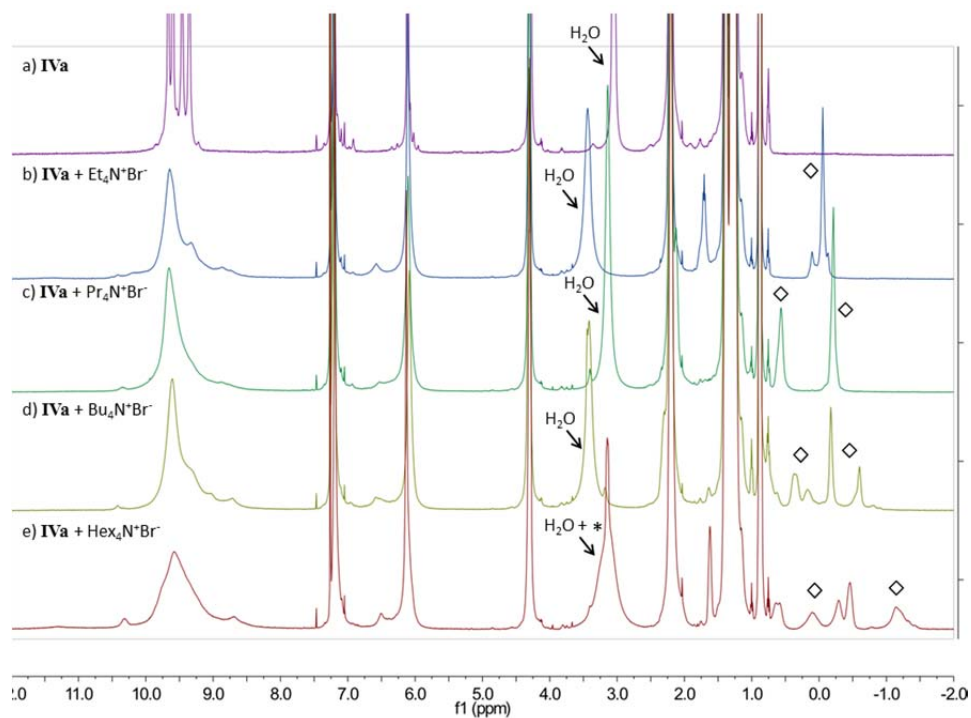
Figure 3.9: Binding studies of resorcinarene capsule **IVa**. a) **IVa** (3.3 mM), with b) Et$_4$N$^+$Br$^-$ (**142a$^+$Br$^-$**) (3.3 mM); c) Pr$_4$N$^+$Br$^-$ (**142b$^+$Br$^-$**) (3.3 mM); d) Bu$_4$N$^+$Br$^-$ (**142c$^+$Br$^-$**) (3.3 mM); e) Hex$_4$N$^+$Br$^-$ (**142d$^+$Br$^-$**) (3.3 mM). Signals corresponding to free and encapsulated guest are highlighted by an asterisk and a square, respectively.
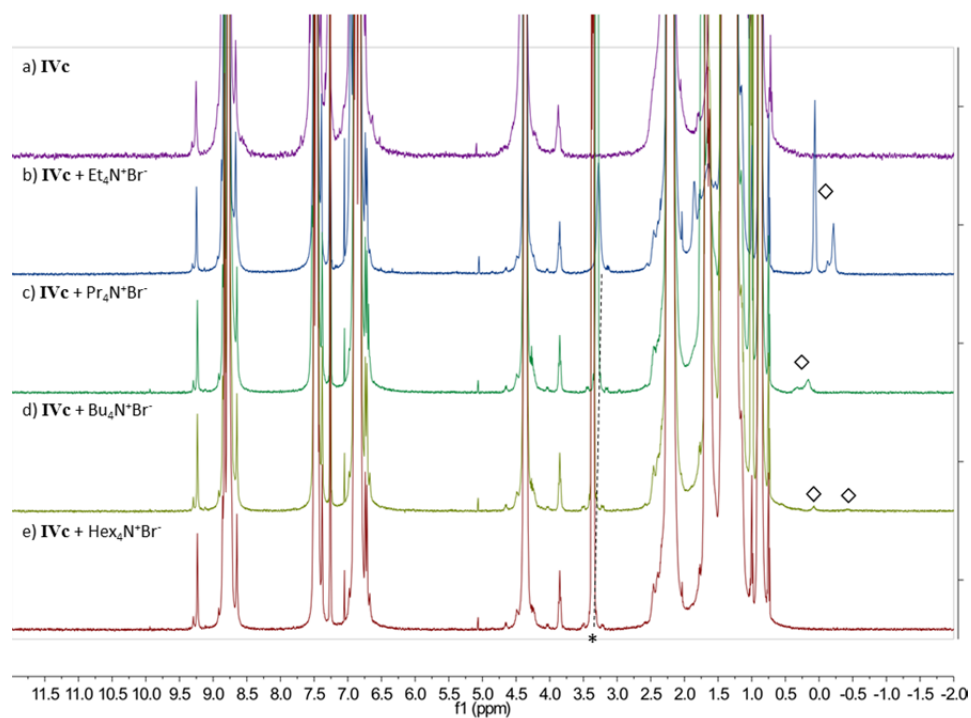
Figure 3.10: Binding studies of pyrogallolarene capsule **IVc**. a) **IVc** (3.3 mM), with b) Et$_4$N$^+$Br$^-$ (**142a$^+$Br$^-$**) (3.3 mM); c) Pr$_4$N$^+$Br$^-$ (**142b$^+$Br$^-$**) (3.3 mM); d) Bu$_4$N$^+$Br$^-$ (**142c$^+$Br$^-$**) (3.3 mM); e) Hex$_4$N$^+$Br$^-$ (**142d$^+$Br$^-$**) (3.3 mM). Signals corresponding to free and encapsulated guest are

highlighted by an asterisk and a square, respectively.
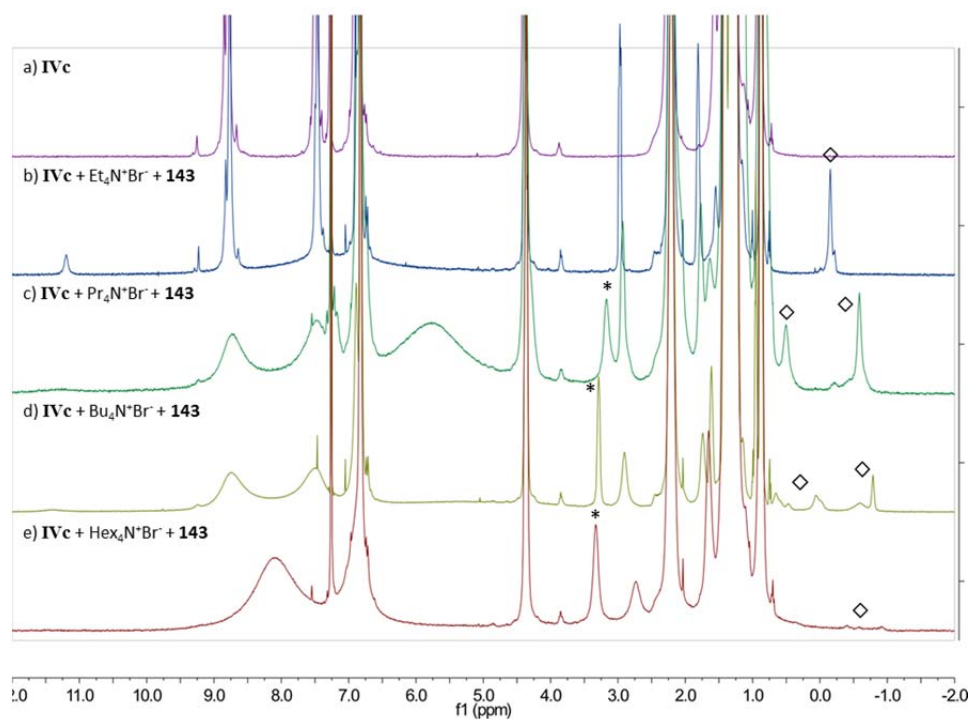
Figure 3.11: Binding studies of pyrogallolarene capsule **IVc**. a) **IVc** (3.3 mM), with b) $Et_4N^+Br^-$ (**142a$^+$Br$^-$**) and trioctadecylamine (**143**), both (3.3 mM); c) $Pr_4N^+Br^-$ (**142b$^+$Br$^-$**) and **143**, both (3.3 mM); d) $Bu_4N^+Br^-$ (**142c$^+$Br$^-$**) and **7**, both (3.3 mM); e) $Hex_4N^+Br^-$ (**142d$^+$Br$^-$**) and **143**, both (3.3 mM). Signals corresponding to free and encapsulated guest are highlighted by an asterisk and a square, respectively.

Investigations concerning the precipitate formed with $Et_4N^+Br^-$ (142a$^+$Br$^-$)

In the binding studies of **II** with $Et_4N^+Br^-$(**142a$^+$Br$^-$**) a precipitate formed. To clarify the reason for precipitate formation, samples of different **7c/142a$^+$Br$^-$**–ratios (Table 3.4) were prepared with tetraethylsilane (Et$_4$Si, **145**) as an internal standard (SiCH_2, 0.53 ppm, q, J = 7.9 Hz, 8H). The amount of precipitate increased with time. The samples were measured 48h after preparation.

Table 3.4: Investigation of the precipitation with $Et_4N^+Br^-$ (**142a$^+$Br$^-$**) and **IVc**.

sample	7c:142a$^+$Br$^-$:145	7c	Δ7c	142a$^+$Br$^-$ (free+encap.)	Δ142a$^+$Br$^-$	Δ7c: Δ142a$^+$Br$^-$
1	6:0:1	1.00eq.	—	—	—	—
2	0:1:1	—	—	1.00eq	—	—
3	6:2:1	4.14eq.	1.86eq.	(0.70+0.37)eq.	0.93eq.	**2.00:1**
4	6:4:1	2.94eq.	3.06eq.	(2.05+0.44)eq.	1.51eq.	**2.03:1**
5	6:6:1	1.68eq.	4.32eq.	(3.37+0.47)eq.	2.16eq.	**2.00:1**

Using Et_4Si as reference, the decrease in pyrogallolarene **7c** and **142a$^+$Br$^-$** was determined by comparing the corresponding integrals with the ones of sample 1 and sample 2 (Table 3.4). These experiments revealed a 2:1 stoichiometry of **7c** and **142a$^+$Br$^-$** in the precipitate and suggest that a dimer complex (**142a$^+$Br$^-$@7c$_2$**) was formed as precipitate. Dimeric capsules of pyrogallolarene (with shorter alkyl feet) containing ammonium species were previously observed in the solid state.[87e, 90] A DOSY-experiment confirmed the integrity of **IVc** as a hexameric assembly in solution when encapsulating **142a$^+$Br$^-$** (Figure 3.12).

The equilibrium between hexameric and dimeric pyrogallolarene capsule is obviously driven to the dimeric species by precipitation. By employing a more bulky guest such as tetrapropylammonium bromide (**142b$^+$Br$^-$**), precipitation was completely suppressed.
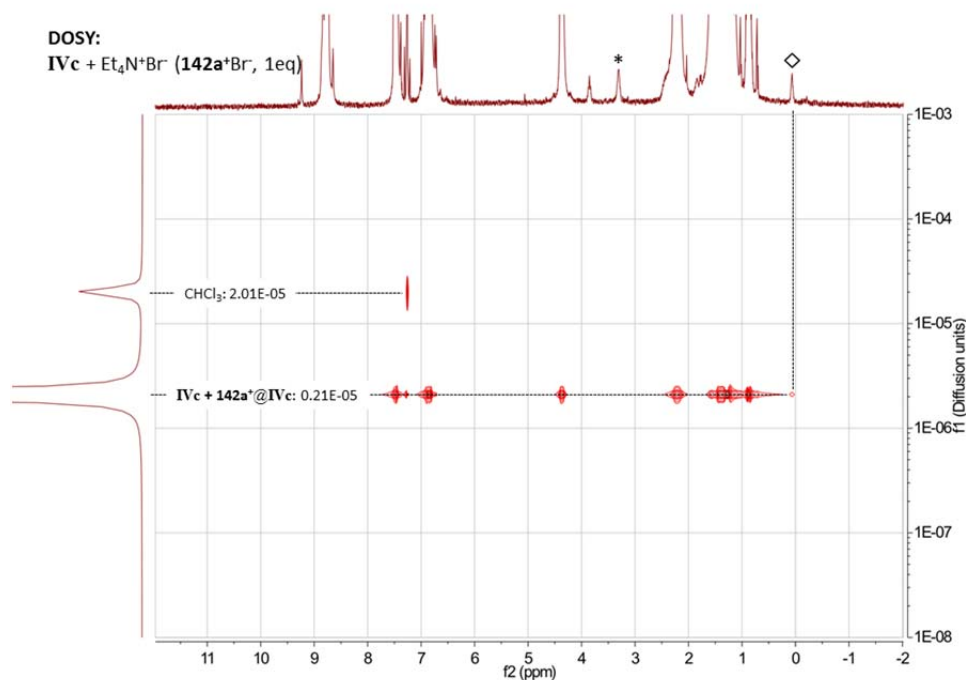
Figure 3.12: DOSY spectrum of pyrogallolarene capsule **IVc** (3.3 mM) with $Et_4N^+Br^-$ (**142a**$^+$**Br**$^-$). The diffusion coefficients are given in cm^2/s. **IVc/142a**$^+$**Br**$^-$ = 1/1. Signals corresponding to free and encapsulated guest are highlighted by an asterisk and a square, respectively.

Encapsulation studies with ethyltripropylammonium mesylate (142e$^+$MeSO$_3^-$)

The ammonium salt (**142e**$^+$**MeSO**$_3^-$) was selected to probe the position of the anion during encapsulation for the following reasons: (1) The medium size of cation **142e**$^+$ (between **142a**$^+$ and **142b**$^+$) not only efficiently prevents the formation of precipitate of the dimeric capsule of **7c**, but also yields a reasonable encapsulation ratio for the binding study. (2) Compared to the original counterion Br^-, $MeSO_3^-$ is detectable by ^{1}H- and ^{13}C-NMR spectroscopy, and, among the available organic counterions, best resembles the Br^- in terms of the acidity of the corresponding conjugated acids.

Synthesis of ethyltripropylammonium mesylate (6e$^+$MeSO$_3^-$): A mixture of ethyl methansulfonate (0.17 mL, 1.6 mmol, 1.0 eq.) and tripropylamine (1.52 mL, 8.0 mmol, 5.0 eq.) was stirred in a pressure tube at 60 ºC. After 24 h, the mixture was allowed to cool to rt and all volatile compounds were evaporated under reduced pressure (4 mbar) at 50 ºC. The residue was washed with Et_2O (3x), to give the product (91 mg, 21%) as a pale yellow wax.

¹H-NMR (500 MHz, CDCl₃): δ 3.53 (q, *J* = 7.2 Hz, **CH₂**CH₃, 2H), 3.28 – 3.19 (m, **CH₂**CH₂CH₃, 6H), 2.76 (s, **Me**SO₃⁻, 3H), 1.79 – 1.70 (m, CH₂**CH₂**CH₃, 6H), 1.37 (t, *J* = 7.2 Hz, CH₂**CH₃**, 3H), 1.05 (t, *J* = 7.3 Hz, CH₂CH₂**CH₃**, 9H).

¹³C-NMR (126 MHz, CDCl₃): δ 60.2 (**CH₂**CH₂CH₃), 54.7 (**CH₂**CH₃), 39.7 (**Me**SO₃⁻), 15.8 (CH₂**CH₂**CH₃), 11.0 (CH₂CH₂**CH₃**), 8.1 (CH₂**CH₃**).

IR (ATR): ṽ (cm⁻¹) = 3447, 2974, 1186, 1039, 768.

Binding studies with 142e⁺MeSO₃⁻
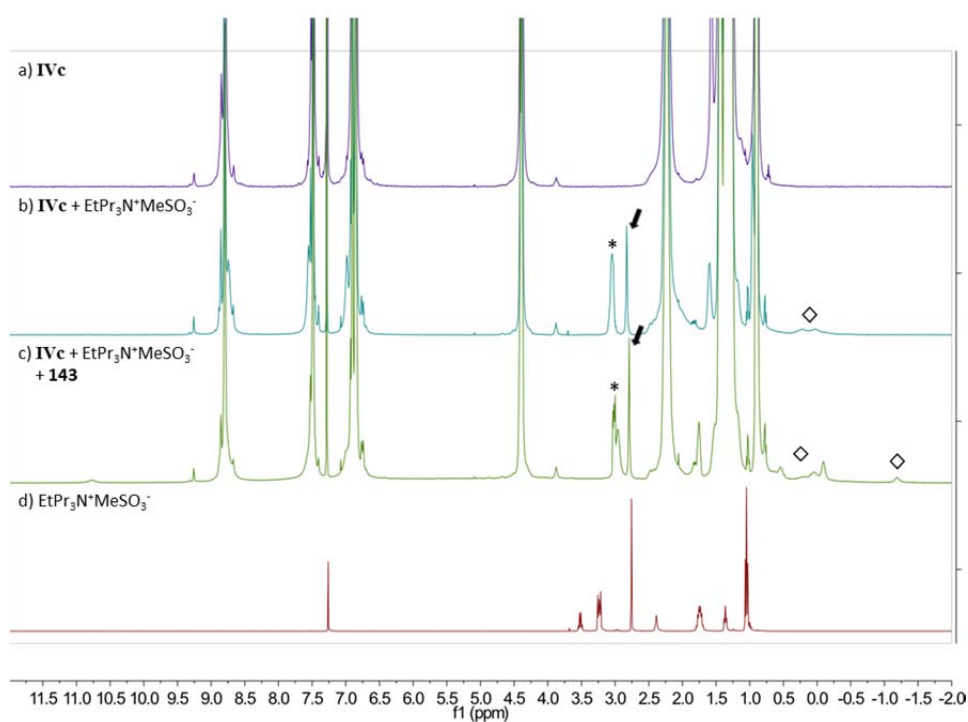
Figure 3.13: Binding studies (¹H-NMR) of pyrogallolarene capsule **IVc**. a) **IVc** (3.3 mM), with b) EtPr₃N⁺MeSO₃⁻ (3.3 mM), integral of MeSO₃⁻: 2.99±0.03 H; c) EtPr₃N⁺MeSO₃⁻ and trioctadecylamine (**143**), both (3.3 mM), integral of MeSO₃⁻: 3.04±0.01 H; d) only EtPr₃N⁺MeSO₃ (3.3 mM). Signals of free guest are highlighted by an asterisk (methylene groups adjacent to N–atoms) and an arrow (*Me*SO₃⁻). Signals of encapsulated guest are highlighted by a square.
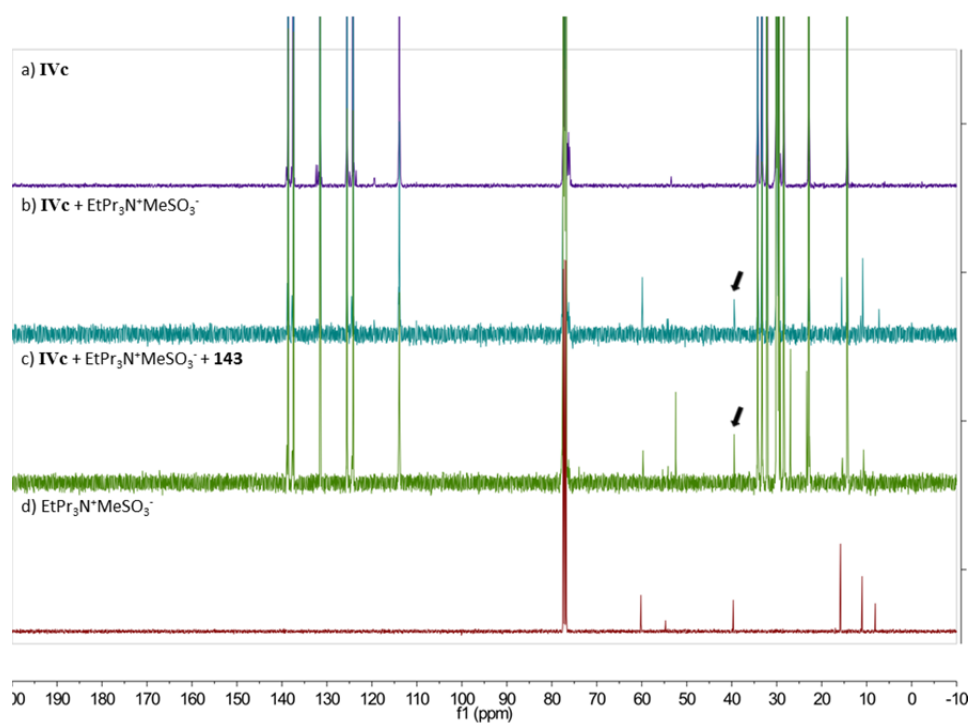
Figure 3.14: Binding studies (^{13}C-NMR) of pyrogallolarene capsule **IVc**. a) **IVc** (3.3 mM), with b) EtPr$_3$N$^+$MeSO$_3^-$ (3.3 mM); c) EtPr$_3$N$^+$MeSO$_3^-$ and trioctadecylamine (**143**), both (3.3 mM). d) only EtPr$_3$N$^+$MeSO$_3$ (3.3 mM). Signal of free mesylate is highlighted by an arrow.
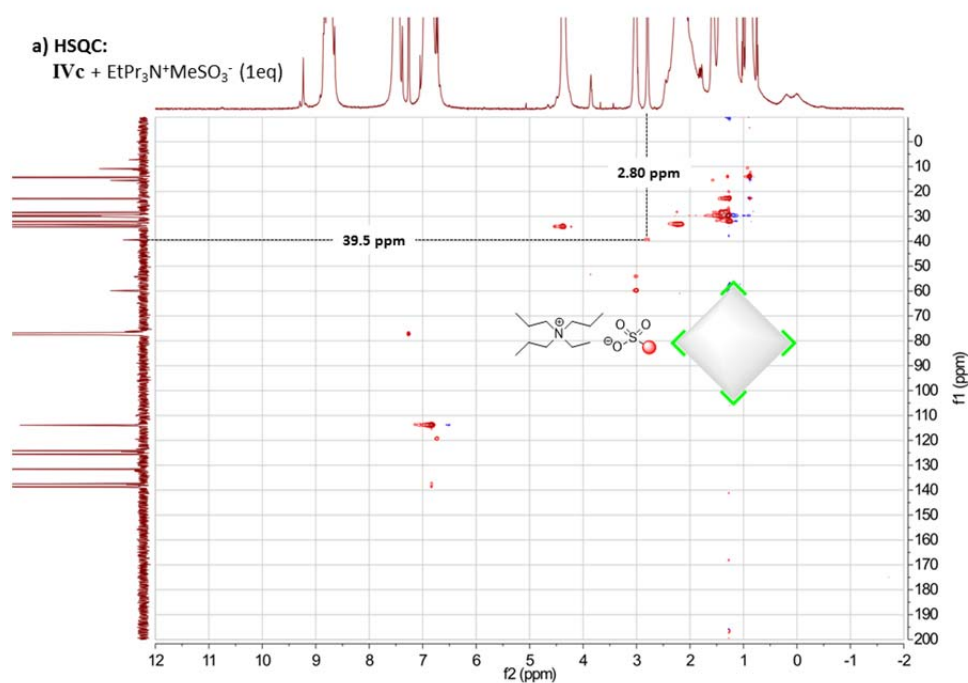
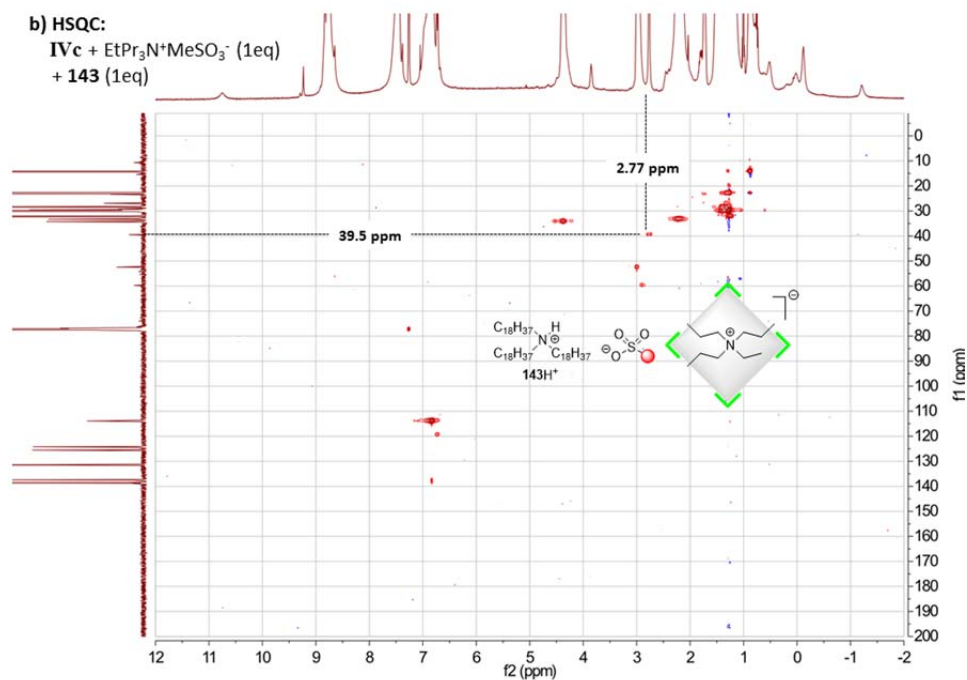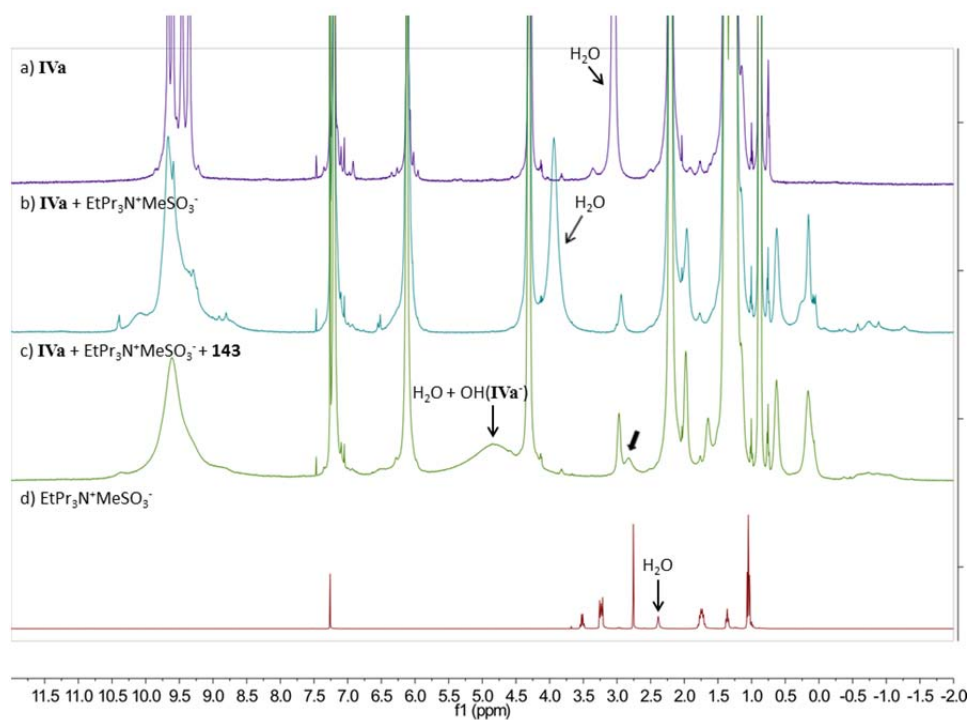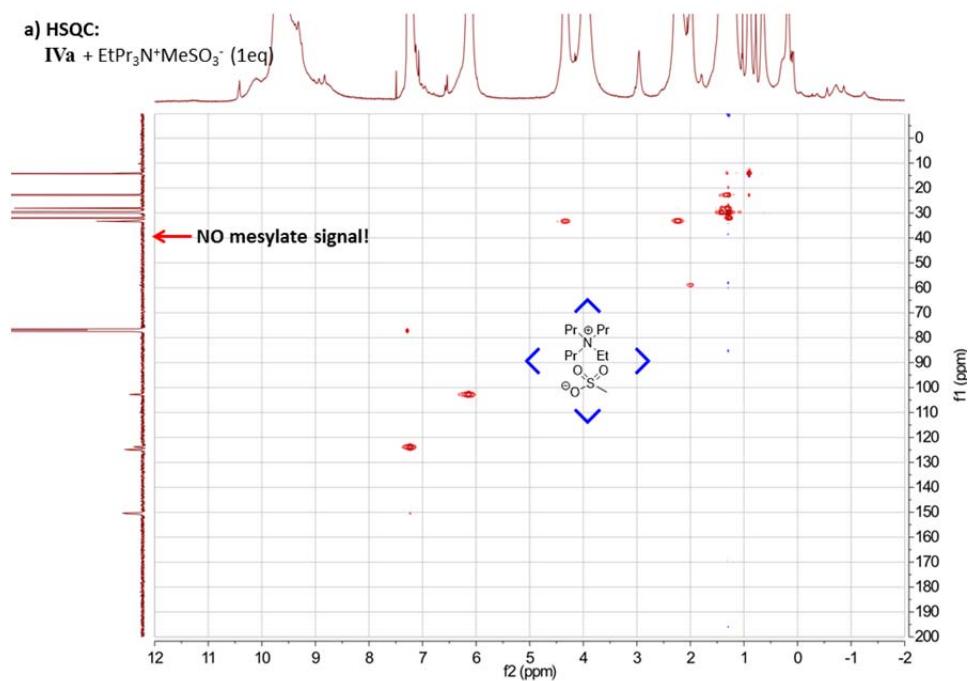**Figure 3.15**: HSQC spectra of pyrogallolarene capsule **IVc** (3.3 mM), with a) EtPr$_3$N$^+$MeSO$_3^-$ (3.3 mM); b) EtPr$_3$N$^+$MeSO$_3^-$ and trioctadecylamine (**143**), both (3.3 mM). Cross peaks of the mesylate group are highlighted.
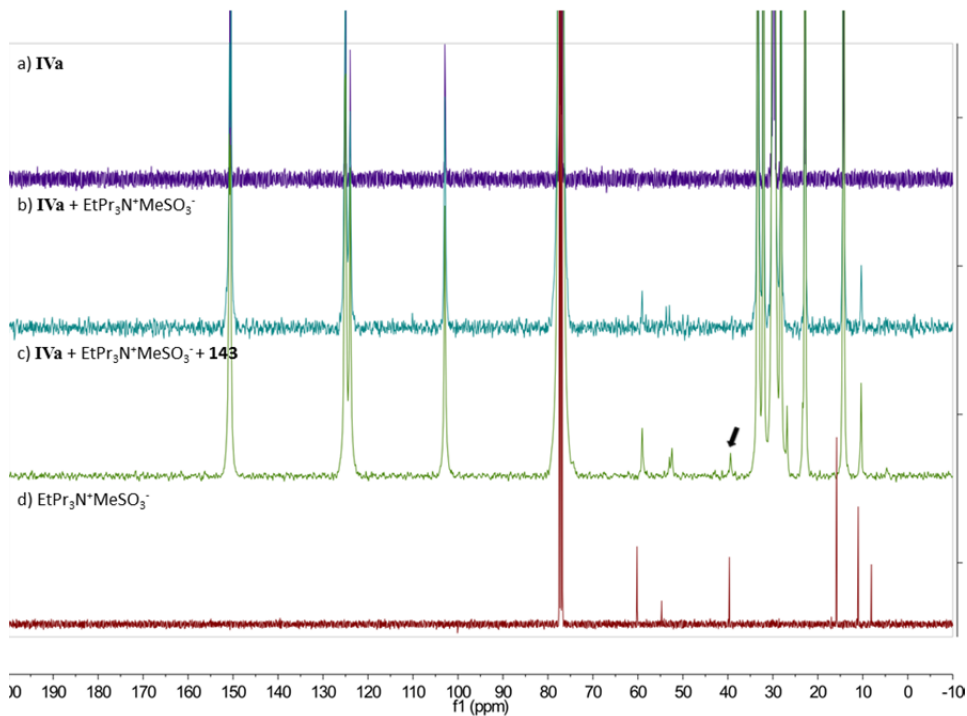
Figure 3.16: Binding studies (^{1}H-NMR) of resorcinarene capsule **IVa**. a) **IVa** (3.3 mM), with b) EtPr$_3$N$^+$MeSO$_3^-$ (3.3 mM); c) EtPr$_3$N$^+$MeSO$_3^-$ and trioctadecylamine (**143**), both (3.3 mM). d) only EtPr$_3$N$^+$MeSO$_3$ (3.3 mM). Signal of the free mesylate is highlighted by an arrow.
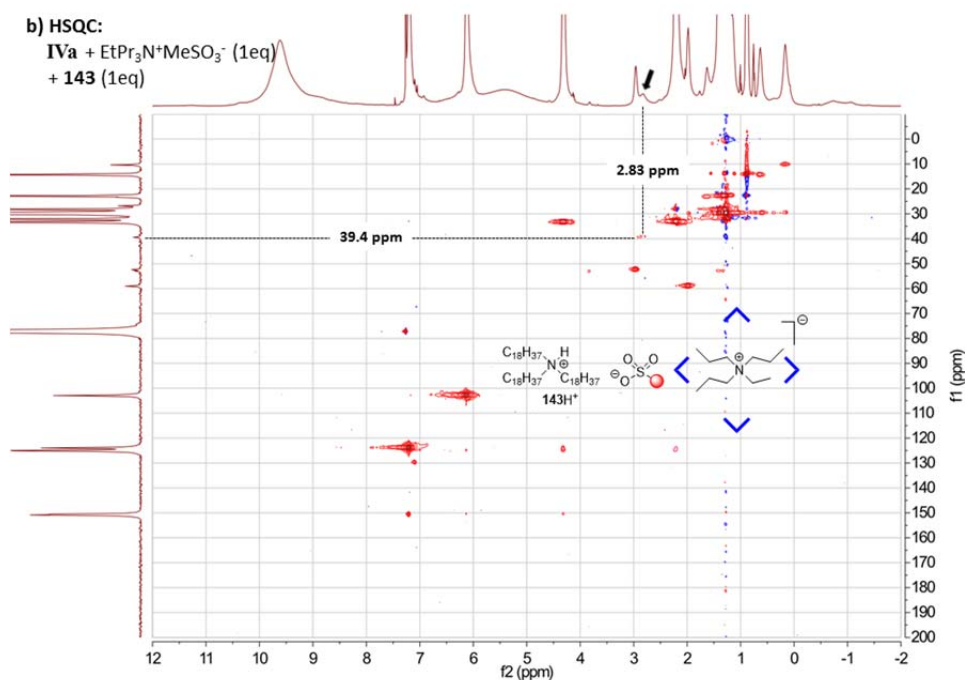
Figure 3.17: Binding studies (^{13}C-NMR) of resorcinarene capsule **IVa**. a) **IV** (3.3 mM), with b) EtPr$_3$N$^+$MeSO$_3^-$ (3.3 mM); c) EtPr$_3$N$^+$MeSO$_3^-$ and trioctadecylamine (**143**), both (3.3 mM). d) only EtPr$_3$N$^+$MeSO$_3$ (3.3 mM). Signal of the free mesylate is highlighted by an arrow.

Figure 3.18: HSQC spectra of resorcinarene capsule **IVa** (3.3 mM) with a) $EtPr_3N^+MeSO_3^-$ (3.3 mM); b) $EtPr_3N^+MeSO_3^-$ and trioctadecylamine (**143**), both (3.3 mM). Cross peaks of the mesylate group are highlighted.

3.2.2.4 Catalysis attempts with pyrogallolarene capsule IVc

Procedure for cyclization reactions

To a solution of substrate (2.9 μL NOH (**131**), 16.7 μmol, 10 eq.) in 0.48 mL $CDCl_3$ was added *n*-decane stock solution in $CDCl_3$ (20 μL, 167 mmol/L, 3.34 μmol, 2.0 eq.). At this point, a sample (approx. 10 μL) was diluted with 0.2 mL *n*-hexane and subjected to GC analysis (initial sample). Afterwards, pyrogallolarene capsule **IVc** (11.7 mg, 1.67 μmol, 1.0 eq.) was added and the reaction was kept at 30 °C. After 1 d, 2 d and 3 d, the reaction was sampled as described above and analyzed by GC. Although DOSY-experiment confirmed the encapsulation of substrate by capsule **IVc**, less than 5% conversions and no formation of cyclized terpene products could be detected after 3 d.
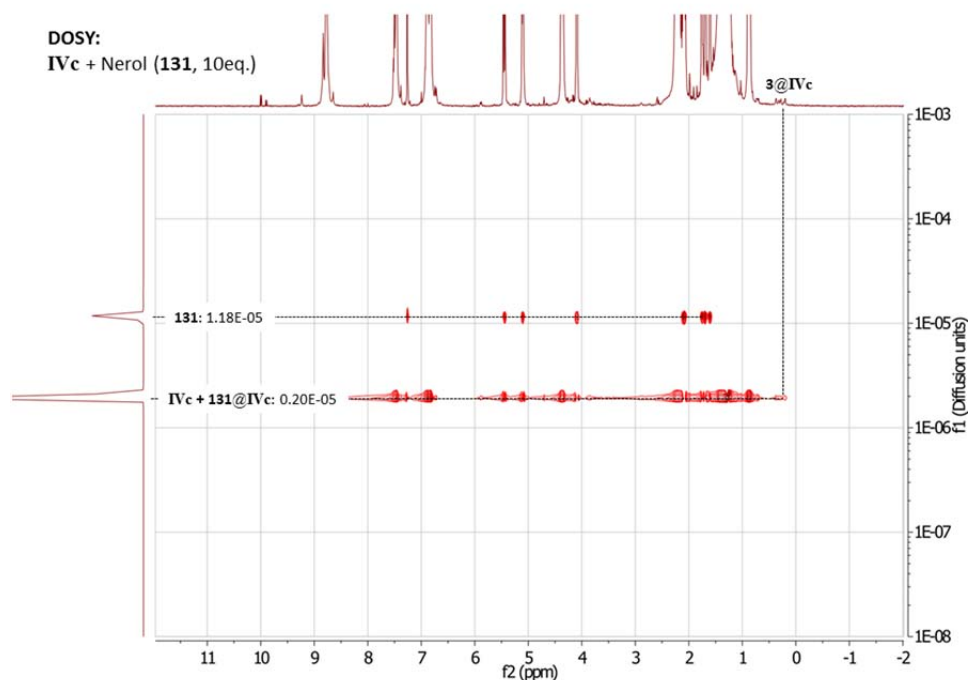
Figure 3.19: DOSY spectrum of pyrogallolarene capsule **IVc** (3.3 mM) with nerol (**131**) (33 mM). The diffusion coefficients are given in cm^2/s.

Determination of the pKa value of pyrogallolarene IVc

The acidity of hexamer **IVc** was determined in analogy to **IVa**,[82] by a series of protonation experiments with amines of different basicity.
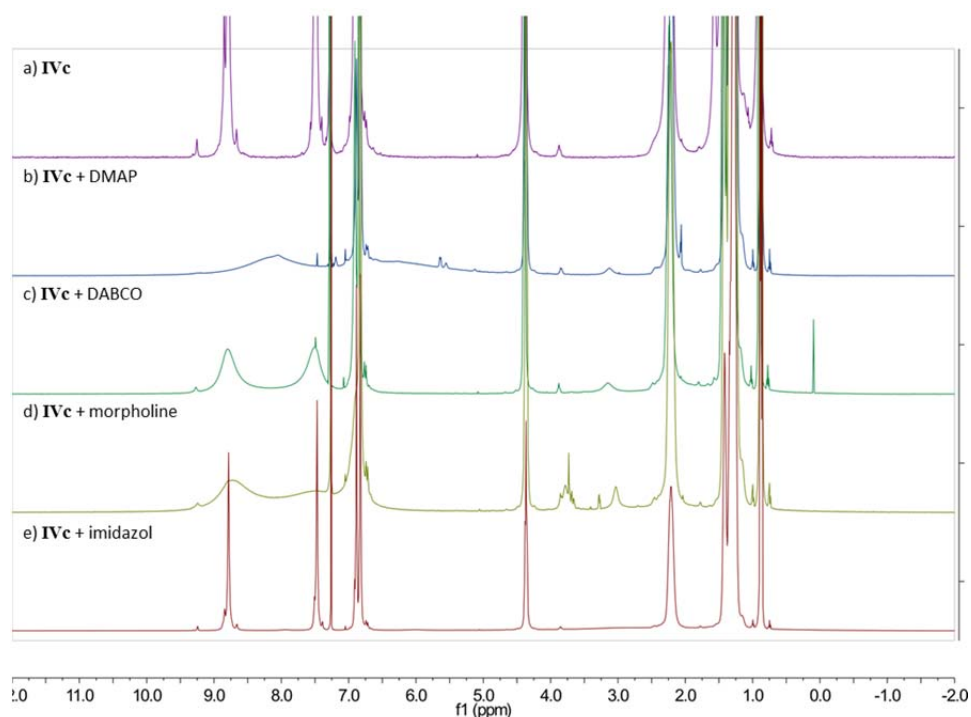
Figure 3.20: ^{1}H-NMR spectra of pyrogallolarene capsule **IVc. a) IVc** (3.3 mM), with b) DMAP (3.3 mM); c) DABCO (3.3 mM); d) morpholine (3.3 mM); d) imidazole (3.3 mM).
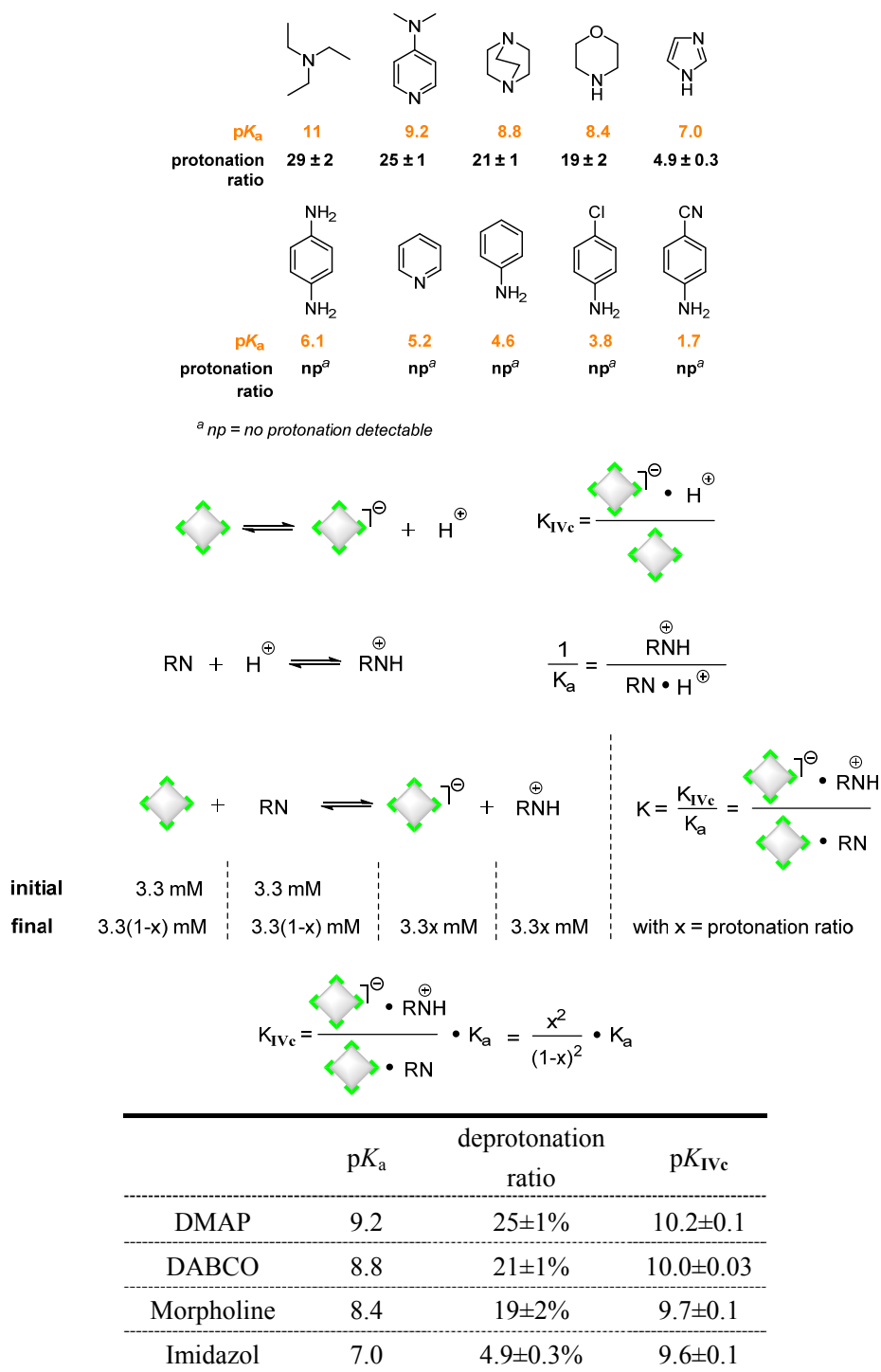

	pK_a	protonation ratio

	triethylamine	DMAP	DABCO	morpholine	imidazole
pK_a	11	9.2	8.8	8.4	7.0
protonation ratio	29 ± 2	25 ± 1	21 ± 1	19 ± 2	4.9 ± 0.3

	1,4-diaminobenzene	pyridine	aniline	4-chloroaniline	4-cyanoaniline
pK_a	6.1	5.2	4.6	3.8	1.7
protonation ratio	np^a	np^a	np^a	np^a	np^a

^{a} np = no protonation detectable

	pK_a	deprotonation ratio	pK_{IVc}
DMAP	9.2	25±1%	10.2±0.1
DABCO	8.8	21±1%	10.0±0.03
Morpholine	8.4	19±2%	9.7±0.1
Imidazol	7.0	4.9±0.3%	9.6±0.1

Figure 3.21: Estimation of the pK_a value of **IVc** by addition of 1.0 eq. of base to a solution of **IVc** in CDCl$_3$ (3.3 mM); SD from three independent experiments are given; pK_a values (measured in water) were taken from literature.[93] The pK_a was estimated to be between 9.5 and 10.

Capsule **IVc** displayed a lower degree of deprotonation, as compared to capsule **IVa**. Bases with a pK_a-value ranging from 11 to 8.4, caused deprotonation ratios ranging

from 29% to 19% (Figure 3.21). The deprotonation ratio dropped to 5% with imidazole ($pK_a = 7$). Weaker bases employed, failed to cause any deprotonation. Based on these results, the pK_a-value of capsule **IVc** was determined to be between 9.5 and 10 (ca. four pK_a units higher than resorcinarene capsule **IVa**).

The surprising acidity difference of **IVa** and **IVc** may arise from mesomeric destabilization (Figure 3.22).[94] The pK_a value for hydroquinone (**146**) (benzene-1,4-diol) is considerably higher (ca. 0.5 pK_a units) than from benzene-1,3-diol (**147**), due to mesomeric destabilization of the phenolate. Benzene-1,3-diol (**147**) is even slightly more acidic than **148**, although the negative charge is stabilized by hydrogen bonding in **148**-. This further highlights the mesomeric destabilization of a phenolate by an *ortho* hydroxy group. The mesomeric destabilization (ca. 0.5 pK_a units) might well be multiplied in capsule **IVc**, due to the high number of destabilizing groups in *ortho*-positions, and therefore may explain the big difference in acidity between **IVa** and **IVc** (ca. four pK_a units).
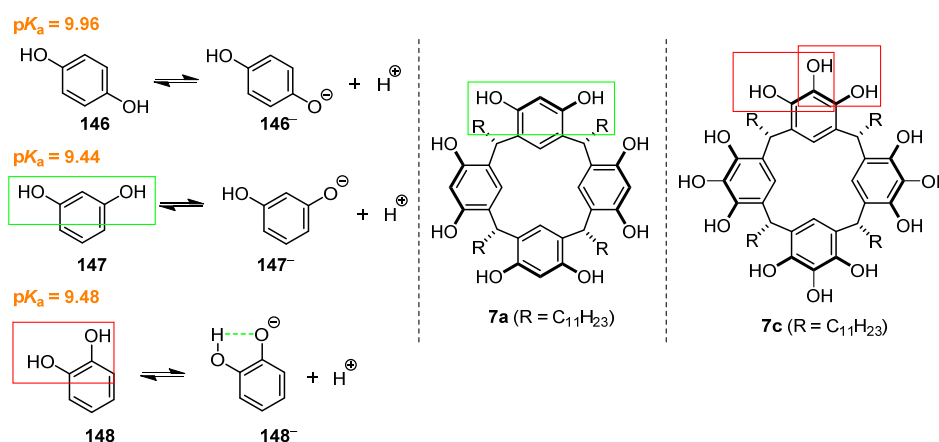

Figure 3.22: Mesomeric destabilization of phenolate anions by *ortho*- and *para*-hydroxy groups.

Catalysis attempts with additional external acids

Since the failed activation of the substrate via protonation by **IVc** is the likely cause of its catalytic incompetence, we tried to initiate the cyclization reaction within **IVc** by the addition of external stronger acids (10 mol% methanesulfonic acid or trifuoroacetic acid; 50 mol% *o*-nitrobenzoic acid, benzoic acid, *p*-nitrophenol or phenol). However, no difference to the background reaction (caused by added external

acid) was detectable, indicating that the reaction only took place outside of **IVc**.

3.2.2.5 Quantum chemical DFT calculations

The structures of resorcinarene (capsule **I**) and pyrogallolarene (capsule **II**) hexamers with 455-486 atoms were optimized at the density functional theory (DFT) level using the dispersion corrected PBE–D3 functional,[95] the multipole accelerated resolution of identity (RI–MARIJ) approximation,[96] and def2–SVP basis sets.[97] The optimizations were performed with and without triethylamine in its protonated ($HNEt_3^+$) and neutral (NEt_3) forms, as well as with tetraethylammonium (NEt_4^+) and its salt ($NEt_4^+Br^-$) using the X–ray structures of the respective empty capsules as starting points. Solvation effects were treated using the conductor like–screening model (COSMO)[98] to model the dielectric screening of trichloromethane with an set to 4.81. Binding affinities of the tetraalkylammonium species in **I** and **II** were also probed at PBE-D3/def2-TZVP level and using different density functionalities (PBE0-D3,[99] TPSS-D3,[100] B3LYP-D3.[101] All quantum chemical calculations were performed using TURBOMOLE v. 5.5–5.6.[102] Visual Molecular Dynamics (VMD) was used for visualization.[103]

Table 3.5. Binding affinity difference of NEt_4^+ (in kcal mol^{-1}) with and without a halogen anion in capsules **IVa** and **IVc** at different density functional theory levels. $\Delta E(NEt_4^+:Br^-)$ and $\Delta E(NEt_4^+)$ refer to the affinity difference between $NEt_4^+Br^-$ and NEt_4^+ towards capsules **IVa** vs. **IVc**, respectively. A negative (positive) sign refers to an exergonic (endergonic) binding of NEt_4^+ to cluster **IVa** in comparison to cluster **IVc**. The medium was modeled as $\varepsilon=4.81$ in all calculations.

	$\Delta E(NEt_4^+Br^-)$	$\Delta E(NEt_4^+)$
PBE-D3/def2-SVP	-3.2	+10.6
PBE-D3/def2-TZVP	-8.8	+4.1
PBE0-D3/def2-SVP	-3.3	+10.6
B3LYP-D3/def2-SVP	-2.7	+12.1
TPSS-D3/def2-SVP	-3.5	+10.7

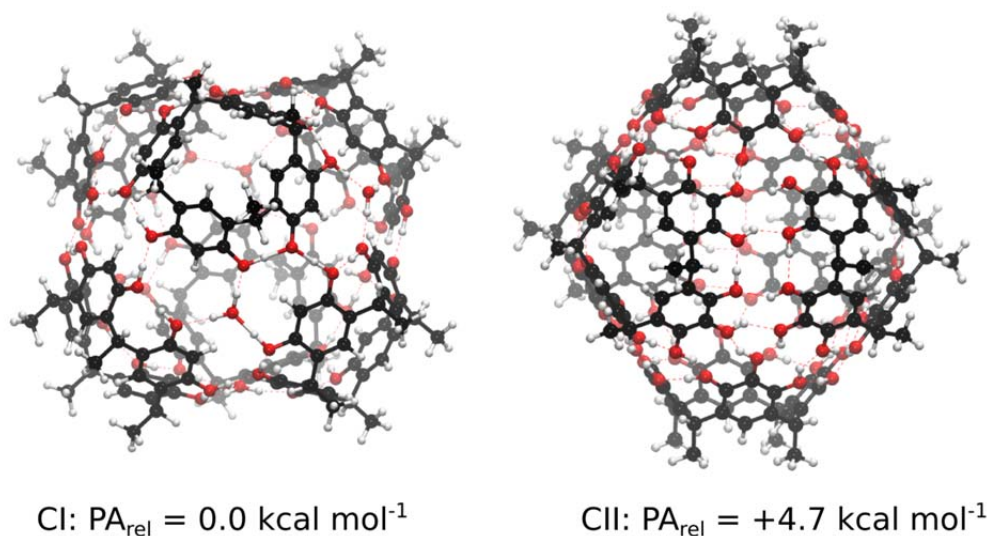CI: PA$_{rel}$ = 0.0 kcal mol^{-1} CII: PA$_{rel}$ = +4.7 kcal mol^{-1}

Figure 3.23: DFT calculations at the PBE–D3/def2–SVP/ε=4.81 level of theory, suggesting that the relative proton affinity (PA) of **IVa** is *ca*. 5 kcal mol^{-1} lower than that of **IVc**. The PAs were estimated relative to the monomeric building blocks **7a** and **7c**.
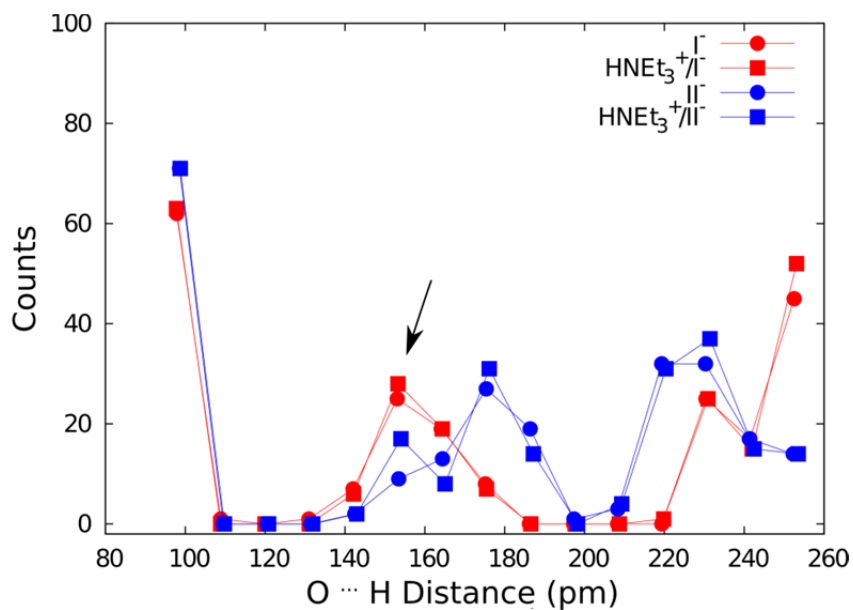

Figure 3.24: Distribution of O⋯H distances (in pm) in capsules **IVa** and **IVc** obtained from PBE-D3/def2-SVP/ε=4.81 optimized structures. Delocalization of the anionic defect across several hydrogen bonds in **IVa** (red), while **IVc** shows a more localized defect (in blue). The delocalization of the anionic defect might lead to a lowering of the relative pK_a in capsule **IVa**.

3.2.2.6 ESP surface map of capsule I and II

The ESP surfaces were calculated with Spartan ´14 (Wavefunction, Irvine, CA, 2014, Version 1.1.8). The fully optimized structures were submitted to a single–point energy calculation on the AM1 level, to obtain the ESP data. It was reported, that the semi–empirical AM1 method produces reliable ESP surfaces.[104] The potential energy values displayed in Figure. 3.3, range from +104.6 kJ/mol (25 kcal/mol) to −104.6 kJ/mol (−25 kcal/mol). The color red is indicating a value equal to or larger than the maximum in negative potential. The color blue is indicating a value equal to or larger than the maximum in positive potential.

4 Summary and Outlook

In pursuit of performing enzyme-like catalysis with artificial catalysts, we identified the hydrogen-bonded supramolecular capsule **IVa** as a promising system. Self-assembling from six copies of the commercially available resorcinarene unit **7a** and eight water molecules in apolar organic solvents, capsule **IVa** surrounds a void of 1375 Å^3. The spacious cavity of **IVa** allows the binding of guests of different sizes and plays a key role in overcoming the notorious product-inhibition issue often encountered in supramolecular catalysis, which arises from the excessive binding of guest molecules.

In an effort to elucidate the puzzling affinity of **IVa** towards tertiary amines, we revealed that **IVa** functions as a Brønsted acid and accommodates the amines in their protonated form. By titrating **IVa** with amines of various basicities, the pK_a-value of **IVa** was determined as approximately 5.5–6. The dramatically increased acidity of **IVa** compared to a normal phenol (pK_a 10) can be explained as a synergistic effect of three factors: (1) the formed ammonium species are stabilized by cation–π interaction. (2) The negative charge of the capsule is delocalized by proton migration within the hydrogen-bond network. (3) The formation of the complex is additionally facilitated by the attractive Coulomb interactions between the ammonium species and the anionic capsule.

We then used **IVa** to impose substrate bias in a stoichiometric reaction. The origin of the bias bears resemblance to those of enzymatic reactions. Capsule **IVa** selectively protonates and encapsulates the suitably sized Wittig ylide **125**, while **IVa** only effects reversible protonation of the larger Wittig ester **126** due to its resistance to encapsulation. Consequently, the large Wittig ylide **126** remained reactive, and it was selectively converted in the presence of **IVa** when the mixture of **125** and **126** was exposed to an aldehyde.

In a follow-up study, we found that capsule **IVa** was capable of catalyzing the acetal hydrolysis reaction in a size-selective fashion. Smaller acetals were more efficiently

encapsulated by **IVa**, thus leading to faster conversions. Several control experiments corroborated that the hydrolysis was facilitated within **IVa**. This example bears close resemblance to the enzymatic catalysis: The suitably-sized substrate is preferentially selected by the reaction host and activated by protonation, the energy of the cationic transition states and intermediates are likely lowered by the cation–π interactions within the aromatic cavity. Finally, the formed product is replaced by a new substrate to close the catalytic cycle.

Most importantly, we succeeded in catalyzing the challenging tail-to-head terpene cyclization with capsule **IVa** as the catalyst. Linear monoterpene alcohols – geraniol, nerol and linalool – were successfully cyclized inside the cavity of **IVa**. By utilizing the less nucleophilic acetate as the leaving group, we were able to suppress the interception of the cationic intermediate and to achieve a non-stop cyclization cascade with geranyl acetate as the substrate. Mechanistic studies conducted with fluoro derivatives disclosed that the neryl substrates cyclized in a concerted fashion (S_N2), while ionization (S_N1) and isomerization preceded the cyclization reaction in the case of geranyl substrates. Our investigations also shed some light on the biosynthesis of terpenes. The different cyclization behavior between geranyl and linalyl acetate provided strong evidence that the direct isomerization of the *transoid* cation into the *cisoid* form, considered so far unlikely in terpene cyclases, is possible inside **IVa**. We also compared the catalytic efficiency of our system to those of natural enzymes. The much higher value of the Michaelis constant in our system suggested a significantly weaker binding of the substrate to capsule **Iva** as compared to natural enzymes.

To understand the origin of the catalytic activity of capsule **IVa**, we became interested in the structurally related pyrogallolarene capsule **IVc**, which is incapable of catalyzing the acetal hydrolysis and the terpene cyclization reactions. As DFT-calculations indicated comparable stabilization of cations by **IVa** and **IVc**, we infer that the much lower acidity of **IVc** (approximately pK_a 9.5–10) is the most likely cause for its catalytic incompetence. We also found an explanation for the low affinity of **IVc** toward alkyl ammonium species, which puzzled the supramolecular

community in the last decade. Evidence showed that **IVc** does not stabilize anions inside its cavity. Therefore, alkyl ammonium salts are encapsulated only to a small extent with concomitant charge separation.

In the THT cyclization catalyzed by **IVa**, the leaving group plays multiple roles: It acts as the binding motif to drive the encapsulation of the substrate; the degree of its lability determines the reactivity of the substrate; the nucleophilicity and the basicity of the cleaved leaving group have a significant impact on the lifetime of the reactive carbocationic intermediates. Therefore, it would be revealing to investigate the influence of additional leaving groups (alcohol, acetate, benzoate, ether, etc.) on the cyclization of monoterpenes. As capsule **IVa** possesses a spacious cavity, it is reasonable to think about the cyclization of sesquiterpenes, to access more complex products (Figure 4.1).
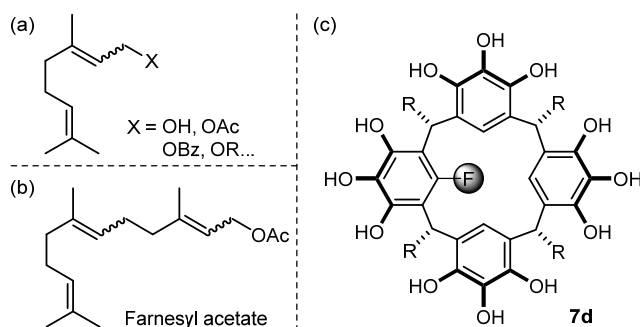
Figure 4.1: Prospective of this thesis: (a) further investigation the influence of leaving groups; (b) cyclization of sesquiterpenes inside **IVa**; (c) synthesis of fluorine-containing pyrogallolarene **7d**.

The design of highly efficient artificial catalysts that rival natural enzymes is a long-term goal of the scientific community. To gain the knowledge for realizing it, modification or optimization of known systems would be a reasonable first step. For this reason, we want to synthesize pyrogallolarene **7d**. Since the low acidity is postulated as the reason for the catalytic incompetence of capsule **IVc**, the introduction of an electron-withdrawing fluorine substituent might increase the acidity of the assembled capsule and render it catalytic activity.

5 Reference

[1]   J. B. Sumner, *J. Biol. Chem.* **1926**, *70*, 97-98.

[2]   C. C. F. Blake, D. F. Koenig, G. A. Mair, A. C. T. North, D. C. Phillips, V. R. Sarma, *Nature* **1965**, *206*, 757-761.

[3]   S. J. Benkovic, S. Hammes-Schiffer, *Science* **2003**, *301*, 1196-1202.

[4]   W. P. Jencks, *Catalysis in Chemistry and Enzymology*, Dover, **1987**.

[5]   D. E. Koshland, *Proc. Natl. Acad. Sci. U.S.A.* **1958**, *44*, 98-104.

[6]   N. C. Ha, M. S. Kim, W. T. Lee, K. Y. Choi, B. H. Oh, *J. Biol. Chem.* **2000**, *275*, 41100-41106.

[7]   A. Warshel, P. K. Sharma, M. Kato, Y. Xiang, H. Liu, M. H. M. Olsson, *Chem. Rev.* **2006**, *106*, 3210-3235.

[8]   W. R. Cannon, S. J. Benkovic, *J. Biol. Chem.* **1998**, *273*, 26257-26260.

[9]   (a) S. Száraz, D. Oesterhelt, P. Ormos, *Biophys. J.* **1994**, *67*, 1706-1712; (b) F. H. Westheimer, *Tetrahedron* **1995**, *51*, 3-20.

[10]   D. L. Nelson, A. L. Lehninger, M. M. Cox, *Lehninger Principles of Biochemistry*, W. H. Freeman, **2008**.

[11]   P. Mattei, F. Diederich, *Helv. Chim. Acta* **1997**, *80*, 1555-1588.

[12]   L. G. Mackay, R. S. Wylie, J. K. M. Sanders, *J. Am. Chem. Soc.* **1994**, *116*, 3141-3142.

[13]   I. Tabushi, *Acc. Chem. Res.* **1982**, *15*, 66-72.

[14]   K. I. Assaf, W. M. Nau, *Chem. Soc. Rev.* **2015**, *44*, 394-418.

[15]   D. J. Cram, H. E. Katz, I. B. Dicker, *J. Am. Chem. Soc.* **1984**, *106*, 4987-5000.

[16]   (a) M. D. Pluth, R. G. Bergman, K. N. Raymond, *Acc. Chem. Res.* **2009**, *42*, 1650-1659; (b) M. Yoshizawa, M. Fujita, *Bull. Chem. Soc. Jpn.* **2010**, *83*, 609-618; (c) T. K. Ronson, S. Zarra, S. P. Black, J. R. Nitschke, *Chem. Commun.* **2013**, *49*, 2476-2490; (d) M. Han, D. M. Engelhard, G. H. Clever, *Chem. Soc. Rev.* **2014**, *43*, 1848-1860.

[17]   (a) F. Hof, S. L. Craig, C. Nuckolls, J. J. Rebek, *Angew. Chem. Int. Ed.* **2002**, *41*, 1488-1508; (b) T. Evan-Salem, I. Baruch, L. Avram, Y. Cohen, L. C. Palmer, J. Rebek, Jr., *Proc. Natl. Acad. Sci. U.S.A.* **2006**, *103*, 12296-12300.

[18]   J. H. Jordan, B. C. Gibb, *Chem. Soc. Rev.* **2015**, *44*, 547-585.

[19]   (a) T. S. Koblenz, J. Wassenaar, J. N. H. Reek, *Chem. Soc. Rev.* **2008**, *37*, 247-262; (b) M. Yoshizawa, J. K. Klosterman, M. Fujita, *Angew. Chem. Int. Ed.* **2009**, *48*, 3418-3438.

[20]   D. L. Caulder, R. E. Powers, T. N. Parac, K. N. Raymond, *Angew. Chem. Int. Ed.* **1998**, *37*, 1840-1843.

[21]   A. V. Davis, K. N. Raymond, *J. Am. Chem. Soc.* **2005**, *127*, 7912-7919.

[22]   D. Fiedler, D. H. Leung, R. G. Bergman, K. N. Raymond, *J. Am. Chem. Soc.* **2004**, *126*, 3674-3675.

[23]   M. Ziegler, J. L. Brumaghim, K. N. Raymond, *Angew. Chem. Int. Ed.* **2000**, *39*, 4119-4121.

[24]   S. M. Biros, R. G. Bergman, K. N. Raymond, *J. Am. Chem. Soc.* **2007**, *129*, 12094-12095.

[25]   A. V. Davis, D. Fiedler, G. Seeber, A. Zahl, R. van Eldik, K. N. Raymond, *J. Am. Chem. Soc.* **2006**, *128*, 1324-1333.

[26]   A. V. Davis, D. Fiedler, M. Ziegler, A. Terpin, K. N. Raymond, *J. Am. Chem. Soc.* **2007**, *129*, 15354-15363.

[27]   C. Zhao, Q.-F. Sun, W. M. Hart-Cooper, A. G. DiPasquale, F. D. Toste, R. G. Bergman, K. N. Raymond, *J. Am. Chem. Soc.* **2013**, *135*, 18802-18805.

[28] P. Mal, D. Schultz, K. Beyeh, K. Rissanen, J. R. Nitschke, *Angew. Chem. Int. Ed.* **2008**, *47*, 8297-8301.

[29] M. M. J. Smulders, S. Zarra, J. R. Nitschke, *J. Am. Chem. Soc.* **2013**, *135*, 7039-7046.

[30] J. L. Bolliger, A. M. Belenguer, J. R. Nitschke, *Angew. Chem. Int. Ed.* **2013**, *52*, 7958-7962.

[31] J. M. Kang, J. Rebek, *Nature* **1996**, *382*, 239-241.

[32] L. C. Palmer, J. J. Rebek, *Org. Biomol. Chem.* **2004**, *2*, 3051-3059.

[33] L. R. MacGillivray, J. L. Atwood, *Nature* **1997**, *389*, 469-472.

[34] L. Avram, Y. Cohen, *J. Am. Chem. Soc.* **2002**, *124*, 15148-15149.

[35] L. Avram, Y. Cohen, *Org. Lett.* **2003**, *5*, 3329-3332.

[36] M. Yamanaka, A. Shivanyuk, J. Rebek, *J. Am. Chem. Soc.* **2004**, *126*, 2939-2943.

[37] (a) S. Slovak, L. Avram, Y. Cohen, *Angew. Chem. Int. Ed.* **2010**, *49*, 428-431; (b) S. Slovak, Y. Cohen, *Chem. Eur. J.* **2012**, *18*, 8515-8520.

[38] (a) A. Shivanyuk, J. Rebek, *Proc. Natl. Acad. Sci. U.S.A.* **2001**, *98*, 7662-7665; (b) I. Philip, A. E. Kaifer, *J. Org. Chem.* **2005**, *70*, 1558-1564.

[39] A. Shivanyuk, J. J. Rebek, *Chem. Commun.* **2001**, 2424-2425.

[40] D. Fiedler, R. G. Bergman, K. N. Raymond, *Angew. Chem. Int. Ed.* **2004**, *43*, 6748-6751.

[41] D. Fiedler, H. van Halbeek, R. G. Bergman, K. N. Raymond, *J. Am. Chem. Soc.* **2006**, *128*, 10240-10252.

[42] C. J. Brown, R. G. Bergman, K. N. Raymond, *J. Am. Chem. Soc.* **2009**, *131*, 17530-17531.

[43] C. J. Hastings, D. Fiedler, R. G. Bergman, K. N. Raymond, *J. Am. Chem. Soc.* **2008**, *130*, 10977-10983.

[44] M. D. Pluth, R. G. Bergman, K. N. Raymond, *Science* **2007**, *316*, 85-88.

[45] M. D. Pluth, R. G. Bergman, K. N. Raymond, *J. Am. Chem. Soc.* **2008**, *130*, 11423-11429.

[46] M. D. Pluth, R. G. Bergman, K. N. Raymond, *Angew. Chem. Int. Ed.* **2007**, *46*, 8587-8589.

[47] M. D. Pluth, R. G. Bergman, K. N. Raymond, *J. Org. Chem.* **2009**, *74*, 58-63.

[48] C. J. Hastings, M. D. Pluth, R. G. Bergman, K. N. Raymond, *J. Am. Chem. Soc.* **2010**, *132*, 6938-6940.

[49] C. J. Hastings, R. G. Bergman, K. N. Raymond, *Chem. Eur. J.* **2014**, *20*, 3966-3973.

[50] C. J. Hastings, M. P. Backlund, R. G. Bergman, K. N. Raymond, *Angew. Chem. Int. Ed.* **2011**, *50*, 10570-10573.

[51] N. Dudareva, D. Martin, C. M. Kish, N. Kolosova, N. Gorenstein, J. Fäldt, B. Miller, J. Bohlmann, *Plant Cell* **2003**, *15*, 1227-1241.

[52] W. M. Hart-Cooper, K. N. Clary, F. D. Toste, R. G. Bergman, K. N. Raymond, *J. Am. Chem. Soc.* **2012**, *134*, 17873-17876.

[53] W. M. Hart-Cooper, C. Zhao, R. M. Triano, P. Yaghoubi, H. L. Ozores, K. N. Burford, F. D. Toste, R. G. Bergman, K. N. Raymond, *Chem. Sci.* **2015**, *6*, 1383-1393.

[54] D. M. Kaphan, F. D. Toste, R. G. Bergman, K. N. Raymond, *J. Am. Chem. Soc.* **2015**, *137*, 9202-9205.

[55] C. Zhao, F. D. Toste, K. N. Raymond, R. G. Bergman, *J. Am. Chem. Soc.* **2014**, *136*, 14409-14412.

[56] Z. J. Wang, C. J. Brown, R. G. Bergman, K. N. Raymond, F. D. Toste, *J. Am. Chem. Soc.* **2011**, *133*, 7358-7360.

[57] Z. J. Wang, K. N. Clary, R. G. Bergman, K. N. Raymond, F. D. Toste, *Nature Chem.* **2013**, *5*, 100-103.

[58]   A. G. Salles, S. Zarra, R. M. Turner, J. R. Nitschke, *J. Am. Chem. Soc.* **2013**, *135*, 19143-19146.

[59]   (a) J. Kang, J. Rebek, *Nature* **1997**, *385*, 50-52; (b) J. Kang, G. Hilmersson, J. Santamaría, J. Rebek, *J. Am. Chem. Soc.* **1998**, *120*, 3650-3656.

[60]   J. Kang, J. Santamaría, G. Hilmersson, J. Rebek, *J. Am. Chem. Soc.* **1998**, *120*, 7389-7390.

[61]   A. Cavarzan, A. Scarso, P. Sgarbossa, G. Strukul, J. N. H. Reek, *J. Am. Chem. Soc.* **2011**, *133*, 2848-2851.

[62]   A. Cavarzan, J. N. H. Reek, F. Trentin, A. Scarso, G. Strukul, *Catal. Sci. Technol.* **2013**, *3*, 2898-2901.

[63]   G. Bianchini, G. L. Sorella, N. Canever, A. Scarso, G. Strukul, *Chem. Commun.* **2013**, *49*, 5322-5324.

[64]   S. Giust, G. La Sorella, L. Sperni, F. Fabris, G. Strukul, A. Scarso, *Asian J. Org. Chem.* **2015**, *4*, 217-220.

[65]   (a) F. G. Fallon, R. M. Herbst, *J. Org. Chem.* **1957**, *22*, 933-936; (b) D. M. Zimmerman, R. A. Olofson, *Tetrahedron Lett.* **1969**, *10*, 5081-5084.

[66]   T. Jin, S. Kamijo, Y. Yamamoto, *Tetrahedron Lett.* **2004**, *45*, 9435-9437.

[67]   G. La Sorella, L. Sperni, G. Strukul, A. Scarso, *ChemCatChem* **2015**, *7*, 291-296.

[68]   S. Shimizu, T. Kiuchi, N. Pan, *Angew. Chem.* **2007**, *119*, 6562-6565.

[69]   S. Shimizu, A. Usui, M. Sugai, Y. Suematsu, S. Shirakawa, H. Ichikawa, *Eur. J. Org. Chem.* **2013**, *2013*, 4734-4737.

[70]   J. S. Dickschat, *Nat. Prod. Rep.* **2011**, *28*, 1917-1936.

[71]   E. Breitmaier, *Terpenes: Flavors, Fragrances, Pharmaca, Pheromones*, Wiley, **2006**.

[72]   W. Eisenreich, A. Bacher, D. Arigoni, F. Rohdich, *CMLS, Cell. Mol. Life Sci.* **2004**, *61*, 1401-1426.

[73]   (a) C. D. Poulter, H. C. Rilling, *Biochemistry* **1976**, *15*, 1079-1083; (b) R. Croteau, *Chem. Rev.* **1987**, *87*, 929-954.

[74]   (a) D. E. Cane, *Chem. Rev.* **1990**, *90*, 1089-1103; (b) D. W. Christianson, *Chem. Rev.* **2006**, *106*, 3412-3442; (c) M. Baunach, J. Franke, C. Hertweck, *Angew. Chem. Int. Ed.* **2015**, *54*, 2604-2626.

[75]   (a) E. J. Corey, J. Lee, *J. Am. Chem. Soc.* **1993**, *115*, 8873-8874; (b) R. A. Yoder, J. N. Johnston, *Chem. Rev.* **2005**, *105*, 4730-4756.

[76]   K. Ishihara, S. Nakamura, H. Yamamoto, *J. Am. Chem. Soc.* **1999**, *121*, 4906-4907.

[77]   A. Sakakura, A. Ukai, K. Ishihara, *Nature* **2007**, *445*, 900-903.

[78]   (a) S. A. Snyder, D. S. Treitler, *Angew. Chem. Int. Ed.* **2009**, *48*, 7899-7903; (b) S. A. Snyder, D. S. Treitler, A. P. Brucks, *J. Am. Chem. Soc.* **2010**, *132*, 14303-14314.

[79]   S. V. Pronin, R. A. Shenvi, *Nature Chem.* **2012**, *4*, 915-920.

[80]   (a) G. Stork, A. W. Burgstahler, *J. Am. Chem. Soc.* **1955**, *77*, 5068-5077; (b) A. Eschenmoser, L. Ruzicka, O. Jeger, D. Arigoni, *Helv. Chim. Acta* **1955**, *38*, 1890-1904.

[81]   S. C. Kampranis, D. Ioannidis, A. Purvis, W. Mahrez, E. Ninga, N. A. Katerelos, S. Anssour, J. M. Dunwell, J. Degenhardt, A. M. Makris, P. W. Goodenough, C. B. Johnson, *Plant Cell* **2007**, *19*, 1994-2005.

[82]   Q. Zhang, K. Tiefenbacher, *J. Am. Chem. Soc.* **2013**, *135*, 16213-16219.

[83]   Q. Zhang, K. Tiefenbacher, *Nature Chem.* **2015**, *7*, 197-202.

[84]   (a) D. M. Vriezema, M. Comellas Aragonès, J. A. A. W. Elemans, J. J. L. M. Cornelissen, A. E.

Rowan, R. J. M. Nolte, *Chem. Rev.* **2005**, *105*, 1445-1490; (b) J. Meeuwissen, J. N. H. Reek, *Nat Chem* **2010**, *2*, 615-621; (c) L. Marchetti, M. Levine, *ACS Catal.* **2011**, *1*, 1090-1118; (d) M. J. Wiester, P. A. Ulmann, C. A. Mirkin, *Angew. Chem. Int. Ed.* **2011**, *50*, 114-137; (e) M. Raynal, P. Ballester, A. Vidal-Ferran, P. W. N. M. van Leeuwen, *Chem. Soc. Rev.* **2014**, *43*, 1734-1787; (f) C. J. Brown, F. D. Toste, R. G. Bergman, K. N. Raymond, *Chem. Rev.* **2015**, *115*, 3012-3035; (g) S. H. A. M. Leenders, R. Gramage-Doria, B. de Bruin, J. N. H. Reek, *Chem. Soc. Rev.* **2015**, *44*, 433-448; (h) S. Zarra, D. M. Wood, D. A. Roberts, J. R. Nitschke, *Chem. Soc. Rev.* **2015**, *44*, 419-432.

[85]   L. Catti, K. Tiefenbacher, *Chem. Commun.* **2015**, *51*, 892-894.

[86]   (a) L. Avram, Y. Cohen, *Org. Lett.* **2002**, *4*, 4365-4368; (b) A. Shivanyuk, J. Rebek, *J. Am. Chem. Soc.* **2003**, *125*, 3432-3433; (c) L. Avram, Y. Cohen, J. Rebek Jr, *Chem. Commun.* **2011**, *47*, 5368-5375; (d) S. Giust, G. La Sorella, L. Sperni, G. Strukul, A. Scarso, *Chem. Commun.* **2015**, *51*, 1658-1661.

[87]   (a) T. Gerkensmeier, W. Iwanek, C. Agena, R. Frohlich, S. Kotila, C. Nather, J. Mattay, *Eur. J. Org. Chem.* **1999**, 2257-2262; (b) J. L. Atwood, L. J. Barbour, A. Jerga, *Chem. Commun.* **2001**, *0*, 2376-2377; (c) A. Shivanyuk, J. Rebek, *Chem. Commun.* **2001**, 2374-2375; (d) L. Avram, Y. Cohen, *J. Am. Chem. Soc.* **2003**, *125*, 16180-16181; (e) A. Shivanyuk, J. C. Friese, S. Döring, J. Rebek, *J. Org. Chem.* **2003**, *68*, 6489-6496; (f) L. Avram, Y. Cohen, *J. Am. Chem. Soc.* **2004**, *126*, 11556-11563; (g) V. Guralnik, L. Avram, Y. Cohen, *Org. Lett.* **2014**, *16*, 5592-5595; (h) J. L. Atwood, L. J. Barbour, A. Jerga, *Proc. Natl. Acad. Sci. U.S.A.* **2002**, *99*, 4837-4841.

[88]   L. Avram, Y. Cohen, *Org. Lett.* **2003**, *5*, 1099-1102.

[89]   S. Yariv-Shoushan, Y. Cohen, *Org. Lett.* **2016**, *18*, 936-939.

[90]   (a) A. Ahman, M. Luostarinen, K. Rissanen, M. Nissinen, *New J. Chem.* **2007**, *31*, 169-177; (b) N. K. Beyeh, K. Rissanen, *Isr. J. Chem.* **2011**, *51*, 769-780.

[91]   S. Bartoli, S. Roelens, *J. Am. Chem. Soc.* **1999**, *121*, 11908-11909.

[92]   M. C. Letzel, C. Agena, J. Mattay, *J. Mass Spectrom.* **2002**, *37*, 63-68.

[93]   J. R. W. P. Jencks, *Ionization constants of acids and bases, Vol. 1*, CRC Press, Cleveland, **1976**.

[94]   We thank Prof. Dr. Ulrich Lüning, Kiel Univerity, for this hypothesis.

[95]   (a) J. P. Perdew, K. Burke, M. Ernzerhof, *Phys. Rev. Lett.* **1996**, *77*, 3865-3868; (b) S. Grimme, J. Antony, S. Ehrlich, H. Krieg, *J. Chem. Phys.* **2010**, *132*, 154104.

[96]   M. Sierka, A. Hogekamp, R. Ahlrichs, *J. Chem. Phys.* **2003**, *118*, 9136-9148.

[97]   F. Weigend, R. Ahlrichs, *Phys. Chem. Chem. Phys.* **2005**, *7*, 3297-3305.

[98]   A. Klamt, G. Schuurmann, *J. Chem. Soc., Perkin Trans. 2* **1993**, 799-805.

[99]   C. Adamo, V. Barone, *J. Chem. Phys.* **1999**, *110*, 6158-6170.

[100]   J. Tao, J. P. Perdew, V. N. Staroverov, G. E. Scuseria, *Phys. Rev. Lett.* **2003**, *91*, 146401.

[101]   (a) A. D. Becke, *J. Chem. Phys.* **1993**, *98*, 5648-5652; (b) C. Lee, W. Yang, R. G. Parr, *Phys. Rev. B* **1988**, *37*, 785-789.

[102]   R. Ahlrichs, M. Bär, M. Häser, H. Horn, C. Kölmel, *Chem. Phys. Lett.* **1989**, *162*, 165-169.

[103]   W. Humphrey, A. Dalke, K. Schulten, *J. Mol. Graphics* **1996**, *14*, 33-38.

[104]   S. Mecozzi, A. P. West, D. A. Dougherty, *Proc. Natl. Acad. Sci. USA* **1996**, *93*, 10566-10571.

6 Bibliographic Data of Complete Publications

This chapter provides the readers with the bibliographic details of the publications summarized in Chapter 3.1 of this thesis to facilitate the retrieval of the complete manuscripts and supporting information.

6.1 Hexameric Resorcinarene Capsule is a Brønsted Acid: Investigation and Application to Synthesis and Catalysis

Qi Zhang and Konrad Tiefenbacher*

Department Chemie, Technische Universität München, D-85747 Garching, Germany

E-mail: konrad.tiefenbacher@tum.de

6.2 Terpene cyclization catalysed inside a self-assembled cavity

Qi Zhang and Konrad Tiefenbacher*

Department Chemie, Technische Universität München, D-85747 Garching, Germany

E-mail: konrad.tiefenbacher@tum.de

6.3 Self-assembled supramolecular structures as catalysts for reactions involving cationic transition states

Lorenzo Catti, Qi Zhang and Konrad Tiefenbacher*

Department Chemie, Technische Universität München, D-85747 Garching, Germany

E-mail: konrad.tiefenbacher@tum.de

Originally published in: *Synthesis.* **2016**, *48*, 313 − 328

DOI: 10.1055/s-0035-1560352

Hyperlink: https://www.thieme-connect.de/DOI/DOI?10.1055/s-0035-1560352

7 Reprint Permissions and Reprints

7.1 American Chemical Society

7.1.1 Reprint Permission

The manuscript published in the *Journal of the American Chemical Society* was reproduced with permission of the American Chemical Society.

7.1.2 Manuscript "Hexameric Resorcinarene Capsule is a Brønsted Acid: Investigation and Application to Synthesis and Catalysis"

# J|A|C|S

JOURNAL OF THE AMERICAN CHEMICAL SOCIETY

Hexameric Resorcinarene Capsule is a Brønsted Acid: Investigation and Application to Synthesis and Catalysis

Qi Zhang and Konrad Tiefenbacher*

Department Chemie, Technische Universität München, D-85747 Garching, Germany

S *Supporting Information*

ABSTRACT: Molecular capsules have attracted interest as simple enzyme mimetics and several examples of catalytic transformations in water-soluble metal−ligand based systems have been reported. This is not the case for hydrogen-bond based molecular capsules, which in contrast can be employed in organic solvents. We describe herein our investigations of such a system: The resorcin[4]arene hexamer is one of the largest hydrogen bond-based self-assembled capsules and has been studied intensively due to its ready availability. We present evidence that the capsule acts as a reasonably strong Brønsted acid (pK_a approximately 5.5−6). This finding explains the capsule's high affinity toward tertiary amines that are protonated and therefore encounter cation-π interactions inside the cavity. We were able to translate this finding into a first synthetic application: A highly substrate-selective Wittig reaction. We also report that this property renders the capsule an efficient enzyme-like catalyst for substrate selective diethyl acetal hydrolysis.
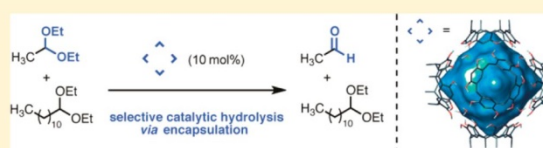
■ INTRODUCTION

Nature's capability to enzymatically catalyze reactions under mild conditions—ambient temperature or slightly higher "body" temperature and necessarily without any precautions against water and oxygen—has been fascinating synthetic organic chemists for decades. Enzymes selectively isolate suitable substrates inside a hydrophobic reaction pocket, adjust them into the reactive orientation and/or conformation, alter or enhance their reactivity by noncovalent or covalent interactions, stabilize the transition state of the reaction, and finally expel the product to complete the catalytic cycle.[1] Additionally, contributions to catalytic efficiency from quantum mechanical tunneling, matching of pK_a values in the transition state and protein dynamics have been identified.[1g]

Naturally, numerous attempts have been made to mimic such biological catalysts: Early examples of discrete entities included functionalized cyclodextrins, cyclic porphyrin oligomers, spherands, and cyclophanes, which were investigated among others by the groups of Breslow, Sanders, Cram, and Diederich, respectively.[1a,b,2] Beside such covalently linked host structures, noncovalently self-assembled structures also have been developed. These molecular capsules spontaneously form in solution via hydrogen bonds, metal−ligand interactions, or the hydrophobic effect and were mainly investigated by the groups of Rebek, Raymond, and Fujita, and Gibb, respectively.[3] Since such host structures self-assemble from smaller components, their preparation usually requires less synthetic effort and, additionally, they completely surround the encapsulated guests. Therefore, attention has shifted toward these systems as enzyme mimics. The investigation of metal−ligand based molecular capsules has yielded numerous examples of catalytic transformation.[4] Interestingly, this is not the case with hydrogen-bonded capsules: There are only two examples of

reactions catalyzed inside such molecular flasks.[5] In most cases, product inhibition prevents a catalytic turnover.[3k,m]

We wanted to explore the possibility of utilizing hydrogen-bonded molecular capsules as catalysts, not only because examples are scarce but mainly due to the fact that such systems are − in contrast to most metal−ligand capsules − soluble in organic media. This should allow the use of reagents which are not compatible with excess water. Since dozens of structurally different hydrogen-bonded molecular capsules have been described in the literature,[3] we screened for the following two properties: (1) ease of preparation: wider applications seem conceivable only if the capsule can be readily synthesized in large quantities; (2) large cavity size: to allow for experiments with a variety of different guest sizes and to prevent excessive binding of substrates (via strong contacts to multiple capsule walls), which usually translates into strong binding of the products (product inhibition). We identified the hexameric resorcin[4]arene capsule **I** (Figure 1), which was reported by the group of Atwood[6] in 1997, as an ideal candidate. It spontaneously forms in apolar solvents from six resorcin[4]-arene units **1**, which are readily prepared in multigram quantities in a single step. And with an internal volume of approximately 1400 Å,[3] it also represents one of the largest hydrogen-bonded molecular capsules.

The structure of **I** was elucidated by single crystal X-ray analysis.[6] In addition to the six resorcin[4]arene units, eight water molecules participate in its formation and indeed also proved essential to its formation in solution.[7] The encapsulation of different guests[8] and the formation of the capsule itself have been investigated extensively in solution.[9] Also, the
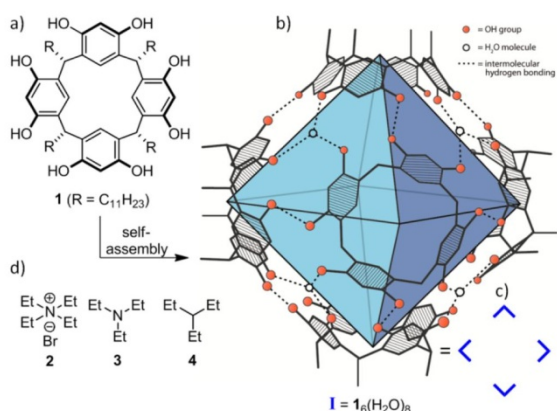
Figure 1. (a) Structure of resorcin[4]arene **1**; (b) schematic representation of the hexameric resorcin[4]arene capsule **I**, emphasizing the octahedral cavity space (blue); alkyl groups have been omitted for clarity; (c) simplified symbolic representation of the hexameric capsule; and (d) guest molecules first investigated for encapsulation in **I**.

stability toward polar additives[10] and the assembling properties in the presence of alcohols has been studied.[11] Besides NMR spectroscopy, EPR spectroscopy[12] and mass spectrometry[13] have been used to analyze molecular capsule **I**. A recent review also discusses the field of hexameric capsules.[14]

■ RESULTS AND DISCUSSION

Acidity of the Hexamer. Our investigations into this field started with the reproduction of an intriguing observation[8e,f,9c] described in the literature: Capsule **I** binds well both tetraalkylammonium salts and trialkylamines. While the strong interactions of alkylammonium compounds can be explained by cation-π stabilization inside the aromatic cavity, the efficient binding of amines was surprising to us. We reinvestigated this issue and quantified the encapsulation by separately adding 0.5 equiv of quaternary ammonium salt **2** (Figure 1) and triethylamine (**3**) to a solution of **I** in water-saturated CDCl$_3$ (3.3 mM in capsule **I**). Indeed, in both cases, the respective guests were completely encapsulated, as evidenced by integration of the upfield-shifted guest signals in the ^{1}H NMR spectrum. This seemed even more interesting, as the carbon analog of triethylamine (**3**), 3-ethylpentane (**4**), completely resisted encapsulation under such conditions, indicating that the amine functionality is responsible for the observed difference. We speculated that the tertiary amine is encapsulated so well only because it was protonated somehow.

Initial evidence in this direction and toward identifying the origin of the proton was found in the ^{1}H NMR spectrum of the experiment with triethylamine (**3**). Integration of the phenolic OH signals of assembly **I** at 9.75−9.31 ppm indicated that approximately 40% had shifted to higher field (broad signal 4.9−3.6 ppm). Evidence that this new signal corresponded to phenolic OH signals was obtained from NOESY-experiments: Correlation to the neighboring *ortho*-aromatic proton and the methine was observed (Supporting Information, SI, Figure 4). A similar pattern is seen with the phenolic protons of assembly **I**. If the capsule itself was acting as Brønsted acid, then the addition of 0.5 equiv of amine **3** would indeed affect up to half of the capsular assemblies and shift their OH signals to higher

field due to the increased electron-density of the anionic species, while the signals of the remaining part would be unaffected. To investigate this phenomenon more closely, a capsule solution was titrated with incremental amounts (0.2 equiv) of triethylamine (**3**) (Figure 2). Several changes can be
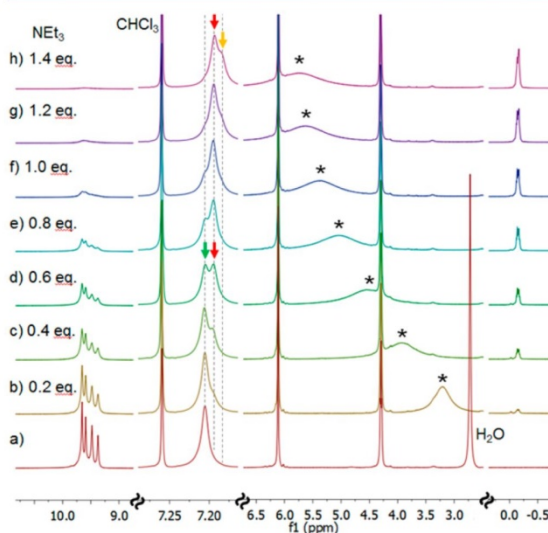

Figure 2. ^{1}H NMR titration of capsule **I** (a) in water-saturated CDCl$_3$ (3.3 mM) with various amounts of NEt$_3$ (b−h). Three different aromatic peaks at 7.20 ppm, indicating the encapsulation of different guests, are observable and are highlighted by colored arrows. The asterisk marks the shifted phenolic signals after deprotonation of the capsule.

observed in the ^{1}H NMR spectra: (1) The integral of the multiplet at 9.75−9.31 ppm, corresponding to the phenolic OH signals of the capsule, decreases inversely with added amounts of NEt$_3$. (2) The aromatic signal of the capsule at 7.20 ppm (*meta* to the phenol groups) is split; indicating in total three different species (highlighted by arrows). These changes are less pronounced in the other aromatic signal at ca. 6.11 ppm. (3) The water peak (which before amine addition appears at 2.72 ppm) is gradually shifted to lower field (indicated with an asterisk) and its integral gradually increases. Careful integration of the broad signal (see SI Table 1) indicated that in fact the phenolic signals at 9.75−9.31 ppm that had disappeared had shifted to the broad peak. Its integral closely matches the original water amount plus the shifted phenolic protons. This indicates a fast exchange of protons between phenols and water, which is not observed in the original capsule **I**. (4) Guest signal peaks appear at −0.10 to −0.15 ppm. Integration indicates that the added guest is completely encapsulated at all concentrations. Accordingly, no free guest signals can be observed in the ^{1}H NMR spectra.

These observations indicate protonation of the added amine by capsule **I**. However, it was not clear if the hexameric capsular structure was still intact as an anionic species after deprotonation, although the strongly high field-shifted guest signals (−0.10 to −0.15 ppm) indicated some form of capsular assembly. DOSY spectroscopy has proven to be the ideal tool to probe the size of the resorcinarene assembly as demonstrated by the Cohen group.[7,9a−d,10b] Therefore, this technique was used to determine the size of the respective species. The

observed diffusion value ($0.24 \pm 0.01 \times 10^{-5}$ cm^{2}s^{-1}; see SI Figure 5) for a sample containing 1.4 equiv of triethylamine (Figure 2, spectrum h; complete deprotonation of **I**) is in very good agreement with the literature values of the hexamer **I** reported by the Cohen group.[7,9a−d,10b] Therefore, a smaller assembly—for instance a dimer, which was observed in crystal structures—[15] can be ruled out.

Taken together, the collected evidence is consistent with the encapsulation of the amine **3** as a protonated species inside the negatively charged capsule **I**—denoted here as HNEt$_3^+$@**I**$^-$ (Figure 3). To some extent, a pairwise encapsulation of a
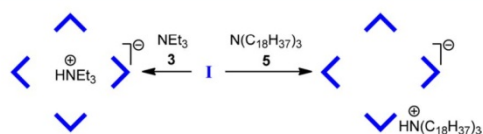
Figure 3. Schematic representation of the protonation and encapsulation of NEt$_3$ (**3**) by **I**. The larger trioctadecylamine (**5**) is protonated by **I** but cannot be accommodated inside the cavity.

protonated amine and regular amine—interacting via the proton—is likely, since we observe complete uptake of 1 equiv of NEt$_3$ but not complete disappearance of the original phenolic capsule **I** signals (e.g., Figure 2f). The pairwise encapsulation of amines could also explain the splitting of the aromatic signal at 7.20 ppm (Figure 2): The peak highlighted in green corresponds to the original capsule **I**; the red arrow marks the peak of HNEt$_3^+$@**I**$^-$; and the yellow arrow refers to assembly Et$_3$N·HNEt$_3^+$@**I**$^-$. Such a pairwise encapsulation of amines was also observed in metal−ligand based capsules by the groups of Bergman and Raymond.[4j]

To corroborate these findings, we tried to obtain direct evidence for the protonation of the tertiary amine: The affected methylene groups of NEt$_3$ (**3**) next to the nitrogen atom were strongly high field-shifted due to encapsulation—concealing any possible low field shift caused by protonation. Therefore, we studied the protonation using trioctadecylamine (**5**), which is too large for encapsulation[8f] and where we therefore could easily observe possible low field shifts of the affected methylene groups in the ^{1}H NMR spectrum. Consistent with protonation of the amine, we observed a shift of the adjacent methylene groups from 2.37 to 2.84 ppm—a value which is in good agreement with the separately synthesized trifluoroacetic acid salt (see SI Figure 7).

After having collected evidence that protonation of tertiary amines is indeed occurring, we wanted to estimate the acidity of assembly **I**. Therefore, we investigated its behavior toward amines of decreasing basicity[16] (Figure 4). Addition of 0.5 equiv of bases with pK_a values ranging from 11−6.1 to a solution of **I** in water-saturated CDCl$_3$ (3.3 mM) resulted in approximately 80% of protonation (as revealed by the residual OH peak at 9.75−9.31 ppm, cf. Figure 2). As discussed before, complete protonation is not observed, since a pairwise encapsulation of a protonated and a regular amine is also observed (Et$_3$N·HNEt$_3^+$@**I**$^-$). Beginning with pyridine (pK_a = 5.2), we observed a lower degree of protonation (53 ± 1%), which is further decreased to 23 ± 2% in the case of aniline (pK_a = 4.6). Amines of lower basicity did not show any degree of protonation as evidenced by ^{1}H NMR spectroscopy. From these results, we estimated the pK_a of hexamer **I** as approximately 5.5−6 (for calculations, see SI).[17]
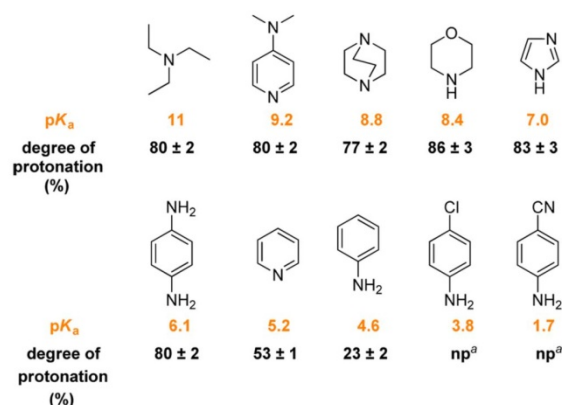

Figure 4. Estimation of the pK_a value of **I** by addition of 0.5 equiv of base to a solution of **I** in water-saturated CDCl$_3$ (3.3 mM); pK_a values (measured in water) were taken from literature.[16] ^{a}No protonation was observed.

Why is the hexameric capsule **I** acting as a relatively strong acid? (1) The protonation leads to thermodynamically more stable complexes due to cation-π interactions. (2) The anion formed is stabilized well by delocalization. The negative charge can be freely shifted between the 48 phenolic groups and the eight water molecules of assembly **I** via proton migration (see Figure 5). (3) Additionally, attractive Coulomb interactions between the ammonium guest and the negatively charged capsule could be involved.
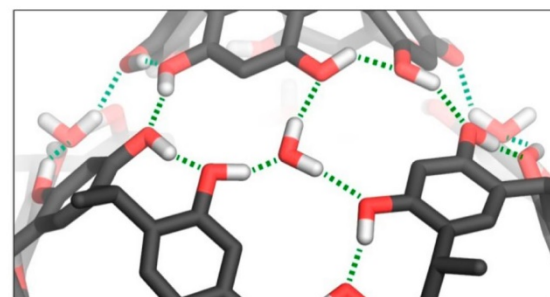

Figure 5. Section of the hydrogen bond seam of capsule **I**.

We next investigated if encapsulation of an ammonium guest influences the acidity of **I**. We chose to synthesize the large dialkyl aniline **6** (Figure 6) as a probe, which due to its pK_a (cf., Figure 4) should not be protonated to a high extent and therefore should allow the observation of increased and decreased protonation. Additionally, due to its size it cannot be encapsulated, and therefore, the addition of the ammonium guest cannot change the encapsulation ratio (which could alter the protonation equilibrium). While we observed 15 ± 1% protonation when adding 1 equiv of **6** to **I** in water-saturated CDCl$_3$ (3.3 mM), the degree of protonation was increased to 22 ± 1% when the capsule was occupied by a tetrabutylammonium guest (1.0 equiv of Bu$_4$NBr was added to the solution of **I**) under otherwise identical conditions. The increased acidity of **I** in this case could stem from the energy gain from Coulomb interactions between the tetrabutylammonium guest and the negatively charged capsule. This observation was interesting in
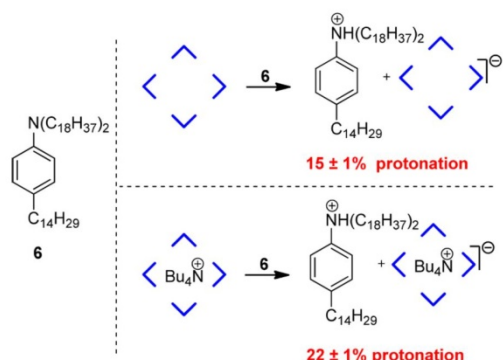
Figure 6. The protonation of aniline **6** by **I** was explored in the presence and absence of the encapsulated tetrabutylammonium salt.

light of potential applications of **I** as an acidic catalyst, since blocking the cavity with the ammonium guest could result in an increased background reaction outside of the capsule during a control reaction.

Synthetic Application via Size-Selective Protonation. After having revealed the acidity of assembly **I**, we next tried to translate these findings into first synthetic applications. We explored the possibility of protonating a stabilized Wittig ylide, which should have an appropriate pK_a value of approximately 8−9.[18] Indeed, the addition of 0.85 equiv of Wittig ethyl ester **7** (Figure 7a) to a solution of **I** (1.0 equiv) in water-saturated CDCl$_3$ (8.0 mM) resulted in complete protonation of the ylide (as evidenced by the integral of the original phenolic OH signals in the ^{1}H NMR spectrum) and complete encapsulation.
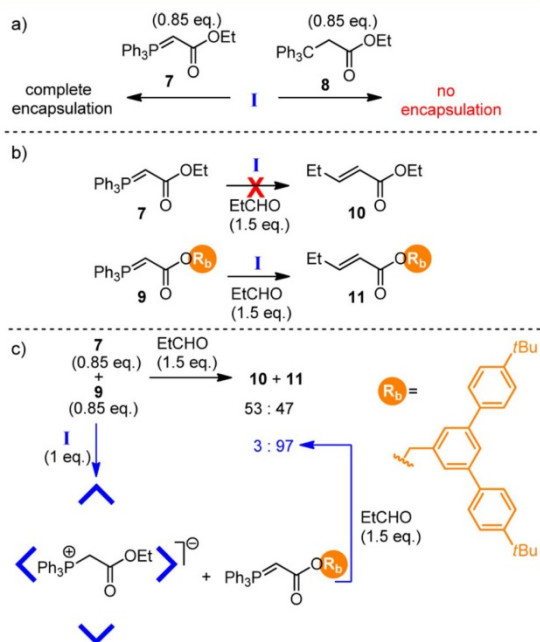

Figure 7. (a) Encapsulation experiments with Wittig ylide **7** and carbon analog **8**; (b) reactivity test of Wittig ylides **7** and **9** in the presence of **I** and EtCHO; and (c) comparison of the selective Wittig reaction in the presence of **I** and the regular reaction in solution.

For comparison, the carbon analog of **7**, namely ethyl 3,3,3-triphenylpropanoate (**8**, Figure 7a), which lacks the ability to accept a proton, was also investigated: It did not yield any detectable amounts of encapsulated species under similar conditions, again emphasizing the role of protonation in the binding of basic compounds. The encapsulated protonated Wittig ylide **7** was tested for its reactivity toward aldehydes. Even the addition of excess propanal (10 equiv) did not produce any alkene product, although the uptake of propanal into the capsule could be observed by the appearance of characteristic signals (SI Figure 10). This lack of reactivity further corroborates our understanding of the acid base chemistry in this system.

We next synthesized a large Wittig ester **9** (Figure 7b), which is not able to fit inside **I**. When 0.85 equiv of **9** were added to a solution of **I** (1.0 equiv) in water-saturated CDCl$_3$ (8.0 mM), as expected, a high degree of protonation (approximately 90%) and no encapsulation was observed via ^{1}H NMR spectroscopy. Addition of 1.5 equiv of propanal to this solution resulted in formation of alkene **11** (66% yield after 16 h), indicating that the protonation of the Wittig ylide outside of **I** was reversible and did not prevent conversion to the alkene. Finally, we tested if capsule **I** can act as a selector in the Wittig reaction of a mixture of ylides **7** and **9** (Figure 7c): Addition of a ylide mixture (0.85 equiv of **7**, 0.85 equiv of **9**) to a solution of **I** in water-saturated CDCl$_3$ (8.0 mM), followed by the addition of propanal (1.5 equiv), led to the highly selective formation of alkene **11** (74% isolated yield, E/Z = 14: 1). Only traces of alkene **10** could be detected by ^{1}H NMR spectroscopy and 72% of ylide **7** could be recovered by basic column chromatography. The selectivity imposed by capsule **I** (ratio of **10**: **11** = 3: 97) was in stark contrast to the unselective reaction without **I** under otherwise identical conditions, which led to a 53:47-mixture of **10** and **11**.

Catalytic Size-Selective Hydrolysis of Acetals. After having demonstrated that the acidity of assembly **I** can be efficiently used to impose substrate selectivity on a stoichiometric reaction, we wanted to explore the potential use of **I** as a selective enzyme-like catalyst. We decided to investigate the hydrolysis of acetals, and after screening several different acetal groups found that 1,1-diethoxyethane (**12**, R = methyl, Figure 8) was a suitable substrate: Addition of 10 equiv of acetal to a solution of **I** in water-saturated CDCl$_3$ (3.3 mM) resulted in good conversion (85%) after 1 h at 25 °C. The control experiment with inhibited catalyst (adding 2.4 equiv of the guest Bu$_4$NBr to the catalyst solution before addition of substrate) only showed a slow background reaction (1% after 1 h). A second control experiment in water-saturated CDCl$_3$ without added catalyst did not show any detectable conversion. These first results were interesting, since they demonstrated that a catalytic conversion is indeed possible with **I** and that the reaction is taking place inside the cavity. Additionally, the successful hydrolysis implies that water is able to enter the cavity of **I**. It is likely that the eight water molecules that are already bound at the surface of **I** (Figure 5) are enabling hydrolysis.

We next investigated the substrate selectivity of the catalytic diethyl acetal hydrolysis by varying the alkyl group R (Figure 8). 1,1-Diethoxypropane **13** (R = ethyl) showed comparable results to 1,1-diethoxyethane **12** (R = methyl), giving approximately 86% conversion after 60 min. When catalyst **I** was blocked with a good guest (Bu$_4$NBr), the hydrolysis of **13** was efficiently slowed down, giving only a weak background
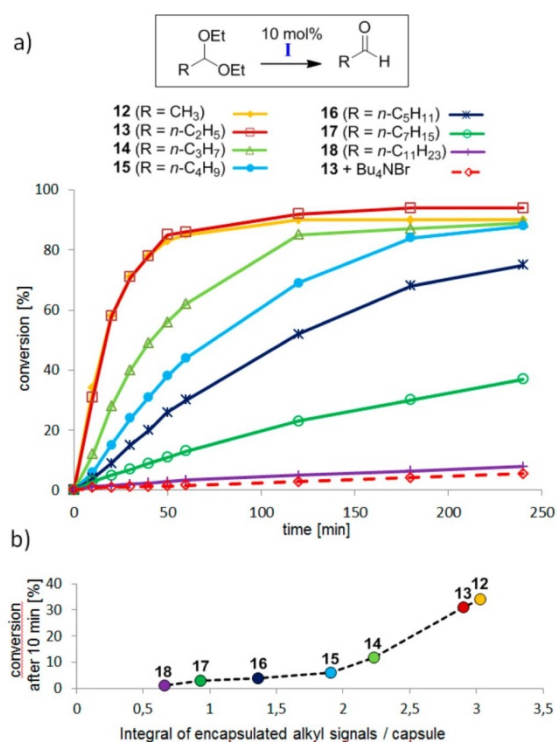
88

Article

a)

b)

Figure 8. (a) Catalytic hydrolysis of various diethyl acetals inside **I** and (b) comparison of the conversion after 10 min to encapsulated alkyl signals (^{1}H NMR region: 0.6 to −2 ppm).

reaction (dotted line in Figure 8), although we observed increased acidity of **I** when occupied by the ammonium guest (see Figure 6). This further demonstrates that the reaction is indeed greatly accelerated *inside* the cavity of **I**. Interestingly, the reaction rate slowed down considerably with longer alkyl groups: 1,1-diethoxybutane **14** (R = propyl) gave 62%, 1,1-diethoxypentane **15** (R = butyl) gave 44%, 1,1-diethoxyhexane **16** (R = pentyl) gave 30%, 1,1-diethoxyoctane **17** (R = heptyl) gave 13% and 1,1-diethoxydodecane **18** (R = undecyl) gave only 3.4% conversion after 60 min. The decreased hydrolysis rate of the longer alkyl acetals cannot be explained by size exclusion arguments. All of the tested acetals can be accommodated well inside the cavity of **I**, as evidenced by the occupation ratio. Even the largest tested acetal (1,1-diethoxydodecane) only occupies 22% of the available space, much less than the optimum of approximately 55%[19] (see SI Table 2). The remaining space would be filled with solvent molecules. To explain the selectivity, we turned to the extent of encapsulation of the different acetals. Unfortunately, we could not determine the encapsulation ratio, since the characteristic acetal-guest signals are not observable after encapsulation, due to signal overlap. We therefore tried to utilize the encapsulated alkyl signals of the acetal, which were shifted to the region of 0.6 to −2 ppm as measure of encapsulation. Since the acetals utilized differ greatly in the number of alkyl protons, and more importantly, it is not known which of the respective alkyl protons are shifted into the observable region due to the anisotropy of the capsule walls, the encapsulation ratio remained elusive. We could only compare the integral of the

encapsulated aliphatic signals (characteristically shifted to the region 0.6 to −2 ppm) in the various experiments. In Figure 8b, these values are plotted versus the respective conversion after 10 min (initial rate). Although the larger acetals (especially **17** and **18**) have more aliphatic protons (which potentially could shift to the high field-region mentioned), we observe a negative correlation of acetal size and alkyl integral. These findings point to a faster encapsulation of the smaller guests, a phenomenon which has been observed in other systems[20] but has not been translated into synthetic applications before. It seems that the smaller acetals are cleaved much more rapidly due to more efficient encapsulation.

Finally we explored the possibility of selectively hydrolyzing one acetal in the presence of another. Indeed, the hydrolysis of a mixture of **12** and **18** (10 equiv each) proceeded in a highly selective fashion (Figure 9): After 60 min, the smaller acetal
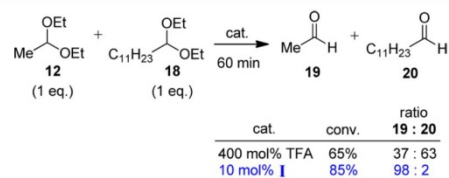

cat.	conv.	ratio **19 : 20**
400 mol% TFA	65%	37 : 63
10 mol% **I**	85%	98 : 2

Figure 9. Selective hydrolysis of acetal **12** in the presence of acetal **18** within catalyst **I**.

was hydrolyzed to a large extent (83%), while the other acetal showed only 2% conversion—resulting in a selectivity of 98:2 at 85% combined conversion. As a control experiment, we wanted to replace capsule **I** with a regular acid of comparable acidity. When utilizing acetic acid (pK_a = 4.8)[16] instead of **I** under otherwise identical conditions, no conversion was observed (monitored for 15 h), although its acidity is approximately one magnitude higher than **I**. This observation indicated the fundamental role of the cavity space in the hydrolysis: We believe that it enables reactions under mild conditions that are not possible in the solution phase by stabilizing cationic intermediates and transition states in the hydrolysis process. To reach comparable hydrolysis rates in solution, we had to turn to the much stronger trifluoroacetic acid (pK_a = 0.2)[16] and use it in large excess (4 equiv per acetal as compared to 10 mol % **I**!). Not surprisingly, the hydrolysis led to mixtures—giving 24% of **19** and 41% of **20** after 60 min (ratio of 37:63). Thus, we could demonstrate selectivity imposed by catalyst **I** in a reaction that is very hard to control in the solution phase.

■ **CONCLUSIONS**

We have provided evidence that the hexameric capsule **I** is acting as a reasonable strong acid ($pK_a \approx 5.5$−6). This finding explains its good binding of tertiary amines, which are protonated to give ammonium ions and then encounter strong cation-π interactions inside the cavity. Further, we demonstrated that the acidity of **I** can be translated into first synthetic and even catalytic applications.[21] The catalytic example presented mimics the basic principle of operation in enzymes: A suitable substrate is selectively isolated inside the reaction pocket, its reactivity is enhanced by protonation, and the cationic transition states likely stabilized by cation-π interactions with the aromatic cavity. Finally, the product is released, since it does not bind strongly to **I**, to complete the catalytic

Article

cycle. We are convinced that our findings will fuel further applications of **I** as a reaction chamber and as an enzyme-like catalyst.

■ ASSOCIATED CONTENT

⑤ Supporting Information

Detailed experimental procedures, characterization data for new compounds and relevant NMR spectra. This material is available free of charge via the Internet at http://pubs.acs.org.

■ AUTHOR INFORMATION

Corresponding Author

konrad.tiefenbacher@tum.de

Notes

The authors declare no competing financial interest.

■ REFERENCES

(1) (a) Kirby, A. J. *Angew. Chem., Int. Ed.* **1996**, *35*, 707. (b) Motherwell, W. B.; Bingham, M. J.; Six, Y. *Tetrahedron* **2001**, *57*, 4663. (c) Garcia-Viloca, M.; Gao, J.; Karplus, M.; Truhlar, D. G. *Science* **2004**, *303*, 186. (d) Zhang, X.; Houk, K. N. *Acc. Chem. Res.* **2005**, *38*, 379. (e) Gao, J.; Ma, S.; Major, D. T.; Nam, K.; Pu, J.; Truhlar, D. G. *Chem. Rev.* **2006**, *106*, 3188. (f) Warshel, A.; Sharma, P. K.; Kato, M.; Xiang, Y.; Liu, H.; Olsson, M. H. M. *Chem. Rev.* **2006**, *106*, 3210. (g) Ringe, D.; Petsko, G. A. *Science* **2008**, *320*, 1428. (h) Kamerlin, S. C. L.; Warshel, A. *Proteins: Struct., Funct., Bioinf.* **2010**, *78*, 1339.

(2) (a) Breslow, R.; Dong, S. D. *Chem. Rev.* **1998**, *98*, 1997. (b) Sanders, J. K. M. *Chem.—Eur. J.* **1998**, *4*, 1378. (c) Vriezema, D. M.; Comellas Aragonès, M.; Elemans, J. A. A. W.; Cornelissen, J. J. L. M.; Rowan, A. E.; Nolte, R. J. M. *Chem. Rev.* **2005**, *105*, 1445.

(3) Selected examples: (a) Wyler, R.; de Mendoza, J.; Rebek, J. *Angew. Chem., Int. Ed.* **1993**, *32*, 1699. (b) Heinz, T.; Rudkevich, D. M.; Rebek, J. *Nature* **1998**, *394*, 764. (c) Caulder, D. L.; Powers, R. E.; Parac, T. N.; Raymond, K. N. *Angew. Chem., Int. Ed.* **1998**, *37*, 1840. (d) Davis, A. V.; Fiedler, D.; Ziegler, M.; Terpin, A.; Raymond, K. N. *J. Am. Chem. Soc.* **2007**, *129*, 15354. (e) Takeda, N.; Umemoto, K.; Yamaguchi, K.; Fujita, M. *Nature* **1999**, *398*, 794. (f) Umemoto, K.; Tsukui, H.; Kusukawa, T.; Biradha, K.; Fujita, M. *Angew. Chem., Int. Ed.* **2001**, *40*, 2620. (g) Gibb, C. L. D.; Gibb, B. C. *J. Am. Chem. Soc.* **2004**, *126*, 11408. (h) Kaanumalle, L. S.; Gibb, C. L. D.; Gibb, B. C.; Ramamurthy, V. *J. Am. Chem. Soc.* **2004**, *126*, 14366. For reviews, see: (i) Hof, F.; Craig, S. L.; Nuckolls, C.; Rebek, J. J. *Angew. Chem., Int. Ed.* **2002**, *41*, 1488. (j) Palmer, L. C.; Rebek, J. J. *Org. Biomol. Chem.* **2004**, *2*, 3051. (k) Koblenz, T. S.; Wassenaar, J.; Reek, J. N. H. *Chem. Soc. Rev.* **2008**, *37*, 247. (l) Rebek, J. *Acc. Chem. Res.* **2009**, *42*, 1660. (m) Yoshizawa, M.; Klosterman, J. K.; Fujita, M. *Angew. Chem., Int. Ed.* **2009**, *48*, 3418. (n) Wiester, M. J.; Ulmann, P. A.; Mirkin, C. A. *Angew. Chem., Int. Ed.* **2011**, *50*, 114. (o) Ajami, D.; Rebek, J. *Acc. Chem. Res.* **2012**, *46*, 990.

(4) (a) Fiedler, D.; Bergman, R. G.; Raymond, K. N. *Angew. Chem., Int. Ed.* **2004**, *43*, 6748. (b) Fiedler, D.; van Halbeek, H.; Bergman, R. G.; Raymond, K. N. *J. Am. Chem. Soc.* **2006**, *128*, 10240. (c) Leung, D. H.; Bergman, R. G.; Raymond, K. N. *J. Am. Chem. Soc.* **2007**, *129*, 2746. (d) Pluth, M. D.; Bergman, R. G.; Raymond, K. N. *Angew. Chem., Int. Ed.* **2007**, *46*, 8587. (e) Pluth, M. D.; Bergman, R. G.;

Raymond, K. N. *Science* **2007**, *316*, 85. (f) Hastings, C. J.; Fiedler, D.; Bergman, R. G.; Raymond, K. N. *J. Am. Chem. Soc.* **2008**, *130*, 10977. (g) Pluth, M. D.; Bergman, R. G.; Raymond, K. N. *J. Am. Chem. Soc.* **2008**, *130*, 11423. (h) Brown, C. J.; Bergman, R. G.; Raymond, K. N. *J. Am. Chem. Soc.* **2009**, *131*, 17530. (i) Pluth, M. D.; Bergman, R. G.; Raymond, K. N. *Acc. Chem. Res.* **2009**, *42*, 1650. (j) Pluth, M. D.; Fiedler, D.; Mugridge, J. S.; Bergman, R. G.; Raymond, K. N. *Proc. Natl. Acad. Sci. U. S. A.* **2009**, *106*, 10438. (k) Hastings, C. J.; Pluth, M. D.; Bergman, R. G.; Raymond, K. N. *J. Am. Chem. Soc.* **2010**, *132*, 6938. (l) Brown, C. J.; Miller, G. M.; Johnson, M. W.; Bergman, R. G.; Raymond, K. N. *J. Am. Chem. Soc.* **2011**, *133*, 11964. (m) Hastings, C. J.; Backlund, M. P.; Bergman, R. G.; Raymond, K. N. *Angew. Chem., Int. Ed.* **2011**, *50*, 10570. (n) Wang, Z. J.; Brown, C. J.; Bergman, R. G.; Raymond, K. N.; Toste, F. D. *J. Am. Chem. Soc.* **2011**, *133*, 7358. (o) Hart-Cooper, W. M.; Clary, K. N.; Toste, F. D.; Bergman, R. G.; Raymond, K. N. *J. Am. Chem. Soc.* **2012**, *134*, 17873. (p) Wang, Z. J.; Clary, K. N.; Bergman, R. G.; Raymond, K. N.; Toste, F. D. *Nature Chem.* **2013**, *5*, 100. (q) Ito, H.; Kusukawa, T.; Fujita, M. *Chem. Lett.* **2000**, 598. (r) Yoshizawa, M.; Sato, N.; Fujita, M. *Chem. Lett.* **2005**, *34*, 1392. (s) Yoshizawa, M.; Tamura, M.; Fujita, M. *Science* **2006**, *312*, 251. (t) Murase, T.; Nishijima, Y.; Fujita, M. *J. Am. Chem. Soc.* **2012**, *134*, 162. (u) Merlau, M. L.; del Pilar Mejia, M.; Nguyen, S. T.; Hupp, J. T. *Angew. Chem., Int. Ed.* **2001**, *40*, 4239. (v) Lee, S. J.; Cho, S.-H.; Mulfort, K. L.; Tiede, D. M.; Hupp, J. T.; Nguyen, S. T. *J. Am. Chem. Soc.* **2008**, *130*, 16828.

(5) (a) Kang, J.; Santamaría, J.; Hilmersson, G.; Rebek, J. *J. Am. Chem. Soc.* **1998**, *120*, 7389. (b) Cavarzan, A.; Scarso, A.; Sgarbossa, P.; Strukul, G.; Reek, J. N. H. *J. Am. Chem. Soc.* **2011**, *133*, 2848.

(6) MacGillivray, L. R.; Atwood, J. L. *Nature* **1997**, *389*, 469.

(7) Avram, L.; Cohen, Y. *Org. Lett.* **2002**, *4*, 4365.

(8) (a) Shivanyuk, A.; Rebek, J. *Proc. Natl. Acad. Sci. U. S. A.* **2001**, *98*, 7662. (b) Shivanyuk, A.; Rebek, J. *Chem. Commun.* **2001**, 2424. (c) Palmer, L. C.; Shivanyuk, A.; Yamanaka, M.; Rebek, J. *Chem. Commun.* **2005**, 857. (d) Evan-Salem, T.; Baruch, I.; Avram, L.; Cohen, Y.; Palmer, L. C.; Rebek, J. *Proc. Natl. Acad. Sci. U. S. A.* **2006**, *103*, 12296. (e) Avram, L.; Cohen, Y. *J. Am. Chem. Soc.* **2003**, *125*, 16180. (f) Slovak, S.; Cohen, Y. *Supramol. Chem.* **2010**, *22*, 803. (g) Philip, I. E.; Kaifer, A. E. *J. Am. Chem. Soc.* **2002**, *124*, 12678. (h) Philip, I.; Kaifer, A. E. *J. Org. Chem.* **2005**, *70*, 1558. (i) Bianchini, G.; Scarso, A.; Sorella, G. L.; Strukul, G. *Chem. Commun.* **2012**, 12082.

(9) (a) Avram, L.; Cohen, Y. *J. Am. Chem. Soc.* **2002**, *124*, 15148. (b) Avram, L.; Cohen, Y. *Org. Lett.* **2003**, *5*, 1099. (c) Avram, L.; Cohen, Y. *J. Am. Chem. Soc.* **2004**, *126*, 11556. (d) Avram, L.; Cohen, Y. *Org. Lett.* **2008**, *10*, 1505. (e) Shivanyuk, A.; Rebek, J. *J. Am. Chem. Soc.* **2003**, *125*, 3432. (f) Yamanaka, M.; Shivanyuk, A.; Rebek, J. *J. Am. Chem. Soc.* **2004**, *126*, 2939. (g) Barrett, E. S.; Dale, T. J.; Rebek, J. *J. Am. Chem. Soc.* **2007**, *129*, 3818. (h) Barrett, E. S.; Dale, T. J.; Rebek, J. *J. Am. Chem. Soc.* **2008**, *130*, 2344.

(10) (a) Atwood, J. L.; Barbour, L. J.; Jerga, A. *Chem. Commun.* **2001**, 2376. (b) Avram, L.; Cohen, Y. *Org. Lett.* **2003**, *5*, 3329.

(11) (a) Ugono, O.; Holman, K. T. *Chem. Commun.* **2006**, 2144. (b) Schnatwinkel, B.; Stoll, I.; Mix, A.; Rekharsky, M. V.; Borovkov, V. V.; Inoue, Y.; Mattay, J. *Chem. Commun.* **2008**, 3873. (c) Slovak, S.; Avram, L.; Cohen, Y. *Angew. Chem., Int. Ed.* **2010**, *49*, 428. (d) Slovak, S.; Cohen, Y. *Chem.—Eur. J.* **2012**, *18*, 8515.

(12) (a) Mileo, E.; Yi, S.; Bhattacharya, P.; Kaifer, A. E. *Angew. Chem., Int. Ed.* **2009**, *48*, 5337. (b) Yi, S.; Mileo, E.; Kaifer, A. E. *Org. Lett.* **2009**, *11*, 5690.

(13) Beyeh, N. K.; Kogej, M.; Åhman, A.; Rissanen, K.; Schalley, C. A. *Angew. Chem., Int. Ed.* **2006**, *45*, 5214.

(14) Avram, L.; Cohen, Y.; Rebek, J., Jr. *Chem. Commun.* **2011**, 5368.

(15) (a) Murayama, K. *Chem. Commun.* **1998**, 607. (b) N. Rose, K. *Chem. Commun.* **1998**, 407. (c) Shivanyuk, A.; Rissanen, K.; Kolehmainen, E. *Chem. Commun.* **2000**, 1107.

(16) W. P. Jencks, , J. R. *Ionization Constants of Acids and Bases*; CRC Press: Cleveland, 1976; Vol. *1*.

(17) The calculated pK_a-value of **I** is based on the reported pK_a-values of pyridine and aniline, which were measured in water. Therefore, the calculated pK_a-value of **I** should be treated as relative

90

value (to compare with reported pK_a-values measured in water) but not as an absolute value.

(18) Zhang, X. M.; Bordwell, F. G. *J. Am. Chem. Soc.* **1994**, *116*, 968.

(19) Mecozzi, S.; Rebek, J. *Chem.—Eur. J.* **1998**, *4*, 1016.

(20) Jiang, W.; Ajami, D.; Rebek, J. *J. Am. Chem. Soc.* **2012**, *134*, 8070.

(21) During the preparation of the manuscript the isonitrile hydration inside I at elevated temperatures was reported. Our findings could explain this observation, since isonitrile hydration usually requires an acidic catalyst. See: Bianchini, G.; La Sorella, G.; Canever, N.; Scarso, A.; Strukul, G. *Chem. Commun.* **2013**, 5322.

7.2 Nature Publishing Group

The manuscript published in the *Nature Chemistry* was reproduced by permission of Nature Publishing Group.

7.2.1 Reprint Permission

7.2.2 Manuscript "Terpene cyclization catalysed inside a self-assembled cavity"

Terpene cyclization catalysed inside a self-assembled cavity

Q. Zhang and K. Tiefenbacher*

In nature, complex terpene natural products are formed by the so-called tail-to-head terpene (THT) cyclization. The cationic reaction cascade is promoted efficiently in complex enzyme pockets, in which cationic intermediates and transition states are stabilized. In solution, the reaction is hard to control and man-made catalysts able to perform selective THT cyclizations are lacking. We herein report the first example of a successful THT cyclization inside a supramolecular structure. The basic mode of operation in cyclase enzymes was mimicked successfully and a catalytic non-stop THT was achieved with geranyl acetate as the substrate. The results presented have implications for the postulated reaction mechanism in cyclase enzymes. Evidence indicates that the direct isomerization of a geranyl cation to the *cisoid* isomer, which so far was considered unlikely, is feasible.

Nature's extraordinary elegance when performing chemical reactions has fascinated and inspired chemists for a long time. Arguably, one of the most complex organic transformations performed in living organisms is the tail-to-head[1] terpene (THT) cyclization[2,3]. It allows the construction of the most diverse class of natural products, namely terpenes, through nature's version of combinatorial chemical synthesis. Thousands of different natural products are formed from just a handful of simple, acyclic starting materials: geranyl pyrophosphate (GPP) (**1** (Fig. 1a), monoterpenes), farnesyl pyrophosphate (**2**, sesquiterpenes) and geranylgeranyl pyrophosphate (**3**, diterpenes). Nature utilizes enzymes, termed cyclases or terpene synthases, to bind the acyclic terpene diphosphate in a hydrophobic reaction pocket. The reaction cascade is initiated by a metal(II)-triggered departure of the diphosphate leaving group, generating, in the case of GPP (**1**), the first carbocationic intermediate **4a** (Fig. 1b)[2–8]. A direct cyclization of cation **4a** into the α-terpinyl cation **6** is not possible; it has to be preceded by isomerization into the *cisoid* conformer **4b**. It was postulated that cation **4a** has to collapse to linalyl pyrophosphate (linalyl-PP) (**5a**) to allow the isomerization to the *cisoid* isomer **5b**, which is suitable for cyclization. It was argued that the free-energy barrier for the direct rotation of the allylic cation **4a** is relatively high (about 55 kJ mol^{-1}) and therefore unlikely[4,9]. We herein present evidence that such a direct isomerization is possible in an enzyme-like catalyst. The α-terpinyl cation **6**, formed by the cyclization of the *cisoid* cation **4b**, is a key intermediate in the biosynthesis. It is converted into a variety of different monoterpene products, depending on the properties of the cyclase. If a water molecule is present in the reaction pocket, α-terpineol (**7**) can be formed, which may be cyclized further into eucalyptol (**8**)[2,4,5,8]. Alternatively, a direct proton elimination of **6** would deliver terpinolene (**9**) or limonene (**10**). If, however, cation **6** is stabilized enough and nucleophiles excluded within the reaction pocket, it is able to undergo alternative intramolecular cyclizations or rearrangements. For example, it can rearrange into cation **11** via a hydride shift and then deliver α-terpinene (**12**). In any case, a wide selection of reaction pathways is available for the high-energy cationic intermediates: intra- or intermolecular substitution reactions, eliminations, rearrangements, oligomerizations and polymerizations. Not surprisingly, in solution THT reactions prove to be hard to

control, and give mixtures of acyclic and, to a much lesser extent, cyclic products. Especially, the conversion of geranyl substrates in solution is problematic[4].

As the acyclic terpene alcohols geraniol (GOH), farnesol and geranylgeraniol are readily available, a direct selective conversion into cyclic terpenes is highly desirable. What are the main differences between THT cyclizations in solution and those in the hydrophobic enzyme pocket? (1) The initial ionization requires harsh conditions (a strong Lewis or Brønsted acid) in solution. In the cyclase, however, the pyrophosphate leaving group is removed under neutral conditions (optimum pH 6–7)[4] with the help of divalent metal ions. (2) In solution, high-energy cationic intermediates are susceptible to undesired side reactions (elimination or quenching by nucleophiles). In the enzyme pocket, cationic key intermediates are stabilized by cation–π and cation–dipole interactions. Specifically, it has been proposed that the aromatic side chains of phenylalanine, tyrosine and tryptophan play a key role in this regard[10,11]. In addition, the enzyme pocket blocks the access of undesired nucleophiles, and thereby prevents premature quenching.

Therefore, we explored the possibility of mimicking the complex cyclase reaction pocket using relatively simple aromatic supramolecular capsules[12–19]. Interestingly, although the field is quite active (for recent examples, see Bocokić *et al.*[20], Dydio *et al.*[21], Wang *et al.*[22], Zhao *et al.*[23,24] and Salles *et al.*[25]), no THT cyclizations in a supramolecular structure have been reported to date. The only reported example of a monoterpene-like cyclization was based on a Prins reaction, which is reproducible in solution[26]. The hexameric resorcinarene capsule **I**[27] (Fig. 2) (for catalysis within **I**, see Cavarzan *et al.*[28], Bianchini *et al.*[29] and Zhang and Tiefenbacher[30]), which is readily available by self-assembly of the monomer **13** in apolar solvents, seemed promising for this study. (1) It forms a large hydrophobic cavity (~1,400 Å^3) that is suitable for accommodating acyclic terpenes. (2) Owing to its aromatic walls, **I** is known to complex cationic guests, such as alkylammonium ions, via cation–π interactions[31,32]. In analogy to the aromatic residues in a terpene cyclase enzyme pocket, the aromatic walls of **I** could potentially stabilize cationic intermediates and transition states. (3) We recently reported that capsule **I** is a mild Brønsted acid (pK_a ~5.5–6) and can function as a catalyst for simple acetal hydrolysis[30]. (4) Guest exchange is facile and is believed to occur

Department Chemie, Technische Universität München, Lichtenbergstraße 4, D-85747 Garching, Germany. *e-mail: konrad.tiefenbacher@tum.de
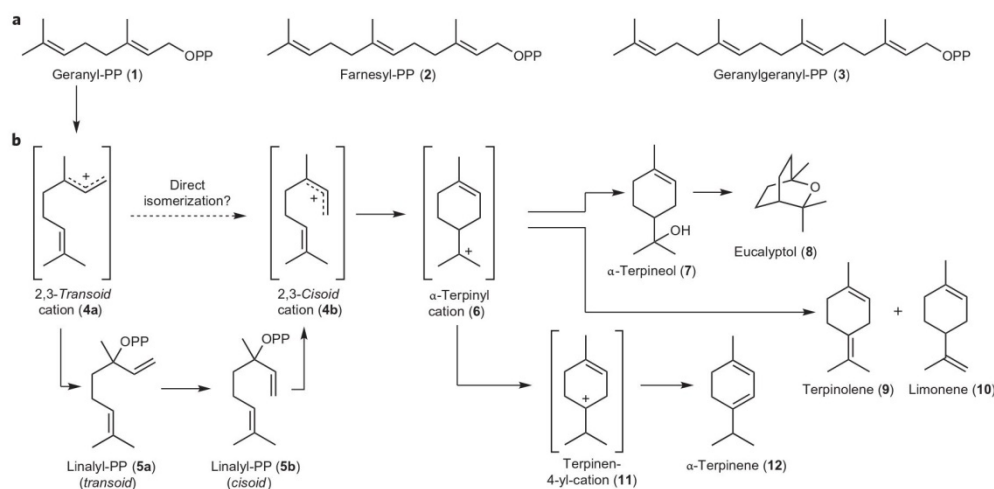
ARTICLES

Figure 1 | Biosynthesis of cyclic terpene natural products. a, Structures of the natural terpene substrates. These are converted into cyclic monoterpenes (geranyl-PP), sesquiterpenes (farnesyl-PP) and diterpenes (geranylgeranyl-PP). **b,** Reaction pathways for the biosynthesis of a selection of monoterpene natural products via THT cyclization. Cleavage of the PP-leaving group forms the *transoid* cation **4a**, which has to isomerize to the *cisoid* form **4b** before cyclization can occur. A direct isomerization is considered unlikely in the literature and therefore a step-wise isomerization that involves reattachment of the pyrophosphate group was proposed. After cyclization to the α-terpinyl cation (**6**), a variety of different reaction paths are available. An attack of water forms α-terpineol (**7**), which can further cyclize to eucalyptol (**8**). Alternatively, elimination delivers terpinolene (**9**) or limonene (**10**). Rearrangements can also occur. A hydride shift, for instance, delivers cation **11**, which yields α-terpinene (**12**) after elimination.

via dissociation of one resorcinarene unit[33]. We speculated that it could potentially activate a suitable leaving group on an acyclic terpene by protonation, and thereby initiate a THT cyclization cascade inside the cavity. Indeed, the system is able to biomimetically catalyse THT cyclizations and herein we report these findings.

Results and discussion

We first investigated the cyclization of monoterpene alcohols. Treatment of a solution of GOH (**14**) in CDCl$_3$ (33 mM) with 10 mol% capsule **I** at 30 °C led to complete conversion of the starting material within 28 hours (Fig. 3a). Identification of the products formed was achieved by comparison with standard solutions of monoterpenes (gas chromatography, ^{1}H NMR spectroscopy). Initially, in analogy to the proposed biosynthesis (Fig. 1b), linalool (LOH) (**15**) was formed as the main product (for the initial rates of formation, see Supplementary Table 9), which indicates that, after protonation of GOH (**14**) and ionization to give cation **4a**, the cleaved water molecule attacked the allylic carbocation. The other two main products formed within the first ten hours were the cyclic α-terpinene (**12**) and α-terpineol (**7**). With progressing reaction time, the concentrations of LOH (**15**) and α-terpineol (**7**) decreased, and eucalyptol (**8**) started to form (for the final yields after 72 hours, see Supplementary Table 4). Alkylation of the phenol groups of monomer **13** (for details, see Supplementary Figs 13–15) and dimerization were observed as side reactions, as evidenced by a multitude of smaller gas chromatography peaks in the diterpene region. For dimerization inside the cavity, two substrates have to be encapsulated simultaneously. It was reported that six chloroform molecules occupy the cavity space if no other guests are present[34]. According to size considerations (see Supplementary Table 8), one substrate would replace two or three of the six chloroform molecules. Several control experiments were performed. When catalyst **I** was omitted, no conversion was observed (12 days). When the catalyst's cavity was blocked with a strongly binding guest (*n*Bu$_4$NBr), no cyclization was observed, although the acidity of the system was thereby increased (see

Supplementary Tables 5 and 6). These experiments provide strong evidence that the cyclization reaction is, indeed, only taking place inside the cavity. Additionally, substrate internalization was evidenced by ^{1}H- and diffusion-ordered NMR spectroscopy (see Supplementary Figs 6–8).

Conversion of nerol (NOH) (**16**) under similar conditions produced contrasting results (Fig. 3b): the conversion was much faster and the dominating product within the first 20 hours was α-terpineol (**7**), which was then converted into eucalyptol (**8**) with good selectivity. Besides α-terpinene (**12**), terpinolene (**9**) was also formed in considerable amounts. Side reactions were greatly reduced.

The product profile of LOH (**15**) (Fig. 3c) could be interpreted as a combination of the GOH (**14**) and NOH (**16**) results to give a
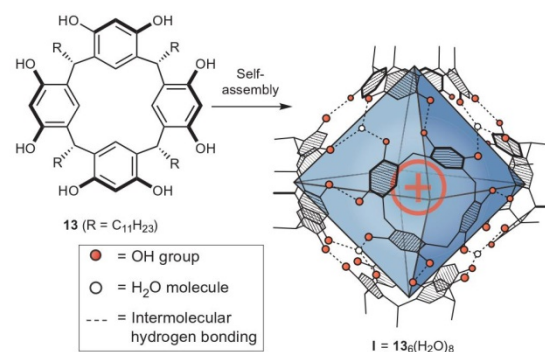
Figure 2 | Structure of the resorcinarene capsule I. This self-assembles via a hydrogen-bond network from six monomer units of **13** and eight water molecules in apolar solvents and encloses a volume of ∼1,400 Å^3. Cationic guests, such as alkylammonium ions, are bound inside the cavity via cation–π interactions. Guest exchange is facile and probably occurs via dissociation of one monomer unit. Capsule **I** is a mild Brønsted acid (pK_a ∼5.5–6).
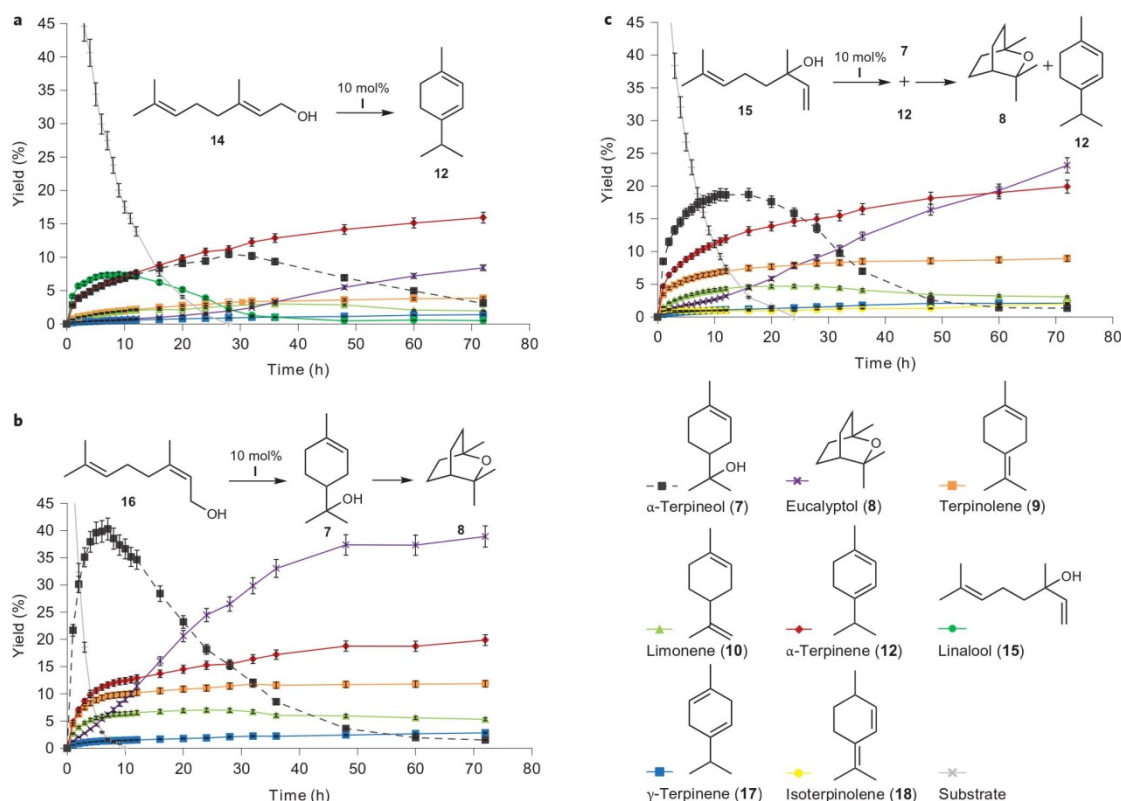
ARTICLES

Figure 3 | Results of the THT cyclizations with catalyst I for the alcohol substrates. Products were identified by gas chromatography and ^{1}H NMR spectroscopy and quantified by gas chromatography. **a**, The cyclization of GOH (**14**) is rather unselective. Initially, in analogy to the proposed biosynthesis, LOH (**15**) was formed. The other main products formed within the first ten hours were α-terpinene (**12**) and α-terpineol (**7**). With progressing reaction time, the concentrations of LOH (**15**) and α-terpineol (**7**) decreased as eucalyptol (**8**) started to form. **b**, NOH (**16**) is first cyclized mainly to α-terpineol (**7**), which is then converted into eucalyptol (**8**). **c**, The reaction profile of LOH (**15**) appears to be a composite of the results from GOH (**14**) and NOH (**16**), and gives a less-pronounced initial maximum of α-terpineol (**7**) and a better selectivity of α-terpinene (**12**) over terpinolene (**9**) than in the case of NOH (**16**). Error bars indicate typical maximal errors (±5%) as evidenced by the experiment, which was run in triplicate (Fig. 4a).

less-pronounced initial maximum of α-terpineol (**7**) and a better selectivity of α-terpinene (**12**) over terpinolene (**9**) than in the case of NOH (**16**). In addition, side reactions were between the two extremes.

The cyclization results are remarkable; for example, eucalyptol (**8**) has not been formed in a cascade reaction from acyclic terpenes before. It was only accessible from cyclic α-terpineol utilizing a strong Brønsted acid[35] or Lewis acid[36], or in a two-step procedure via phenylselenoetherification[37]. Nevertheless, we wanted to suppress the interception of cationic intermediates by the cleaved leaving group, which resulted, for example, in the formation of α-terpineol (**7**) as an intermediate. We therefore tested leaving groups with a reduced nucleophilicity and found that the acetate proved to be well suited in that regard.

Submitting geranyl acetate (GOAc) (**14a**) to the described reaction conditions resulted in the selective formation of α-terpinene (**12**) (Fig. 4a). The interception of reactive cationic intermediates was suppressed successfully, as evidenced by the disappearance of LOH and α-terpineol derivatives. The α-terpinyl cation formed (**6**) (Fig. 1b) is not quenched by nucleophiles or elimination, but is able to propagate via a 1,2-hydride shift to form cation **11** in good selectivity. Therefore, this reaction represents a true 'non-stop'[38] THT cyclization cascade, which is hard to achieve in

solution (for a different approach to 'non-stop' THT cyclizations, see Pronin and Shenvi[1]). As described for GOH (**14**), a series of control experiments were performed with **14a** and confirmed that the reaction did, indeed, only take place inside the cavity (see Supplementary Fig. 2 and Supplementary Table 6). Additionally, **14a** was converted selectively inside **I** in the presence of the extended derivative **19** (Fig. 4d) (for the details, see Supplementary Fig. 4 and Supplementary Scheme 1). For comparison, several Brønsted and Lewis acids were tested for the cyclization of GOAc (**14a**) and showed only traces of cyclic monoterpene products (see Supplementary Fig. 3).

In the case of neryl acetate (NOAc) (**16a**) (Fig. 4b), the product profile also changed dramatically. As expected, only trace amounts of α-terpineol (**7**) were observed. Nevertheless, a small fraction of α-terpinyl acetate (**7a**) was formed. More significantly, the initial product ratio between α-terpinene (**12**) and terpinolene (**9**) changed dramatically, with the latter dominating in the first 36 hours of the reaction. The product spectrum of linalyl acetate (LOAc) (**15a**), as in the case of the free alcohols, appears to be a composite of the results of GOAc and NOAc (Fig. 4c). Additionally, GOAc was formed initially, which could indicate an equilibration to the thermodynamically more stable isomer.
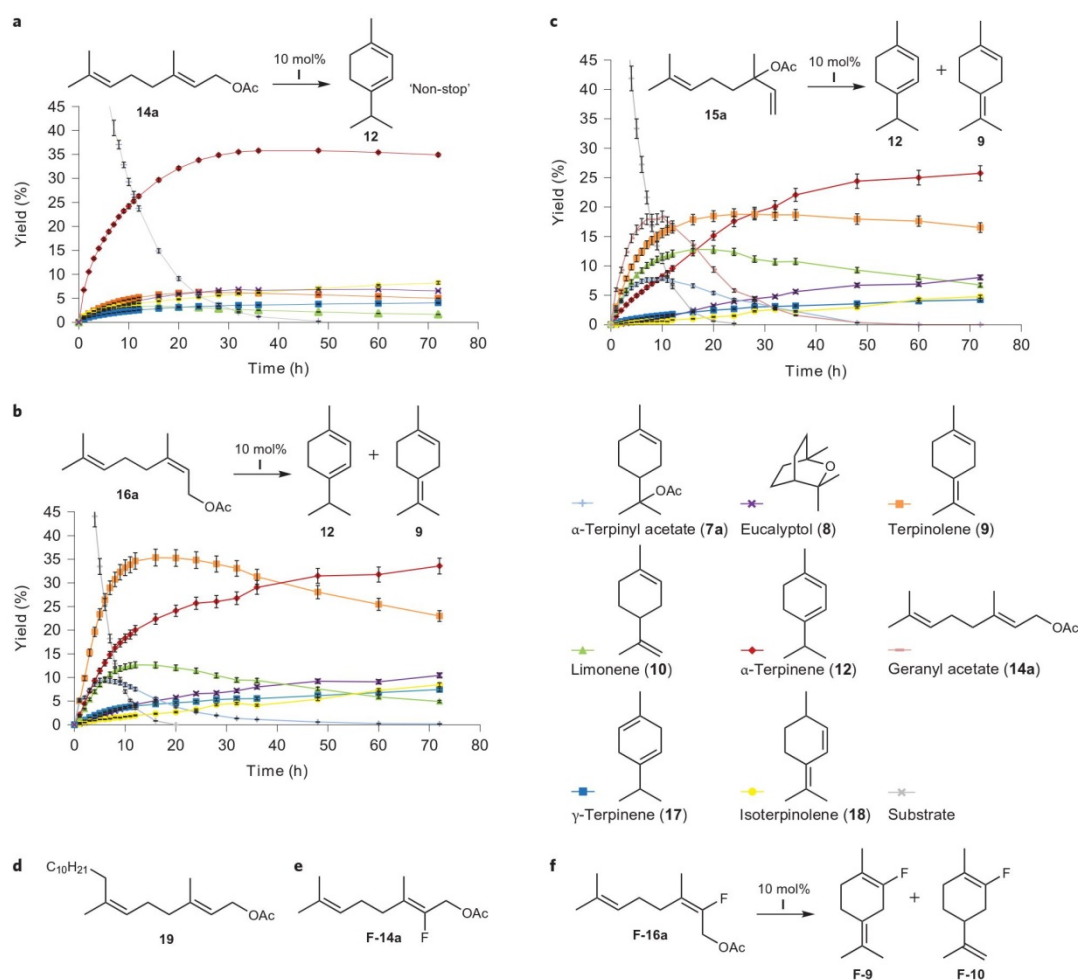
Figure 4 | Results of the THT cyclizations with catalyst I for the acetate substrates. a, The cyclization of GOAc (**14a**) led to α-terpinene (**12**) in good selectivity. It represents a 'non-stop' THT cyclization because the cationic intermediates were not quenched by nucleophiles or elimination—as evidenced by the disappearance of LOH and α-terpineol derivatives. **b**, NOAc (**16a**) cyclized mainly to α-terpinene (**12**) and terpinolene (**9**), with the latter dominating in the first 36 hours. **c**, The product profile of LOAc (**15a**) appears to be a composite of the results from GOAc (**14a**) and NOAc (**16a**). Initially, GOAc was formed, which could indicate an equilibration to the thermodynamically more stable isomer. **d**, The extended geranyl substrate **19** used for the control experiments. **e,f**, Fluoro derivatives explored in the cyclization. 2-Fluorogeranyl acetate (**F-14a**) did not undergo cyclization within I (**e**). 2-Fluoroneryl acetate (**F-16a**) produced fluoroterpinolene (**F-9**) and fluorolimonene (**F-10**) as the only main products (**f**), which indicates that these products are formed predominantly via a concerted (S_N2) mechanism, whereas α-terpinene (**12**) is formed predominantly via an S_N1-mechanism within I. Error bars in **a** represent the standard deviation from the mean value (the experiment was run in triplicate). Error bars in **b** and **c** indicate typical maximal errors (±5%), as evidenced by the results in **a**.

The dramatically different product profiles for GOAc (**14a**) and LOAc (**15a**) were striking. If GOAc (**14a**) formed the *cisoid* cation **4b** (Fig. 1b) via LOAc (**15a**) as an intermediate, as proposed in the biosynthesis, such a difference would not be expected. Additionally, no LOAc (**15a**) was observed as an intermediate in the cyclization of GOAc (**14a**). In contrast to natural enzymes, intermediates can be detected during cyclization in I, as can be seen in Figs 3a–c and 4b,c. Based on these results, we propose that the allylic cation **4a** is, indeed, directly undergoing the *transoid–cisoid* isomerization into **4b** inside I. As there is no direct evidence for the formation of linalyl-PP as an intermediate in cyclase enzymes[4] and the isomerization energy barrier of 55 kJ mol⁻¹ (gas phase)[9] can be overcome relatively quickly at ambient conditions

(half-life < 0.5 milliseconds, short compared to typical turnovers of every 1–100 seconds in cyclase enzymes[4]), a direct isomerization should no longer be excluded in cyclase enzymes.

Compared to NOH (**16**) and LOH (**15**), the reactions of NOAc (**16a**) and LOAc (**15a**) led to an increased initial formation of terpinolene (**9**) and limonene (**10**), respectively, as compared to α-terpinene (**12**). This may be attributed to the presence of the acetate/acetic acid leaving group in the reaction pocket, which could function as a general base to deprotonate the α-terpinyl cation **6** (Fig. 1b)[1]. The high degree of deprotonation in the cases of NOAc (**16a**) and LOAc (**15a**), as compared with the results of GOAc (**14a**), might seem surprising at first because all the substrates have to converge to the common intermediate α-terpinyl

ARTICLES

cation **6**. We speculated that this may indicate a different reaction mechanism. In the case of GOAc (**14a**), because of its 2*E*-alkene geometry, ring formation has to be preceded by ionization and isomerization. Thereby, the leaving group is cleaved in a distinct step before the α-terpinyl cation **6** is generated. As the isomerization is considered a slow step[4,9], the leaving group may be able to diffuse away from the reaction centre. LOAc and NOAc, however, can react in a concerted fashion (S_N2'/S_N2-like). In these cases the leaving groups would be liberated simultaneously with the formation of the α-terpinyl cation **6**, and thus they have a greater probability to assist in deprotonation. Evidence in this direction was obtained by the investigation of the cyclization behaviour of 2-fluoro derivatives.

The electron-withdrawing fluoro substituent suppresses the formation of neighbouring cationic species. Thereby, ionization-dependent reaction pathways are efficiently slowed down, whereas concerted (S_N2-type) displacements remain viable. In cyclases, 2-fluorogeranyl-pyrophosphate and 2-fluorolinalyl-pyrophosphate were utilized to elucidate the reaction mechanism[39].

When submitting 2-fluorogeranyl acetate (**F-14a**) (Fig. 4e) to catalyst **I**, no formation of the corresponding cyclic products was observed (19 days), which confirms that, indeed, ionization is required to initiate the reaction cascade in this case. 2-Fluoroneryl acetate (**F-16a**), however, showed conversion, although at a reduced rate (8%; see Supplementary Table 7), to produce fluoro-terpinolene **F-9** and fluorolimonene **F-10** as the only main products (see Supplementary Fig. 5). The reduced rate can be explained by the decreased uptake in the catalyst (fluoro-containing substrates have generally shown a lower degree of encapsulation) and by the inhibition of the S_N1 reaction path. The observed rate reduction, both in absolute terms as well as in comparison with 2-fluorogeranyl acetate (**F-14a**), does not indicate an ionization-dependent (S_N1-type) reaction path. In contrast to regular NOAc (**16a**), only traces of α-terpinene (**12**) were formed. These results indicate that terpinolene (**9**) and limonene (**10**) are formed predominantly via a concerted mechanism (S_N2' in the case of LOAc, and S_N2 in the case of NOAc), whereas α-terpinene (**12**) is formed predominantly via an S_N1 mechanism within **I**. These results are in line with the hypothesis that the local concentration of the leaving group influences product selectivity. Interestingly, these results are in contrast with solvolysis studies of neryl mesylate, in which a 160-fold rate reduction was observed for the 2-fluoroneryl substrate[40]. As, in that case, the rate decrease was comparable to that observed with the 2-fluorogeranyl substrate, it was argued that both react via an ionization (S_N1) mechanism. As expected, 2-fluorolinalyl acetate (**F-15a**) also produced fluoroterpinolene (**F-9**) and fluorolimonene (**F-10**) as the only main products. Additionally, these results could explain the different degrees of side reactions (alkylation of phenolic groups of monomer **13** and dimerization) observed during cyclization. Geranyl derivatives, which require the formation of acyclic cations, displayed the highest degree. Linalyl and neryl derivatives, able to react in a concerted fashion and thereby avoid acyclic cationic intermediates, displayed a much lower tendency.

To compare the catalytic efficiency of the system to that of natural cyclase enzymes, the kinetics of the conversion of GOAc (**14a**) inside capsule **I** were investigated (see Supplementary Figs 9–12 and Supplementary Table 10). The obtained k_{cat} value of 0.00079 ± 0.00006 s^{-1} is only about two orders of magnitude lower than that observed in natural cyclase enzymes (0.01–1 s^{-1})[4]. However, a large difference can be seen when comparing the K_m values (0.078 ± 0.007 M inside **I**, as compared to low micromolar values in natural cyclase enzymes[4]). As K_m is related to the inverse of the binding constant, this translates into a much weaker binding of the substrate in the presented capsule catalyst than in natural enzymes. One reason for the much higher affinity

of natural substrates to cyclase enzymes may be the strong interaction of the pyrophosphate group with magnesium ions in the enzyme pocket[4].

Conclusions

Two main conclusions can be drawn from this work. (1) The presented evidence indicates that direct isomerization of the *transoid* cation **4a** into the *cisoid* form **4b**, considered unlikely in the biosynthesis[4,9], is possible inside cavity **I**. Therefore, a direct isomerization should also be considered in the biosynthesis. (2) It was demonstrated for the first time that a relatively simple aromatic cavity is catalytically competent in complex THT cyclizations. The catalytic power of the system relies, as with enzyme pockets, on the stabilization of the cationic intermediates and transition states. These findings set the stage for the development of catalysts able to revolutionize the total synthesis of complex terpene natural products.

References

1. Pronin, S. V. & Shenvi, R. A. Synthesis of highly strained terpenes by non-stop tail-to-head polycyclization. *Nature Chem.* **4**, 915–920 (2012).
2. Christianson, D. W. Structural biology and chemistry of the terpenoid cyclases. *Chem. Rev.* **106**, 3412–3442 (2006).
3. Miller, D. J. & Allemann, R. K. Sesquiterpene synthases: passive catalysts or active players? *Nat. Prod. Rep.* **29**, 60–71 (2012).
4. Croteau, R. Biosynthesis and catabolism of monoterpenoids. *Chem. Rev.* **87**, 929–954 (1987).
5. Degenhardt, J., Köllner, T. G. & Gershenzon, J. Monoterpene and sesquiterpene synthases and the origin of terpene skeletal diversity in plants. *Phytochemistry* **70**, 1621–1637 (2009).
6. Cane, D. E. Enzymic formation of sesquiterpenes. *Chem. Rev.* **90**, 1089–1103 (1990).
7. Dickschat, J. S. Isoprenoids in three-dimensional space: the stereochemistry of terpene biosynthesis. *Nat. Prod. Rep.* **28**, 1917–1936 (2011).
8. Wise, M. L. & Croteau, R. in *Comprehensive Natural Products Chemistry* Vol. 2 (eds Barton, D., Nakanishi, K. & Meth-Cohn, O.) 97–153 (Pergamon, 1999).
9. Allinger, N. L. & Siefert, J. H. Organic quantum chemistry. XXXIII. Electronic spectra and rotational barriers of vinylborane, allyl cation, and related compounds. *J. Am. Chem. Soc.* **97**, 752–760 (1975).
10. Lesburg, C. A., Zhai, G., Cane, D. E. & Christianson, D. W. Crystal structure of pentalenene synthase: mechanistic insights on terpenoid cyclization reactions in biology. *Science* **277**, 1820–1824 (1997).
11. Starks, C. M., Back, K., Chappell, J. & Noel, J. P. Structural basis for cyclic terpene biosynthesis by tobacco 5-epi-aristolochene synthase. *Science* **277**, 1815–1820 (1997).
12. Hof, F., Craig, S. L., Nuckolls, C. & Rebek, J. J. Molecular encapsulation. *Angew. Chem. Int. Ed.* **41**, 1488–1508 (2002).
13. Palmer, L. C. & Rebek, J. J. The ins and outs of molecular encapsulation. *Org. Biomol. Chem.* **2**, 3051–3059 (2004).
14. Koblenz, T. S., Wassenaar, J. & Reek, J. N. H. Reactivity within a confined self-assembled nanospace. *Chem. Soc. Rev.* **37**, 247–262 (2008).
15. Rebek, J. Molecular behavior in small spaces. *Acc. Chem. Res.* **42**, 1660–1668 (2009).
16. Yoshizawa, M., Klosterman, J. K. & Fujita, M. Functional molecular flasks: new properties and reactions within discrete, self-assembled hosts. *Angew. Chem. Int. Ed.* **48**, 3418–3438 (2009).
17. Wiester, M. J., Ullmann, P. A. & Mirkin, C. A. Enzyme mimics based upon supramolecular coordination chemistry. *Angew. Chem. Int. Ed.* **50**, 114–137 (2011).
18. Ajami, D. & Rebek, J. More chemistry in small spaces. *Acc. Chem. Res.* **46**, 990–999 (2012).
19. Raynal, M., Ballester, P., Vidal-Ferran, A. & van Leeuwen, P. W. N. M. Supramolecular catalysis. Part 2: artificial enzyme mimics. *Chem. Soc. Rev.* **43**, 1734–1787 (2014).
20. Bocokić, V. et al. Capsule-controlled selectivity of a rhodium hydroformylation catalyst. *Nature Commun.* **4**, 2670 (2013).
21. Dydio, P., Detz, R. J. & Reek, J. N. H. Precise supramolecular control of selectivity in the Rh-catalyzed hydroformylation of terminal and internal alkenes. *J. Am. Chem. Soc.* **135**, 10817–10828 (2013).
22. Wang, Z. J., Clary, K. N., Bergman, R. G., Raymond, K. N. & Toste, F. D. A supramolecular approach to combining enzymatic and transition metal catalysis. *Nature Chem.* **5**, 100–103 (2013).

ARTICLES

23. Zhao, C. *et al.* Chiral amide directed assembly of a diastereo- and enantiopure supramolecular host and its application to enantioselective catalysis of neutral substrates. *J. Am. Chem. Soc.* **135,** 18802–18805 (2013).

24. Zhao, C., Toste, F. D., Raymond, K. N. & Bergman, R. G. Nucleophilic substitution catalyzed by a supramolecular cavity proceeds with retention of absolute stereochemistry. *J. Am. Chem. Soc.* **136,** 14409–14412 (2014).

25. Salles, A. G., Zarra, S., Turner, R. M. & Nitschke, J. R. A self-organizing chemical assembly line. *J. Am. Chem. Soc.* **135,** 19143–19146 (2013).

26. Hart-Cooper, W. M., Clary, K. N., Toste, F. D., Bergman, R. G. & Raymond, K. N. Selective monoterpene-like cyclization reactions achieved by water exclusion from reactive intermediates in a supramolecular catalyst. *J. Am. Chem. Soc.* **134,** 17873–17876 (2012).

27. MacGillivray, L. R. & Atwood, J. L. A chiral spherical molecular assembly held together by 60 hydrogen bonds. *Nature* **389,** 469–472 (1997).

28. Cavarzan, A., Scarso, A., Sgarbossa, P., Strukul, G. & Reek, J. N. H. Supramolecular control on chemo- and regioselectivity via encapsulation of (NHC)-Au catalyst within a hexameric self-assembled host. *J. Am. Chem. Soc.* **133,** 2848–2851 (2011).

29. Bianchini, G., Sorella, G. L., Canever, N., Scarso, A. & Strukul, G. Efficient isonitrile hydration through encapsulation within a hexameric self-assembled capsule and selective inhibition by a photo-controllable competitive guest. *Chem. Commun.* **49,** 5322–5324 (2013).

30. Zhang, Q. & Tiefenbacher, K. Hexameric resorcinarene capsule is a Brønsted acid: investigation and application to synthesis and catalysis. *J. Am. Chem. Soc.* **135,** 16213–16219 (2013).

31. Shivanyuk, A. & Rebek, J. Reversible encapsulation by self-assembling resorcinarene subunits. *Proc. Natl Acad. Sci. USA* **98,** 7662–7665 (2001).

32. Avram, L. & Cohen, Y. Spontaneous formation of hexameric resorcinarene capsule in chloroform solution as detected by diffusion NMR. *J. Am. Chem. Soc.* **124,** 15148–15149 (2002).

33. Yamanaka, M., Shivanyuk, A. & Rebek, J. Kinetics and thermodynamics of hexameric capsule formation. *J. Am. Chem. Soc.* **126,** 2939–2943 (2004).

34. Shivanyuk, A. & Rebek, J. Assembly of resorcinarene capsules in wet solvents. *J. Am. Chem. Soc.* **125,** 3432–3433 (2003).

35. Leão Lana, E. J., da Silva Rocha, K. A., Kozhevnikov, I. V. & Gusevskaya, E. V. Synthesis of 1,8-cineole and 1,4-cineole by isomerization of α-terpineol catalyzed by heteropoly acid. *J. Mol. Catal. A* **259,** 99–102 (2006).

36. Kelly, B. D., Allen, J. M., Tundel, R. E. & Lambert, T. H. Multicatalytic synthesis of complex tetrahydrofurans involving bismuth(III) triflate catalyzed intramolecular hydroalkoxylation of unactivated olefins. *Org. Lett.* **11,** 1381–1383 (2009).

37. Bugarčić, Z. M., Dunkić, J. D. & Mojsilović, B. M. A simple, convenient and expeditious approach to cineol. *Heteroatom Chem.* **15,** 468–470 (2004).

38. Eschenmoser, A., Ruzicka, L., Jeger, O. & Arigoni, D. Zur Kenntnis der Triterpene. 190. Mitteilung. Eine stereochemische Interpretation der biogenetischen Isoprenregel bei den Triterpenen. *Helv. Chim. Acta* **38,** 1890–1904 (1955).

39. Croteau, R. Evidence for the ionization steps in monoterpene cyclization reactions using 2-fluorogeranyl and 2-fluorolinalyl pyrophosphates as substrates. *Arch. Biochem. Biophys.* **251,** 777–782 (1986).

40. Poulter, C. D. & King, C. H. R. Model studies of terpene biosynthesis. A stepwise mechanism for cyclization of nerol to α-terpineol. *J. Am. Chem. Soc.* **104,** 1422–1424 (1982).

Author contributions
K.T. conceived the project and wrote the manuscript with Q.Z. Q.Z. planned and carried out the experiments. K.T. and Q.Z. discussed the experiments and results.

Additional information
Supplementary information and chemical compound information are available in the online version of the paper. Reprints and permissions information is available online at www.nature.com/reprints. Correspondence and requests for materials should be addressed to K.T.

Competing financial interests
The authors declare no competing financial interests.

7.3 The Royal Society of Chemistry

Figure 1.4 is partly reproduced from reference[32] with the permission of the Royal Society of Chemistry.

98

**ROYAL SOCIETY OF CHEMISTRY LICENSE
TERMS AND CONDITIONS**

Dec 03, 2015

This is a License Agreement between Qi Zhang ("You") and Royal Society of Chemistry ("Royal Society of Chemistry") provided by Copyright Clearance Center ("CCC"). The license consists of your order details, the terms and conditions provided by Royal Society of Chemistry, and the payment terms and conditions.

All payments must be made in full to CCC. For payment instructions, please see information listed at the bottom of this form.

License Number	3761560770748
License date	Dec 03, 2015
Licensed content publisher	Royal Society of Chemistry
Licensed content publication	Organic & Biomolecular Chemistry
Licensed content title	The ins and outs of molecular encapsulation
Licensed content author	Liam C. Palmer, Julius Rebek, Jr.
Licensed content date	Oct 13, 2004
Volume number	2
Issue number	21
Type of Use	Thesis/Dissertation
Requestor type	academic/educational
Portion	figures/tables/images
Number of figures/tables/images	1
Format	print and electronic
Distribution quantity	40
Will you be translating?	no
Order reference number	None
Title of the thesis/dissertation	Enzyme-like catalysis in self-assembled aromatic cavities
Expected completion date	Jan 2016
Estimated size	150
Total	0.00 EUR

Terms and Conditions

This License Agreement is between {Requestor Name} ("You") and The Royal Society of Chemistry ("RSC") provided by the Copyright Clearance Center ("CCC"). The license consists of your order details, the terms and conditions provided by the Royal Society of Chemistry, and the payment terms and conditions.

RSC / TERMS AND CONDITIONS
INTRODUCTION
The publisher for this copyrighted material is The Royal Society of Chemistry. By clicking "accept" in connection with completing this licensing transaction, you agree that the following terms and conditions